LITHIUM ION BATTERY-SUPERCAPACITOR HYBRID USING BIMATERIAL ELECTRODES

Ph.D. THESIS

by

SOBHIT SAXENA

**DEPARTMENT OF METALLURGICAL AND MATERIALS
ENGINEERING
INDIAN INSTITUTE OF TECHNOLOGY ROORKEE
ROORKEE-247 667 (INDIA)
JULY, 2017**

LITHIUM ION BATTERY-SUPERCAPACITOR HYBRID USING BIMATERIAL ELECTRODES

A THESIS

*Submitted in partial fulfilment of the
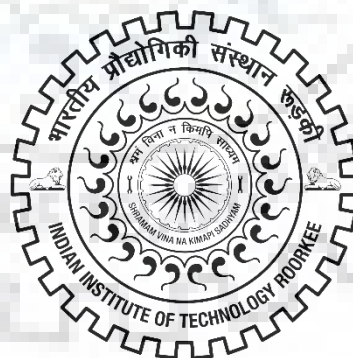requirements for the award of the degree*

of

DOCTOR OF PHILOSOPHY

in

METALLURGICAL AND MATERIALS ENGINEERING

by

SOBHIT SAXENA

**DEPARTMENT OF METALLURGICAL AND MATERIALS
ENGINEERING
INDIAN INSTITUTE OF TECHNOLOGY ROORKEE
ROORKEE-247 667 (IDIA)
JULY, 2017**

INDIAN INSTITUTE OF TECHNOLOGY ROORKEE
ROORKEE

<u>CANDIDATE'S DECLARATION</u>

I hereby certify that the work which is being presented in the thesis entitled "**LITHIUM ION BATTERY-SUPERCAPACITOR HYBRID USING BIMATERIAL ELECTRODES**" in partial fulfilment of the requirements for the award of Degree of Doctor of Philosophy and submitted in the Department of Metallurgical and Materials Engineering of the Indian Institute of Technology Roorkee, Roorkee is an authentic record of my own work carried out during a period from July, 2011 to July, 2017 under the supervision of Dr. Anjan Sil, Professor, Department of Metallurgical and Materials Engineering, Indian Institute of Technology Roorkee, Roorkee.

The matter presented in the thesis has not been submitted by me for the award of any other degree of this or any other Institute.

(Sobhit Saxena)

This is to certify that the above statement made by the candidate is correct to the best of my knowledge.

(Anjan Sil)
Supervisor

The Ph.D. Viva-Voce Examination of **Sobhit Saxena** , Research Scholar, has been held on _____.

Chairman, SRC   **External Examiner**

This is to certify that the student has made all the corrections in the thesis.

Anjan Sil (Supervisor)   **Head of the Department**

Dated: _____

Dedicated to

My parents (Shri. Girish Kumar Saxena and Smt. Usha Saxena)
&
mother in law (Smt. Suresh Kanta)
whose support
has been a continuous source of motivation

and

my wife (Seema Saxena) & beloved daughter (Avyukta Saxena)
for being omnipresent

ABSTRACT

The electrochemical energy storage system stores the electrical energy in the form of chemical energy while charging and delivers electrical energy while discharging. This type of device is a green system as it does not generate pollution. One of the distinctive characteristics of the electric power sectors is that the amount of electricity that can be generated is relatively fixed with time, although demand of electricity fluctuates throughout the day. Thus storage of electrical energy is very much required so that it can be available to meet the demand whenever needed. The electrochemical energy storage devices can be very effective for the same. They are also useful for energy storage in large-scale solar or wind-based electricity generations. Electrochemical energy storage systems are also required to enable the widespread use of hybrid electric vehicles (HEV), plug-in hybrids, and all-electric vehicles. These systems had already proven their efficiency in the modern portable electronic devices such as laptops and smart phones.

Lithium ion battery is an electrochemical energy storage system, which is characterized by a high specific energy. A lithium-ion battery utilizes lithium insertion materials in both the negative and positive electrodes. Supercapacitor is an electrochemical energy storage device characterized by an inherently high specific power. The electrochemical double layer capacitor typically consists of two activated carbon (AC) based electrodes soaked with an organic electrolyte. The hybridization of supercapacitors with lithium ion batteries, with a view to combining the high specific power of the supercapacitor with the high specific energy of the lithium ion battery has been persuaded in the last decade with different approaches. Readily available batteries and electrochemical capacitors can be externally hard wire connected, in serial or in parallel. By analogy, the same approaches can be proposed at the internal level within one device, leading to the internal serial or the internal parallel hybrids. The internal parallel hybrids provide a specific energy greater than that of the capacitor and a specific power greater than that of the battery. Thus, the internal parallel hybrids improve the capacitor in terms of specific energy and the battery in terms of specific power.

This Ph.D. thesis is based on preparation of internal parallel hybrid of lithium ion battery and supercapacitor consisting of bimaterial electrode. Bai et al. has patented different approaches of making bimaterial electrodes. A novel bimaterial electrode configuration is adopted in this

work based on one of the existing configuration with some modifications which makes the hybrid system a three terminal device in relation to conventional two terminal devices.

$Li_4Ti_5O_{12}$ (LTO) and AC are chosen as battery material and supercapacitor material respectively. Sol-gel process is adopted for synthesis of the above mentioned materials throughout the work. The properties of LTO are enhanced by making it nanoporous and also by doping with vanadium. The role of calcination atmosphere on the electrochemical performance of vanadium doped LTO is studied as the samples are calcined in air and argon atmospheres separately. A comparative study of LTO, nanoporous LTO and vanadium doped LTO based bimaterial electrodes with AC in the three terminal hybrid system is done. All the hybrid systems are also subjected to pulsating input current to test their performance in power application. The thesis content is presented in seven chapters as given below:

Chapter 1 Introduction

This chapter presents brief overview on importance of electrochemical energy storage devices, lithium ion batteries and supercapacitors stating their advantages, limitations and the need of hybridization between battery and supercapacitor. This chapter also introduces the objective of the Ph.D. dissertation.

Chapter 2 Literature Review

This chapter describes properties of lithium ion battery and supercapacitor as energy storage devices. The performance of different types of materials as anode of lithium ion battery is surveyed and presented. LTO is chosen as anode material based on the properties and drawbacks of different anode materials. Efforts made by the researchers to overcome the limitations of LTO to enhance the electrochemical performance as anode of lithium ion battery are also discussed. The need of hybridization due to limitations of lithium ion battery and supercapacitor is discussed and different configurations of hybrid system are described. The problem formulation for thesis and scope of the research work are described.

Chapter 3 Experimental Techniques

The purpose of the present work is to prepare and characterize the hybrid of lithium ion battery and supercapacitor which includes synthesis of LTO, nanoporous LTO and vanadium doped LTO as battery materials. Characterization of synthesized samples using X-ray diffractometer (XRD), Field emission-scanning electron microscope (FE-SEM) along with Energy dispersive spectroscopy (EDS), Transmission electron microscope (TEM), X-ray photoelectron spectrometer (XPS), Electrochemical impedance spectroscopy (EIS) analyser and Brunauer–Emmett–Teller (BET) analyser for surface area measurement of porous samples is performed. Electrochemical analysis of the samples using charge-discharge, cyclic voltammetry etc. is done following the steps given below:

(i)   Preparation of electrodes of lithium ion cell as well as of hybrid cell using AC as supercapacitor material with all above mentioned battery material synthesized.

(ii)   Formation of cell assembly under the inert gas atmosphere.

(iii)   Electrochemical tests using Arbin Cycler.

Chapter 4 LTO and nanoporous LTO

This chapter presents the results and discussion on synthesis and characterization of LTO with pure phase. Occurrence of rutile TiO_2 phase in the compound LTO (synthesized with stoichiometric ratio Li: Ti = 4:5) is due to loss of Li during calcination at higher temperature and is independent of synthesis method (Shin, Chung, Ryu, Park, & Yoon, 2012). Pure LTO phase is desired as rutile TiO_2 does not contribute to lithium intake process while charging at room temperature due to unique primitive tetragonal packing in rutile TiO_2. The cation radius of octahedral sites is 0.40 Å but the Li ion radius is normally 0.68 Å. Christiansen et al. 1988 shows that rutile TiO_2 does not have any discharge capacity at room temperature (Christiansen, West, Jacobsen, & Atlung, 1988). Quantitative analysis of the impurity phase (Rutile TiO_2 observed by XRD analysis) was done by PDXL software using relative intensity ratio (RIR) method. According to the weight% of both phases obtained, theoretical calculations were performed to estimate the excess Li required to synthesize phase pure LTO free from the TiO_2 impurity phase. $Li_{4+x}Ti_5O_{12}$ (x = 0.2, 0.4 and 0.6) are synthesized by following sol-gel route (as described in chapter 3). Electrochemical analysis is performed to understand the effect of excess Li on the capacity of LTO. Morphological analysis of LTO is performed using TEM image analysis.

This chapter also describes results and discussion on synthesis and characterization of nanoporous LTO using carbon nano beads as pore former. Carbon nano beads were synthesized

using CVD process and incorporated at precursor level during synthesis of LTO. Since the calcination temperature of LTO is 800°C, carbon nano beads got oxidized (at about 650°C) to become CO_2 resulting in porous LTO. The surface area of the particles was measured following BET analysis. Average pore size of the powder was calculated from the SEM micrographs of the powder. Effect of porous morphology on electrochemical performance is also studied.

Chapter 5 Vanadium doped LTO

LTO with enhanced properties can replace the conventional carbonaceous anode material of lithium ion battery. Vanadium (V) doped LTO ($Li_4Ti_{5-x}V_xO_{12}$, x = 0, 0.05, 0.1, 0.15) materials are synthesized by sol-gel process followed by calcination of dried gel in air and argon atmospheres separately to examine the role of calcination atmosphere on the oxidation state of V and Ti. The electronic conductivity and electrochemical performance of the synthesized samples as anode of lithium ion battery are reported in this chapter. It is understood from the literature that both doping and synthesis in reducing atmosphere increase the conductivity of the material and the probable cause of the enhancement is the reduction of Ti^{4+} to Ti^{3+} (Yi et al., 2009, 2010a; Yu et al., 2011). However, it is not clear whether the reduction of Ti ion occurs either due to doping or calcination in reducing atmosphere. An attempt to study the oxidation states of V and Ti by XPS is made to understand the fact. EIS is performed to estimate of lithium ion diffusion coefficient.

For electronic conductivity measurements, the powder samples are compacted in the form of cylindrical pellets by hydraulic press and the samples are heat treated. Ohmic contact for electrical conductivity measurement were developed by applying silver paste onto flat surfaces of pellets.

Chapter 6 Hybrid system having bimaterial electrode of LTO and AC

In chapters 4 and 5 LTO, nanoporous LTO and V doped LTO as electrode materials of lithium ion battery are discussed. This chapter describes the electrochemical behavior of AC based supercapacitor. A new internal hybrid system of lithium ion battery and supercapacitor is investigated. This hybrid is a three terminal device. The bimaterial electrodes using LTO, nanoporous LTO or V doped LTO as battery material and AC as supercapacitor material are

explored in terms of its electrochemical properties comparative to both LTO based lithium ion battery and AC based supercapacitor.

All the three systems are tested for pulse applications by studying the electrochemical behavior on application of pulsating charge-discharge current. Argon calcined V doped LTO based hybrid system shows superior performance for all the pulsating charge-discharge currents.

Chapter 7 presents the major conclusions of the present study and scope of the future work.

List of Publications

Peer reviewed Journals:

1. **Sobhit Saxena** and Anjan Sil "Role of calcination atmosphere in vanadium doped $Li_4Ti_5O_{12}$ for lithium ion battery anode material" Material Research Bulletin (2017), Vol. 96, 449-457.

2. Hari Raj, **Sobhit Saxena** and Anjan Sil "Improved electrochemical performance of $Li_4Ti_5O_{12}$ by reducing rutile TiO_2 phase impurity and particle size", Materials Technology (2017), Vol. 32, No. 3, 196-201.

3. **Sobhit Saxena** and Anjan Sil "Nanoporous $Li_4Ti_5O_{12}$ Material for the Electrode of Lithium Ion Battery" IETE Technical Review (2016), Vol. 33, No. 1, 60-63.

4. Hari Raj, **Sobhit Saxena** and Anjan Sil "Internal Hybrid System of Li-Ion Battery and Supercapacitor" Journal of Basic and Applied Engineering Research (2015) Vol. 2, No. 11, 937-940.

Conference Proceedings/Symposium:

1. Anjan Sil and **Sobhit Saxena** "Electrochemical characteristics of battery-supercapacitor hybrid device having bimaterial electrode" 3rd World Congress on Materials Science & Engineering, Scientific Future Group, Barcelona, Spain, August 24-26, 2017.

2. **Sobhit Saxena** and Anjan Sil "Excess Li in synthesis of sol-gel derived phase pure $Li_4Ti_5O_{12}$" International Conference on Advanced Functional Materials (ICAFM-2017), Anna University, Chennai, 6-8 January, 2017.

3. Hari Raj, **Sobhit Saxena** and Anjan Sil "Internal Hybrid System of Li-Ion Battery and Supercapacitor", 3rd International Conference on "Applied Sciences, Environmental Engineering and Clean Energy Technologies for Sustainable Development" Jawaharlal Nehru University, New Delhi, April 25-26, 2015.

4. **Sobhit Saxena** and Anjan Sil "Nanoporous $Li_4Ti_5O_{12}$ material for electrode of lithium ion battery" 2nd IEEE International Conference on Emerging Electronics (ICEE-2014), IISc Bangalore, 3-6 December, 2014.

5. **Sobhit Saxena** and Anjan Sil "Synthesis of nanoporous $Li_4Ti_5O_{12}$ by using carbon nano beads as pore former" International Conference on Functional Materials (ICFM-2014), IIT Kharagpur, 5-7 February, 2014.

6. **Sobhit Saxena** "Synthesis of template based porous nano-structured $Li_4Ti_5O_{12}$ with graphene coated surface as anode material for lithium ion battery" International Workshop on Nanomechanical Sensing", IIT Bombay, 6-8 June, 2012.
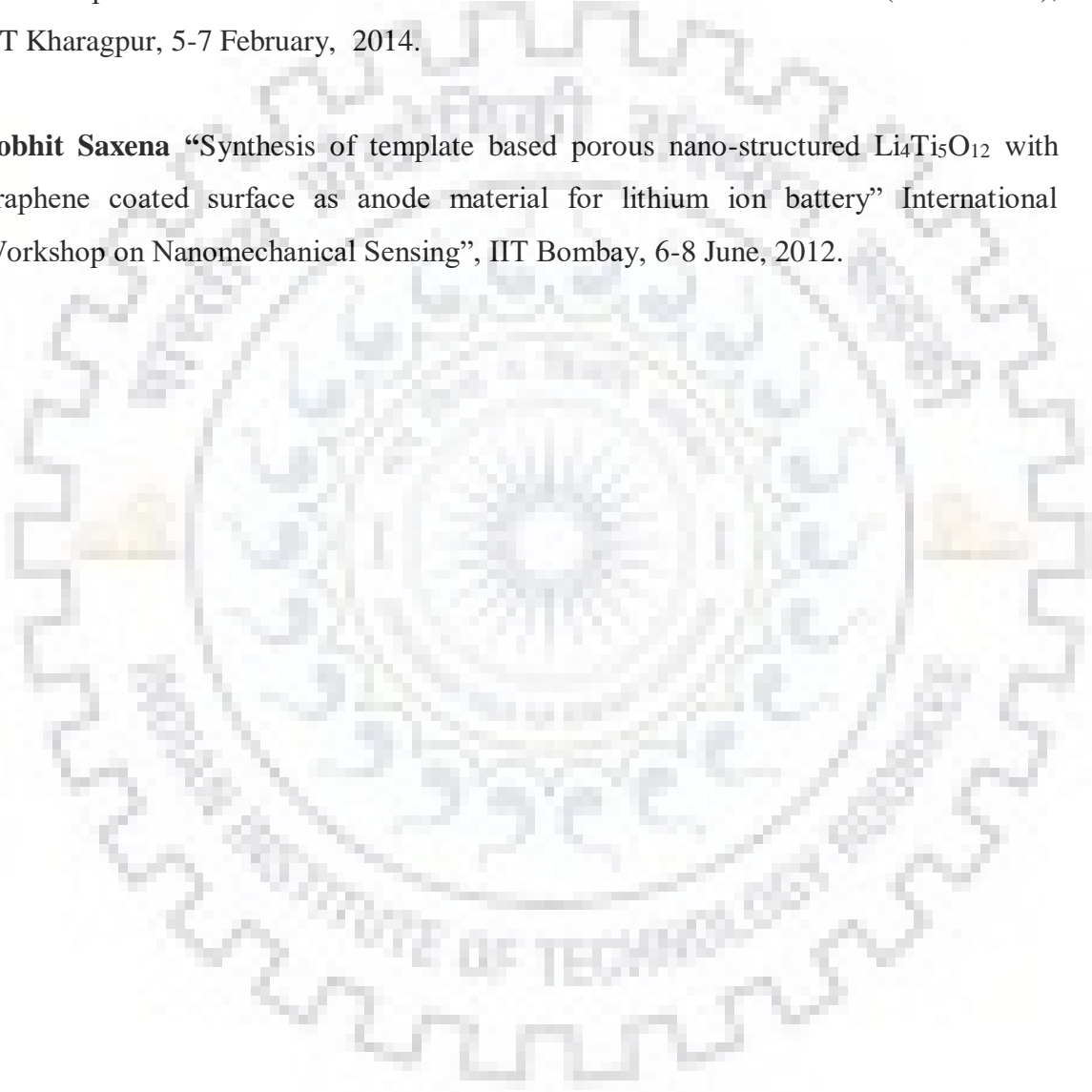
Acknowledgements

A doctoral thesis comes to fruition by the combined effort of many people and it gives me great pleasure to acknowledge and thanks the people involved directly or indirectly with my dissertation work.

First and foremost, my utmost gratitude goes to Almighty God for giving me patience and courage to successfully complete my dissertation work. I am eternally grateful to my family for their unremitting support. It goes without saying that none of this would have been possible without them.

My sincere thanks and earnest gratitude to my supervisor Dr. Anjan Sil, Professor and Head, Department of Metallurgical and Materials Engineering, Indian Institute of Technology Roorkee. Without his timely help, intellectual input, constructive criticism and painstaking efforts, it would not have been possible for me to complete this thesis in the present form. He molded my outlook towards the science of materials. His comprehensive knowledge and incisive insight in this field of research had always inspired me. Besides the guidance in research he was always with me throughout my Ph.D. Whenever I was depressed, he was there to boost my morale and helped me in getting out of that depression. I feel lucky to have him as my Ph.D. supervisor.

I would like to acknowledge the other members of my S.R.C. committee, Prof. B.S.S. Daniel, Prof. Tashi Nautiyal and Dr.Vikram Dabhade who monitored my work and took effort in reading and providing me with valuable comments on earlier versions of this thesis.

I convey my sincere thanks to Prof. Anil Kumar, Department of Chemistry, Prof. G.P. Choudhari, Department of Metallurgical and Materials Engineering and Dr. P. Gopinath, Centre of Nanotechnology from whom my knowledge related to materials was enriched during my Ph.D. course work.

I wish to place my sincere thanks to the technical and the administrative staff of the Department of Metallurgical and Materials Engineering specially to Mr. Dhan Prakash, Mr. R.K. Sharma, Mr. R.S. Sharma, Mr. Narendra, Mr. Ramveer Singh who have helped me in many ways during the course of my Ph.D. Thanks are also due to Mr. S.D. Sharma, Mr. Anil Saini, Mr. Shiv Kumar of IIC, for providing all the necessary help.

I would also like to thank my seniors and lab mates for creating an interacting and enthusiastic research atmosphere. I wish to thank Dr. Malay Jana, Dr. Rajeev Sehrawat, Dr. Rajni Sharma and Dr. Soumya Shankar Ghosh from whom I learn to progress in Ph.D. work. A special

thanks Mr. Siddharth, Scientist-C, CECRI, Kolkata for taking all the pains in performing XPS characterization of my samples.

I would especially like to thanks Mr. Abhishek Gupta & Mr. Hari Raj for their gracious and vital help along the way in completing the work. Their excitement and willingness to provide feedback made the completion of this research an enjoyable experience.

I owe my sincere gratitude and a very special thanks to family members for bearing me throughout my Ph.D tenure. I bow in ovation to my wife and my daughter for their care and kindness. The two noble ones stood by me all through with patience and tolerance. My words of thanks cannot compensate their contribution, yet with all humility I thank them for their noble gesture and splendid support.

Last but not the least I would like to acknowledge the financial support from Ministry of Human Resource & Development (MHRD).

(Sobhit Saxena)

Contents

List of Figures

List of Tables

List of Abbreviations

AC	Activated Carbon
BET	Brunauer–Emmett–Teller
BSH	Battery Supercapacitor Hybrid
CA	Citric Acid
CNT	Carbon Nanotube
CPE	Constant Phase Element
CTAB	Cetyl Trimethylammonium Bromide
CV	Cyclic voltammetry
CVD	Chemical Vapour Deposition
D_{Li+}	Li-ion Diffusivity
DMC	Dimethyl Carbonate
EC	Ethylene Carbonate
EDLC	Electrochemical double layer capacitor
EIS	Electrochemical Impedance Spectroscopy
EPH	Internal Parallel Hybrid
ESH	External Series Hybrid
FESEM	Field Emission Scanning Electron Microscope
H_2O_2	Hydrogen peroxide
IPH	Internal Parallel Hybrid
ISH	Internal Series Hybrid
JCPDS	Joint Committee on Powder Diffraction Standards
Li_2CO_3	Lithium carbonate
Li_2MnO_3	Lithium Manganese Oxide
Li_2TiO_3	Lithium Titanate
$Li_4Ti_5O_{12}$ (LTO)	Lithium Titanate
$LiAsF_6$	Lithium Hexafluoroarsenate
$LiClO_4$	Lithium Perchlorate
$LiCo_{1/3}Ni_{1/3}Mn_{1/3}O_2$	Lithium Cobalt Nickel Manganese Oxide
$LiCoO_2$	Lithium Cobalt Oxide
$LiCoPO_4$	Lithium Cobalt Phosphate

LiFePO4	Lithium Iron Phosphate
$LiMnPO_4$	Lithium Manganese Phosphate
$LiNi_{0.5}Mn_{0.5}O_2$	Lithium Nickel Manganese Oxide
$LiNiPO_4$	Lithium Nickel Phosphate
LiOH	Lithium Hydroxide
$LiPF_6$	Lithium Hexafluorophosphate
LiPF6	Lithium Hexafluorophosphate
LTO-P	Nanoporous LTO
NEC	Nippon Electric Company
NMP	N-methyl-2 pyrrolidone
PVA	Poly(vinyl alcohol)
PVB	Polyvinyl Butyral
PVDF	Poly(vinylidene fluoride)
R_b	Bulk Resistance
R_{ct}	Charge Transfer Resistance
RIR	Relative Intensity Ratio
SAED	Selected Area Electron Diffraction
SEI	Surface Electrolyte Interphase
SEM	Scanning Electron Microscopy
SPE	Solid Polymer Electrolyte
TEA	Triethanolamine
TEM	Transmission Electron Microscopy
TiO_2	Titanium Dioxide
TTIP	Titanium (IV) isopropoxide
XPS	X-ray photoelectron spectroscopy
XRD	X-ray Diffraction
ZnO	Zinc Oxide
Z_w	Warburg Impedance
σ_w	Warburg impedance coefficient

Introduction

2

INDRODUCTION

In today's world there is a continuous increase in demand of energy. Fossil fuels viz. coal, natural gas, and oil produce most of the required electricity but with significant and harmful consequences. They produce the vast majority of global warming emissions. They release toxic chemicals that pollute air atmosphere and water. Renewable energy has the potential to reduce pollution and slowdown the global warming. It is clean and safe but totally depends upon the natural circumstances which are not same for every time. Hence there is a need of energy storage devices which can store the energy when generated and the stored energy is utilized when required. The electrochemical energy storage system stores the energy in the form of chemical energy while charging and delivers electrical energy while discharging. This type of device is a green system as it does not create pollution.

The demand of electricity varies frequently throughout the day while the generated electricity is relatively fixed. Thus storage of electrical energy is very much required so that it can be utilized according to the requirement of the consumer. The electrochemical energy storage devices can be very effective for the same. They are also useful for energy storage in solar plants and wind based electricity. Electrochemical energy storage systems are the base of future electric vehicles and also successfully contribute to make hybrid electrical vehicles and plug-in hybrids popular. These systems had already proven their efficacy in the electronic gadgets like laptops, smart phones, etc.

The electrochemical energy storage systems can be broadly classified on the basis of charge storage mechanism into two categories viz. rechargeable battery and supercapacitor. The charge is stored by chemical transformation which takes place by means of oxidation and reduction of electrode materials. Commonly known rechargeable battery systems include lead -acid, nickel-cadmium and lithium-ion battery. Supercapacitor stores charge in the form of double layer on the electrode-electrolyte interface and hence is called electrochemical double layer capacitor (EDLC). These capacitance of EDLC is much higher than electrolytic and solid state capacitors.

Lithium ion battery has high energy density but low power density while supercapacitor has reverse characteristics of high power density and low energy density. There is a demand of a device having high energy density as well as high power density to fulfill the requirements of

many applications. Neither supercapacitor nor lithium ion battery alone can fulfill the requirements. Thus hybridization of lithium ion battery and supercapacitor is required for the same. Figure 1.1 shows ragone plots of different rechargeable batteries and supercapacitor with expected performance area of hybrid of lithium ion battery and supercapacitor denoted as BSH (Battery Supercapacitor Hybrid).
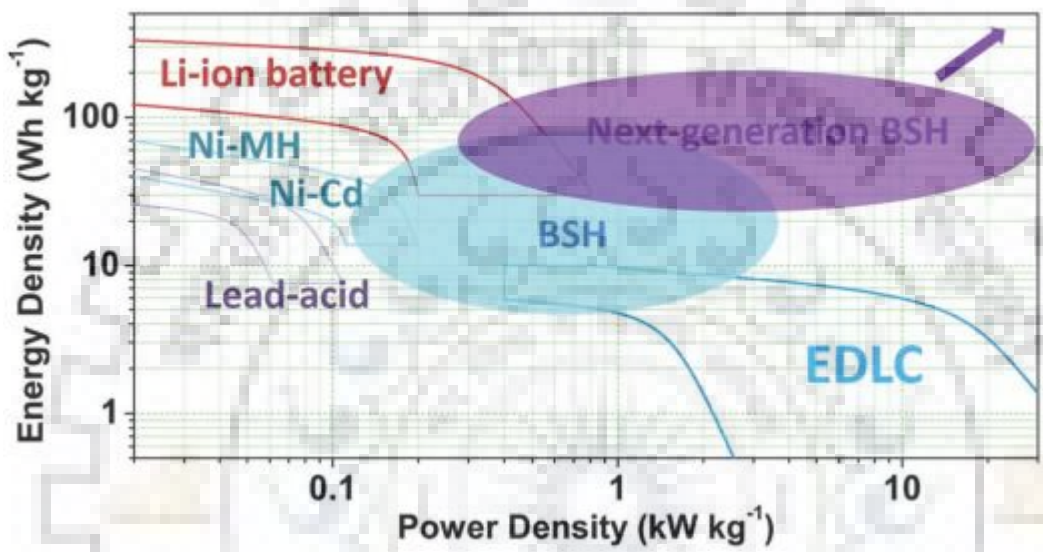
Figure 1.1. Ragone plots of different rechargeable systems (Zuo et al., 2017)

The hybridization of lithium ion battery and supercapacitor can be accomplished in an external manner by connecting the already available lithium ion battery and supercapacitor in either series or parallel configuration. The other approach is the internal connection in which one of the electrodes of supercapacitor is replaced by lithium ion battery electrode. This device is called as asymmetric capacitor or internal series hybrid. In the internal parallel hybrid configuration both the electrodes consist of lithium ion battery material as well as supercapacitor material. This type of electrode consisting of two active materials having different charge storing mechanisms is known as bimaterial electrode. The hybrid systems with only one bimaterial electrode and the other electrode of either lithium ion battery material or supercapacitor material are also categorized under the category of internal parallel hybrid.

The hybridization of supercapacitor with lithium ion battery considering that the high specific power of supercapacitor can be combined with the high specific energy of lithium ion battery has potential to fulfill the current requirements and has become the subject of interest for researchers in energy storage field for the last few decades.

4

The external hybrids (series and parallel) were investigated by many researchers and they have observed that the parallel configuration has the capability to improve the high rate and pulse performance of lithium ion battery due to the reason that the high current pulses are accepted and released by the supercapacitor. The lithium ion battery remains idle during the pulse period which in turn increases the battery life. During the no-pulse period the supercapacitor gets charged by the battery and becomes prepared for the next high current pulse. But the voltage mismatch issues and extra electronic circuitry required for the same escalates the cost and the space occupation of the hybrid system.

In the case of internal hybrids, the series configuration was widely investigated and reported (Duffy, Baldsing, & Pandolfo, 2008; Idota, 1997; Wang & Yoshio, 2006; Wang, Yoshio, Thapa, & Nakamura, 2007; Yuan & Zhang, 2006). This was demonstrated that by replacing one supercapacitor electrode with lithium ion battery electrode the specific energy of the hybrid device can be increased compared to that of supercapacitor with similar electrodes. The specific power of such systems still depend upon the lithium ion battery material and hence the research is now focused on improved battery materials to meet the power requirement. A very few research work is published on internal parallel hybrids (Cericola, Novák, Wokaun, & Kötz, 2011; Lam & Louey, 2006). There are many bimaterial electrode design presented and patented by Bai et al. in 1998 but the only design with intermixing of lithium ion battery and supercapacitor materials is mainly adopted by other researchers so far (Cericola et al., 2011). It is demonstrated that the specific energy provided by the device is greater than that of the supercapacitor alone and the specific power provided is greater than that of the lithium ion battery. The maximum specific energy attained by the internal parallel hybrid of lithium ion battery and supercapacitor is lower than the specific energy of the battery and the maximum specific power attained is lower than the specific power of the supercapacitor. The electrode material components of the hybrid systems are the same as those of individual battery and supercapacitor. Indeed, the hybrid system is a device which can provide moderate specific energy and power.

In this work a different approach is applied in designing the internal parallel hybrid of lithium ion battery and supercapacitor. Instead of replacing one battery electrode with supercapacitor electrode or mixing of battery and supercapacitor materials for making a bimaterial electrode, a three terminal hybrid system is constructed. This hybrid system consists of a bimaterial electrode having battery material and supercapacitor material sharing the common current collector (copper foil) on either sides, an electrode of battery material and an electrode of

supercapacitor material. The first terminal is connected to a bimaterial electrode, the second terminal is connected to a battery material electrode facing battery material of bimaterial electrode and third terminal is connected to a supercapacitor material electrode facing the supercapacitor material of bimaterial electrode. Such arrangement leads to internal parallel hybrid system by shorting the second and third terminals of the system externally through wire.

The performance of any electrochemical device is greatly influenced by the properties of the electrode materials and the electrolyte used. The commercially used anode and cathode materials for lithium ion battery are graphite and lithium cobalt oxide ($LiCoO_2$) respectively with the $LiPF_6$ dissolved in organic solvent as electrolyte. Carbon based materials having high surface area viz. activated carbon, carbon nanotubes, graphene etc. are used as supercapacitor material. A lot of research is ongoing for the last few decades to either improve the properties of existing electrode materials or to prepare new materials which will have better properties than those of conventionally used materials.

Material selection for hybrid of lithium ion battery and supercapacitor plays a very important role to get the desired performance of the device. The battery material chosen for making the bimaterial electrode in this work is spinel lithium titanate, $Li_4Ti_5O_{12}$ (LTO) as this material is considered to be one of the best high rate performance anode materials. The material has the capability to perform well for the future applications such as in electric vehicles and energy storage devices related to natural energy sources like sunlight and wind. The LTO based electrode charges and discharges at a flat plateau of around 1.55 V vs. Li^+/Li which is quite above the reduction potential of commonly used electrolyte and hence electrolyte decomposition and metal deposition is avoided which can create short circuiting. An important property of LTO is structural stability while charging and discharging. There is negligibly small change in volume with lithium insertion and de-insertion. All the above properties made this material very safe with long cycle life. The theoretical specific capacity of LTO is 175 $mAhg^{-1}$ which is quite low compared to other type of anode materials. However, LTO has an advantage over other materials in terms of the safety features and long cycle life. The other drawbacks of LTO are its poor electrical conductivity and low lithium ion diffusion coefficient which can be improved.

Efforts were made by the researchers to improve the properties of LTO by reducing the particle size, developing porous structure, carbon coating, doping, synthesis in reducing atmosphere etc. (Gu, Guo, & Liu, 2014; Shao, He, Luo, & Liu, 2012; Wolfenstine & Allen, 2008; Yi et al., 2010a). The LTO with improved properties has not been used in internal parallel hybrid of lithium ion battery and supercapacitor, so far, by researchers.

The aim of the thesis is to study the performance of the proposed hybrid system using LTO with improved properties. The activated carbon is used as supercapacitor material. Two different methods are adopted to improve the properties of LTO. First is the development of nanoporous LTO using carbon nanobeads as template with a target to achieve the pore size less than 100nm which is not reported so far to the best of the author's knowledge. Second is the synthesis of vanadium doped LTO with the aim to enhance the electronic conductivity and lithium ion diffusivity in the LTO material. Lastly hybrid configuration were made separately with LTO and modified LTO viz. nanoporous LTO and vanadium doped LTO to study their relative performance in electrochemical behaviour.

Literature Review

LITERATURE REVIEW

This chapter describes the properties and applications of lithium ion battery as an important device for energy storage. Influence of different materials as basic components of lithium ion battery viz. cathode, electrolyte and anode on battery performance is explained. The chosen anode material LTO is explored in terms of its properties and limitations. A review on the efforts done by the researchers to overcome the limitations of LTO so that its electrochemical performance can be enhanced as anode material of lithium ion battery is presented. Supercapacitor as another important energy storage device is described. The need of hybridization to overcome limitations of lithium ion battery and supercapacitor is discussed and different configurations of possible hybrid systems are explained. The problem formulation for thesis and scope of the research work are described.

2.1 Lithium Ion Battery

Lithium ion battery is an important energy storage device. It has been considered as one of the most promising power sources for various applications like mobile phones, laptops and other electronic gadgets. The following are the characteristics of the lithium ion battery.

(i)   It is very light and smaller in size compared to traditional batteries viz. lead-acid battery, nickel-cadmium etc.

(ii)   It has very low rate of self-discharge and therefore has long standby time.

(iii)   It has a large working temperature range (0 to 45°C).

Thus, it has gained a lot of commercial interest.

Lithium ion battery is characterized by a high specific energy up to 200 Wh/kg and low specific power which is less than 1KW/Kg. As far as electric and hybrid vehicles are concerned, lithium ion battery is still in developing stage and require more investment on research and development to become the efficient power storage for the future market of electric and hybrid vehicles. The major issues are cost, safety, energy, power and cycle life in the successful adoption of the lithium ion battery technology for transportation and stationary electrical energy storage, and these parameters are in turn depend on the materials used in electrolyte and electrodes i.e.

anode and cathode which are the basic components of lithium ion battery (Goodenough & Kim, 2010).

2.1.1 Principle of operation

Lithium-ion battery is constructively a two electrode device in which electrodes are electronically isolated with the help of separator and ionically connected by means of a medium called electrolyte. The electrolyte consists of an electrolytic solution of lithium salt dissolved in a non-aqueous solvent. The two electrodes are distinguished as cathode or anode depending upon which electrode acts as a source of lithium ions and which one acts as a sink. While charging, cathode becomes the source of lithium ions and releases them and anode becomes the sink and stores them. On discharging, anode releases the lithium ions and cathode takes them back. The direction of the flow of electrons i.e. current in the outer circuit and lithium ion movement inside the battery is shown in Figure 2.1.
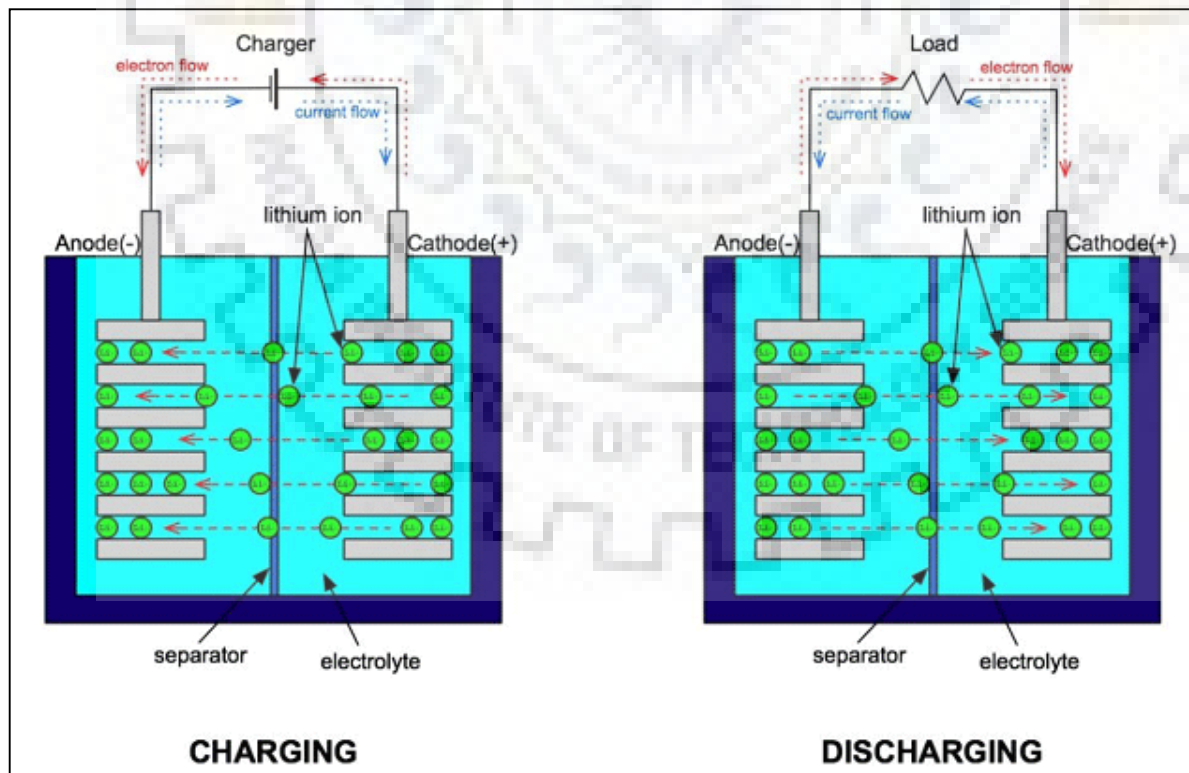
Figure 2.1. Charging- discharging mechanisms of lithium ion battery

The electrode material of lithium ion battery must have intercalation-deintercalation characteristics implying that they must be capable of incorporating lithium ion reversibly within their crystal structure (Winter, Besenhard, Spahr, & Novák, 1998). In this process, the rate at which the lithium ions intercalate or deintercalate into the cathode and anode significantly influences on the battery performance.

The lithium metal is very unsafe to be used as electrode inside the cell as it can create short circuiting easily. In case of other electrode materials having intercalation properties the small lithium ions reside within the crystal structure. The overall chemical reaction followed in charge and discharge of the cell considering $LiCoO_2$ as cathode and graphite as anode is shown below:

$$LiCoO_2 + 6C \longleftrightarrow Li_{(1-x)}CoO_2 + Li_xC_6 \qquad\qquad .... (2.1)$$

The charge reaction proceeds towards right and discharge proceeds towards left side (Kalhammer et al. 1995). During charging, the lithium ions move out from the $LiCoO_2$ and travel towards carbon which stores them inside it (for $x = 1$). In reality, all the ions are not transported back and forth i.e. $0 < x < 1$.

2.1.2 Components

2.1.2.1 Cathode

A cathode is a positive electrode of an electrochemical system in which reduction takes place during the electrochemical discharging process of the battery. Cathode materials are typically oxides of the transition metals which undergo changes to higher oxidation states during delithiation. Mizushima et al. first demonstrated $LiCoO_2$ as cathode material for rechargeable lithium battery and is the most dominant material of this class (Mizushima et al, 1980). Sony Corporation successfully introduced $LiCoO_2$ in 1991 to market and since then it has been used in the small electronic devices (Nishi et al, 1990). The material $LiCoO_2$ has good electrochemical stability which results in long cyclability. But the limited availability of Co makes the $LiCoO_2$ material expensive, moreover Co is toxic which creates environmental problem. Therefore the research has focused from $LiCoO_2$ to its derivatives which replace the Co ion partially or fully to nontoxic and high abundant metal ions in the structure. In this respect the materials

$LiNi_{0.5}Mn_{0.5}O_2$ and $LiCo_{1/3}Ni_{1/3}Mn_{1/3}O_2$ were proposed to have good Li-ion storage capacity. Ohzuku et al initially reported the electrochemical performance of $LiNi_{0.5}Mn_{0.5}O_2$ (Ohzuku et al, 2001). The material system $LiCo_{1/3}Ni_{1/3}Mn_{1/3}O_2$ exhibits high discharge capacity, high thermal stability and good cyclability. Thackeray et al. proposed an integrated composite having layer by layer like structure $xLi_2MO_3-(1-x)LiMn_{0.33}Co_{0.33}Ni_{0.33}O_2$ (for M = Co, Mn, Ni) as another high potential (>3V) cathode materials which shows superior performance with structural stability and outcastes the cathode materials currently used (Rossouw, M. H. and Thackeray, 1991). Sagar Mitra et al. investigated $0.7Li_2MnO_3-0.3LiMn_{0.33}Co_{0.33}Ni_{0.33}O_2$ composite and achieved relatively more stable reversible capacity of about 192 $mAhg^{-1}$ by cycling at C/10 rate after stabilization of Li_2MnO_3 at 20°C (Rajarathinam, Mitra, & Petla, 2013). The microemulsion synthesis of $LiCo_{1/3}Ni_{1/3}Mn_{1/3}O_2$ composites shows excellent electrochemical reversibility as cathode material. In this technique, well crystallized nanoparticles (size ~ 45 nm) of $LiCo_{1/3}Ni_{1/3}Mn_{1/3}O_2$ were synthesized at low temperature. The $LiCo_{1/3}Ni_{1/3}Mn_{1/3}O_2$ cathode electrode exhibits a discharge capacity of 198 $mAhg^{-1}$ when charging and discharging is done in between 2.5 V and 4.6 V.

The spinel $LiMn_2O_4$ is another promising cathode material for Li-ion battery and was first purposed by the Thackeray et al in 1983 (Thackeray et al, 1983). The olivine structure $LiMPO_4$ can be formed with M as transition metal ions such as Mn, Co, Ni and Fe. The redox potentials of $LiMnPO_4$, $LiCoPO_4$ and $LiNiPO_4$ are 4.1, 4.8 and 5.1V respectively which are higher than $LiFePO_4$ (3.4 V) (Xu et al, 2012). West et al. investigated $Li_2FeMn_3O_8$ as novel 5V spinel cathode for lithium ion battery (Kawai, Nagata, Tabuchi, Tukamoto, & West, 1998). The olivine structured $LiFePO_4$ has gained the intense attention as a potential cathode material. The material $LiFePO_4$ is very near to an ideal cathode material having high theoretical discharge capacity of 170 mAh/g, moderate discharge potential 3.4 V (vs Li_+/Li), excellent thermal stability at charged and discharge state, lower cost, environment friendly, high cyclability and flat discharge voltage plateau. The low electronic conductivity of $LiFePO_4$ can be enhanced by carbon coating and doping. S. Ghosh et al. has developed the ZnO doped $LiFePO_4/C$ composite with functionalized surface as cathode of lithium ion battery (Saroha, Panwar, Sharma, Tyagi, & Ghosh, 2017). Muldar et.al demonstrated template based 3D structure of $LiFePO_4$ for high rate performance as cathode of lithium ion battery (Singh et al. 2013).

2.1.2.2 Electrolyte

Electrolyte is very important part of lithium ion battery or any other electrochemical device as it is the medium through which electrodes are ionically connected and electronically isolated. The properties of an electrolyte highly influence the performance of the device. Following are some of the basic requirements for an electrolyte of lithium ion battery:

(i)   Ionic conductivity should be high.

(ii)   Chemical stability against decomposition with reducing anode and oxidizing cathode.

(iii)   Electrochemical stability for high cell voltages.

(iv)   Thermal stability for proper functioning of the device at required temperatures.

(v)   Low cost and nontoxic.

(vi)   In case of solid electrolytes mechanical strength should be high.

The commonly used lithium salts are $LiClO_4$, $LiAsF_6$ and $LiPF_6$ dissolved in organic liquids. Polymer based electrolytes are also developed for lithium ion battery. Solid polymer electrolytes are having good mechanical strength but low ionic conductivity and gel polymer electrolytes have good ionic conductivity and low mechanical strength (Armand, 1994). Solid oxide electrolytes of wide varieties are used in solid oxide fuel cells. S. Ghosh et al. presented a review on low temperature solid oxide electrolytes (Singh, Ghosh, Aich, & Roy, 2017).

2.1.2.3 Anode

The anode is known as the negative electrode of the battery because while charging it is connected to negative terminal of the electrical source to attract lithium ions and stores them into the structure. The lithium ions get stored by means of chemical reaction called oxidation. The amount of lithium ions gets stored is decided by the specific capacity of the electrode material and is expressed in terms of $mAhg^{-1}$. Different materials have different specific capacities and higher capacity is desirable. But there are many other features which have to be considered for selecting the material as anode viz. safety, cyclability, lithium ion diffusion rate, self-leakage etc. There is always a trade-off between the features depending upon the application. In this section different anode materials are discussed which are categorized into three types on the basis of lithium ion storage mechanism. These are the following:

(i)   Intercalation/de-intercalation materials

(ii)   Alloy/de-alloy materials and

(iii)   Conversion materials

A brief and systematic comparison of above mentioned categories is done by (Goriparti et al., 2014) and is represented in Table 2.1. The intercalation/de-intercalation materials include carbonaceous (hard carbons, CNTs, graphene) and titanium oxides (TiO_2, $Li_4Ti_5O_{12}$) Alloy/de-alloy materials include silicon, germanium, tin, antimony, tin oxide and SiO_2. The conversion materials include metal oxides viz. Fe_2O_3, Fe_3O_4, Cu_2O, RuO_2 etc., metal phosphides/sulphides/nitrides viz. M_xX_y where M=Fe, Mn, Ni and Cu; X= P, S and N. The all above mentioned materials are compared for their theoretical discharge capacity, advantages and the common issues involved.

Table 2.1: Most common anode materials used for lithium ion batteries. (Goriparti et al., 2014)

Active anode material	Theoretical capacity (mAh g^{-1})	Advantages	Common Issues
Insertion/de-insertion materials			
A. Carbonaceous			
a) Hard carbons	200-600	Good working potential	Low Columbic efficiency
b) CNTS	1116	Low cost	High voltage hysteresis
c) Graphene	780/1116	Good safety	High irreversible capacity
B. Titanium oxides			
a) $Li_4Ti_5O_{12}$	175	Extreme safety	Very low capacity
b) TiO_2	330	Good cycle life	Low energy density
Low cost			
High power capability			
Alloy/de-alloy materials			
a. Silicon	4212	Higher specific capacities	Large irreversible capacity
b. Germanium	1624	High energy density	Huge capacity fading
c. Tin	993	Good safety	Poor cycling
d. Antimony	660		
e. Tin oxide	790		
f. SiO_2	1600		
Conversion materials			
a. Metal oxides	500-1200	High capacity	Low coulombic efficiency

16

Fe$_2$O$_3$, Fe$_3$O$_4$, CoO ,Co$_3$O$_4$, Mn$_x$O$_y$, Cu$_2$O/CuO, NiO, Cr$_2$O$_3$, RuO$_2$, MoO$_2$/MoO$_3$ etc.		High energy Low cost Environmental-compatibility	Unstable SEI formation Large potential hysteresis Poor cycle life
b. Metal phosphides /sulfides/nitrides (M$_x$X$_y$; M = Fe, Mn, Ni, Cu, Co etc. and X = P, S, N)	500-1800	High specific capacity Low operation potential and Low polarization than counter oxides	Poor capacity retention Short cycle life High cost of production

2.1.3 Carbonaceous materials

The anode of commercially used lithium ion battery is graphite based which has the specific capacity of 372 mAhg^{-1} and operating potential < 0.1 volt. The solid electrolyte interface (SEI) layer formed on the interface of graphite and electrolyte reduces reversible capacity of graphite and upon lithiation, its operating potential approaches to that of lithium metal (Zhang, 2006). This can cause lithium plating and dendrite formation leading to short circuiting. Also there is a volume expansion in the graphite electrode as the interplanar distance increases from 3.35Å to 3.70Å upon lithiation (Song & Kinoshita, 1996). Due to these safety issues researchers are on continuous search of developing alternative anode materials. S. Bandyopadhyay et al. reviewed electrical and mechanical properties of graphite in detail (Sengupta, Bhattacharya, Bandyopadhyay, & Bhowmick, 2011). The carbon nanotubes (CNT) and grapheme are much better options than graphite in terms of safety and reversible capacity.

2.1.4 Alloy/de-alloy materials

Several lithium alloy anode materials Li$_x$M$_y$ have attracted much attention due to their high capacity. A few examples of such materials are Li$_{3.75}$Si (3578mAh/g) (Ng et al., 2006), Li$_{3.75}$Ge (1385mAh/g) (Yoon, Park, & Sohn, 2008), Li$_{4.4}$Sn (993mAh/g) (Idota, 1997) and Li$_3$Sb (660mAh/g) (Yang, Takeda, Imanishi, & Yamamoto, 1999). Also a few alloys have operating voltage above reduction potential of electrolyte which avoids lithium plating (SEI formation), ensuring the enhancement in the safety. One of the major issues with the alloy anodes is the severe capacity fading with the number of cycles which arises due to a large change in volume occurs during the charging and discharging (lithium alloying/de-alloying) process. This large volume change creates the lattice stress which can cause cracks and crumbs in the alloy particles.

The degradation during cycling results in rapid loss of capacity in just a few cycles of charge and discharge.

Figure 2.2 shows an illustration of active anode materials in terms of its intercalation potential and specific capacity. Titanium oxides have potential well above reduction potential of electrolyte and has low specific capacity. LTO with the spinel structure has emerged as an attractive alternative as its operating voltage of 1.55 V versus Li/Li$^+$ is quite high to prevent the formation of SEI layer with the electrolyte and hence very safe anode material (Ferg, Gummow, & Kock, 1994; Reale et al., 2004). Due to its safety features it has become one of the most promising anode materials for large scale applications of lithium ion battery like electric vehicles and renewable energy storage devices.
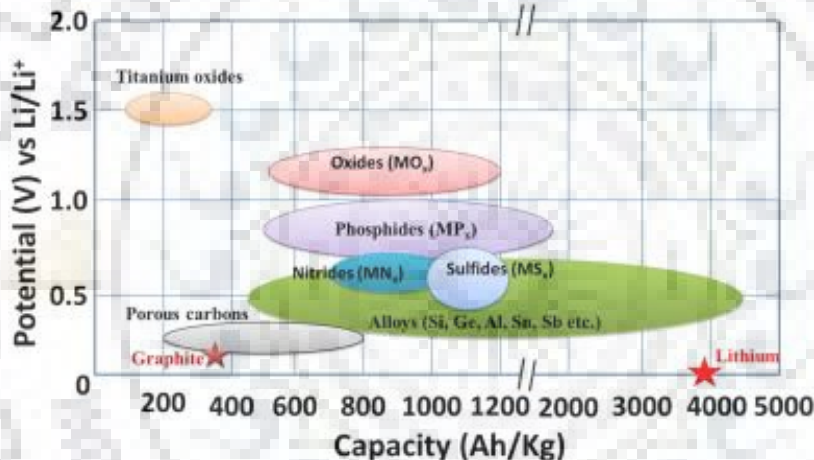
Figure 2.2. Intercalation potential (w.r.t. Li/Li$^+$) and the corresponding capacity of different anode materials (Goriparti et al., 2014)

2.1.5 LTO

2.1.5.1 History of LTO

LTO was first reported in 1956 by Jonker. LTO is also reported as $Li_{4/3}Ti_{5/3}O_4$ and $Li_{1.33}Ti_{1.67}O_4$. The stoichiometric formula with site occupancies will be $[Li]_{8a}[Li_{1/3}Ti_{5/3}]_{16d}[O_4]_{32e}$. LTO has a spinel structure according to the chemical formula AB_2O_4, where the array of oxygen ions in a cubically closed packing (ccp) occupies the 32e sites. The two types of interstitial sites viz. tetrahedral (8a, 8b, 48c) and octahedral (16c, 16d) are partially occupied by the cations A and B. A.R. West et al. described lithium conduction pathways in complex spinels (Reeves-Mclaren, Smith, & West, 2011).

LTO is an important family member of $Li_{3+x}Ti_{6-x}O_{12}$ (for $0 < x < 1$), which was initially known among researchers for its superconductivity property. $LiTi_2O_4$ belongs to $Li_{3+x}Ti_{6-x}O_{12}$ (for $x = 0$) and exhibits superconductivity at temperatures below 10 K (Johnston, Prakash, & Zachariasen, 1973; Moshopoulou, 1999). LTO which also belongs to $Li_{3+x}Ti_{6-x}O_{12}$ (for $x = 1$), has the characteristics of semiconductor at liquid helium temperatures (Chen, Spears, Wondre, & Ryan, 2003). The capability for intercalation of Li ion inside the LTO material was first reported by Murphy et al. (Murphy, Cava, Zahurak, & Santoro, 1983). Colbow et al. were the first to perform the galvanostatic charge–discharge test of LTO material in a half-cell with lithium as counter electrode in 1989. They observed that LTO exhibits a flat plateau in its discharging profile and its cyclic performance is quite stable up to 100 cycles (Colbow, Dahn, & Haering, 1989).

2.1.5.2 Structure and properties of LTO

In 1971, Deschanvres et al. reported first time the single crystal based detailed structural analysis of LTO (Deschanvres et al. 1971). In LTO the tetrahedral 8a sites are occupied only by Li^+ ions, while the octahedral 16d sites are randomly occupied by 1/6 Li^+ ions and 5/6 Ti^{4+} ions as shown in Figure 2.3 (a)
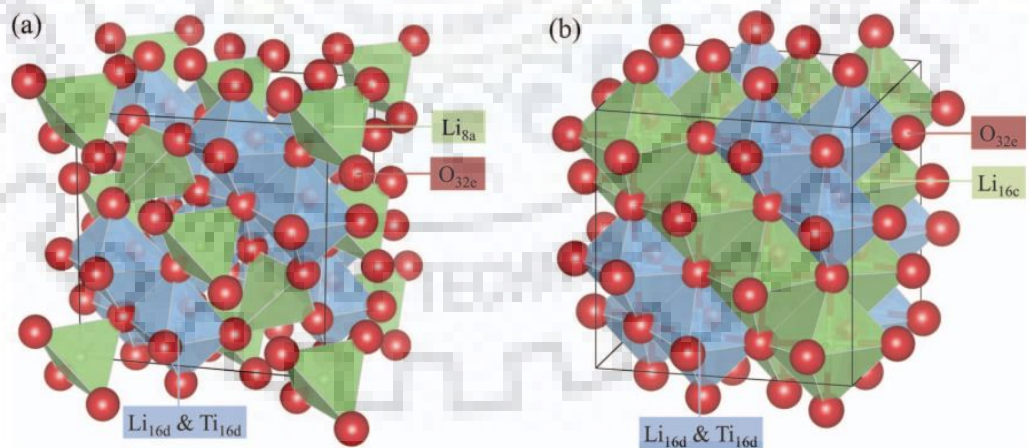
Figure 2.3. Unit cells of the (a) $Li_4Ti_5O_{12}$ and (b) $Li_7Ti_5O_{12}$ phases (Tsai, Hsu, & Lin, 2014)

Green tetrahedrons	---	Li ions at the 8a site,
Green octahedrons	---	Li ions at the 16c site,
Blue octahedrons	---	Li and Ti ions at the 16d site and
Red spheres	---	O ions at the 32e site.

The basic crystal structure of LTO is a cubic spinel with an Fd3m space group and a unit cell parameter reported to be between $a = 8.352$ and 8.370 Å (Harrison et al. 1984; Ohzuku et al. 1995; Mosa et al. 2012) Lithium reacts with $Li_4Ti_5O_{12}$ according to the reaction

$$Li_4Ti_5O_{12} + 3Li + 3e \rightarrow Li_7Ti_5O_{12} \qquad \qquad \text{... Eq. 2.1}$$

The Li^+ inserted to the structure of LTO while charging of LTO based lithium ion battery and resides at 16c octahedral sites. The Li^+ already resides at 8a tetrahedral sites also moves to 16c sites leaving 8a sites empty (Safronov et al. 2012; Scharner et al. 1999). This phenomenon is accompanied by a progressive phase transition from a spinel to a rock salt type structure as shown in Figure 2.3.

LTO spinel has a potential to be used anode material in lithium ion battery due to its unique features like very flat plateau and no SEI formation at interface with electrolyte (Gao, Jiang, Ying, & Wan, 2006). LTO is a zero strain material. It exhibits negligible increase in unit cell volume during charge-discharge processes (Ohzuku, Ueda & Yamamota, 1995). This material has a theoretical specific capacity of 175 $mAhg^{-1}$ and exhibits a practical specific capacity at maximum 160 $mAhg^{-1}$ after 100 deep discharge cycles.

2.1.5.3 Synthesis methods of LTO

Solid-state synthesis of LTO is normally conducted by mixing of solid raw materials using ball milling and then the mixtures are calcined at high temperature. The precursors commonly used are lithium carbonate Li_2CO_3 and TiO_2. A lot of researchers follow this route because of the simplicity of this method. The disadvantages of the solid state reaction method is long heating time, several intermediate grinding steps, irregular morphology, wide particle size range, agglomeration and inhomogeneous composition. Scharner et al. synthesized LTO using Li_2CO_3 and TiO_2 as precursors by solid state process (Scharner et al. 1999). Lu et al. synthesized LTO by a solid-state reaction with anatase TiO_2 and Li_2CO_3 at 800°C (Lu, Belharouak, Liu, & Amine, 2007).

Sol-gel process is a wet-chemical technique widely used in the fields of materials science and ceramic engineering. A colloidal suspension (sol) acts as the precursor for an integrated network (or gel) of either discrete particles or polymeric structures. Typical precursors are metal alkoxides, metal salts (such as chlorides and acetates), and organic metal compounds which

undergo various forms of hydrolysis and polycondensation reactions. Bach et al. first applied a sol–gel process to the preparation of LTO; they conducted the synthesis in a non-aqueous medium with lithium acetate and titanium (IV) isopropoxide (TTIP) as the raw materials (Bach, 1999). Hao et al. applied triethanolamine (TEA) and citric acid (CA) as complexing agents for the titanium ion during the sol–gel synthesis of LTO using tetrabutyl (ortho) titanate as the titanium source (Hao, T, Xu, Liu, & Ji, 2005). Venkateswarlu et al. successfully prepared high-purity nanosized $Li_4Ti_5O_{12}$ with a crystal size of 39 nm, using a sol–gel process after further calcination at 800°C for 12 h with TTIP and lithium acetate dihydrate as the raw materials (Venkateswarlu et al., 2005). A. Garg et al. successfully synthesized thin films and doped ceramics using sol-gel process (Sharma et al. 2017; Garg et al. 2007).

Hydrothermal synthesis is autoclave based process under controlled temperature and/or pressure in which the reaction with water takes place further followed by calcination. J. Chen et al. synthesized hierarchical mesoporous nest-like LTO preparation by hydrothermal reaction of LiOH with water-soluble titanium complex $[NH_4^+]_4[H^+]_2[Ti_4(C_2H_2O_3)_4(C_2H_3O_3)_2(O_2)_4O_2]^{6-}$. Surfactant CTAB was employed as the template to obtain this hierarchical structure (Chen, Yang, Fang, Hirano, & Tachibana, 2012). J. Liu et al. reported microwave-assisted hydrothermal synthesis of LTO nanoparticles and nanoflower like structure. The precursors used are LiOH, H_2O_2 and titanium tetra iso-propoxide. The heat treatment was done at 130 and 170°C in the autoclave (Liu et al., 2012).

Solvothermal method uses nonaqueous solvent. The difference between solvothermal and hydrothermal method is that in solvothermal process instead of water other solvent is used in the preparation process. Since a variety of organic solvents with high boiling points can be selected by using solvothermal method, the temperature can be elevated much higher than that in hydrothermal method. Lim et al. synthesized nanoparticles of LTO adopting solvothermal route. The precursors used were LiOH, TTIP and $(HOCH_2CH_2)_2O$ in polyol medium (Lim et al., 2011).

Sonochemical synthesis is performed inside an ice bath using ultrasonication apparatus. The solution prepared by mixing of precursors in a solvent goes through sonication operation followed by calcination process after drying into powder form. S. Mitra et al. reported

sonochemical synthesis of phase-pure LTO anode along with its electrochemical performance for the first time (Ghosh, Mitra, & Barpanda, 2016).

Spray Drying technique is a direct process which develops ceramic powders directly from solutions/slurries. In this process decomposition of precursor molecules is occurred at a high temperature.
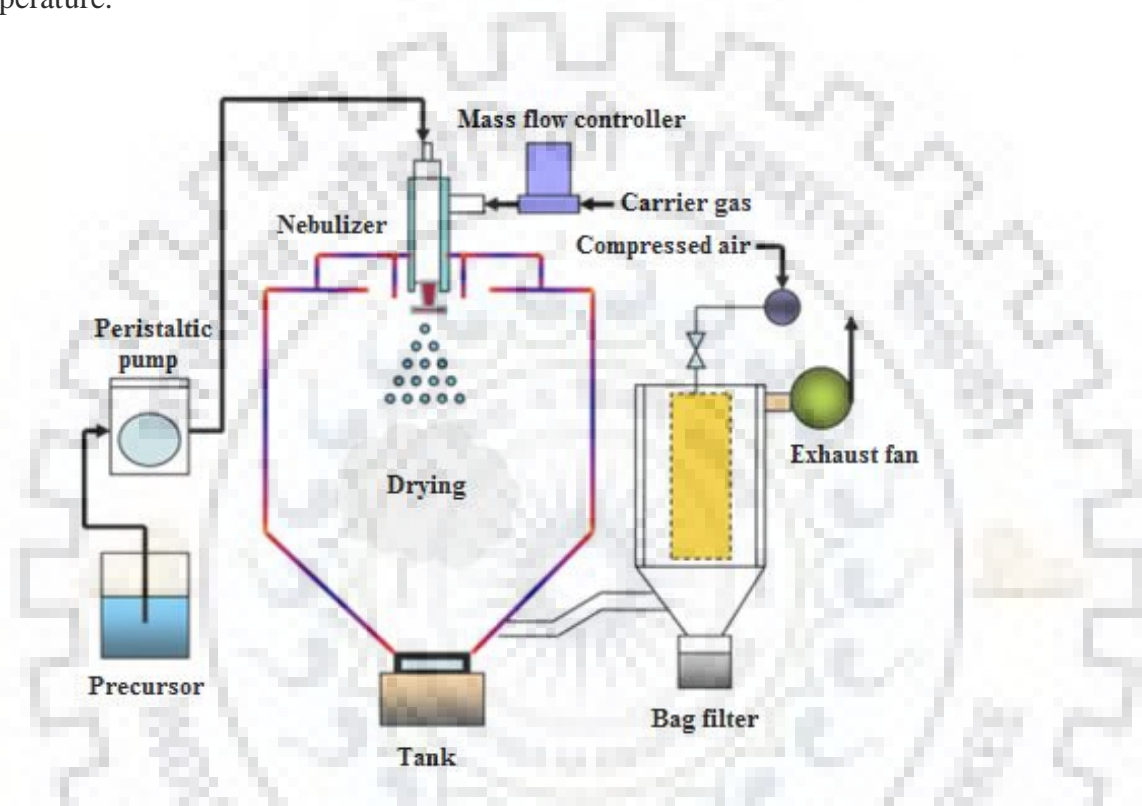
Figure 2.4. Block diagram representation of spray drying process (Hsiao, Liao, & Chen, 2008)

A typical block diagram representing the spray drying process is shown in Figure 2.4. Z. Wen et al. synthesized spherical LTO powder which are porous in nature following spray drying process using Li_2CO_3 and rutile TiO_2 as precursors and PVB as forming agent of pores (Wen et al., 2005). Hsiao et al. synthesized porous as well as dense $Li_4Ti_5O_{12}$ powders following spray drying precursor slurries of the LiOH and TiO_2 particles (Hsiao et al., 2008).

Most of the researchers have reported the synthesis of LTO using solid state method as it is comparatively easy and cost effective method than other synthesis methods. However, A. Mahmoud et al. compared three different synthesis methods viz. solid state, self-combustion and

sol-gel. He found that sol-gel is the best synthesis method for optimum performance of LTO as anode material of lithium ion battery (Mahmoud, Amarilla, Lasri, & Saadoune, 2013).

2.1.5.4 Limitations of LTO

LTO has empty Ti 3d-states in its electronic structure and is characterized by an energy band gap of 2 to 3 eV which give rise to an insulating behavior of this material (Ouyang, Zhong, & Lei, 2007). Poor electronic and ionic conductivity limit its high rate-capability.

2.1.5.5 Efforts to overcome the limitations

To overcome these limitations a lot of efforts including reduction in particle size (Gu et al., 2014), preparing the material in nanoporous form (Shao et al., 2012) , carbon coating (Hu, Lin, Yang, Huai, & Deng, 2011), doping of alkali and alkaline earth metals ions (Zhang et al. 2013; Chen et al. 2001), doping of transition metal ions having higher valency than Ti (4+) (Wolfenstine & Allen, 2008; Yi et al., 2009, 2010a) and synthesis in oxygen deficient atmosphere (Song et al., 2014; Wolfenstine, Lee, & Allen, 2006) were made by researchers. F. M. Mulder et al. described impact of particle size on the properties of lithium inserted material (Shen, Chen, Klaver, Mulder, & Wagemaker, 2014). LTO synthesis in oxygen deficient atmosphere leads to re-oxidation over time if the material is maintained in air and consequently its performance degrades. H. Song et al. suggested doping as a solution to resist re-oxidation for LTO synthesized in reducing atmosphere.

2.1.6 Porous LTO

The functionality of lithium ion battery depends upon intercalation phenomenon of Li^+ ions inside the electrode materials which causes volume expansion and contraction. This cyclic volume changes damage the morphology of the electrode and hence the performance of the battery degrades. In Figure 2.4, four different types of electrode materials with the effect of intercalation phenomenon on morphology are shown. Thin films and particles got cracked, wire array got disturbed. Zangari et al. performs electrochemical characterization of nanoporous film (Rouya, Cattarin, Reed, Kelly, & Zangari, 2012) . Open pores allow better accommodation for the volume changes without causing performance deterioration than solid non-porous materials. Porous materials can quickly store large numbers of Li^+ ions due to large surface area and short

Li^+ diffusion path lengths. Porous materials can be used as a template for the production of nanometer-sized arrays (Zangari & Lambeth, 1994).
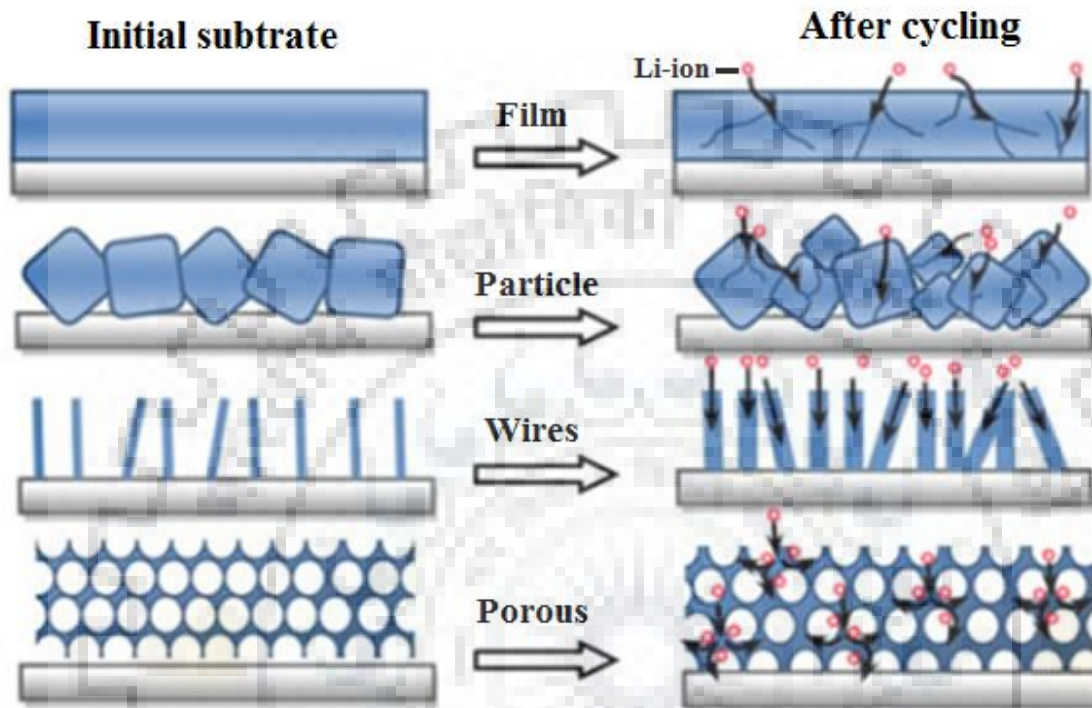
Figure 2.4. Schematic of morphological changes and electron transport that occur in anode material during electrochemical cycling (Shao et al., 2012)

Attempts were made to make $Li_4Ti_5O_{12}$ porous (as well as mesoporous), few of which are described below:

- Shao et al. reports the synthesis of nanoporous LTO by sol–gel method using polystyrene spheres as templates (Shao et al., 2012).
- Y. Lv et al. reports phenol–formaldehyde resin-assisted synthesis of pure porous LTO (Lv, Zhang, Cao, Wang, & Wang, 2011).
- K.-C. Hsiao et al. reports porous LTO powders fabricated by spray drying process (Hsiao et al., 2008).
- Sorensen et al. reports synthesis of three-dimensionally ordered macroporous LTO (Sorensen et al., 2006).

2.1.7 Doped LTO

One of the most effective method to improve poor electronic and ionic conductivity of LTO is doping with highly conductive metal ions or doping of ions having higher oxidation states. The doping of element with 5+ oxidation state will increase the electronic concentration and hence increase the electronic conductivity. Thakur et al. describes the structural and electrical properties of Nb^{5+} substituted PZT ceramics (Thakur & Prakash, 2009). Effect on dielectric properties by doping and effect of preparative parameters on electrical conduction are investigated by P. Gopalan et al. (Bobade, Gulwade, Kulkarni, & Gopalan, 2005; Gopalan, Bhandari, Kulkarni, & Palkar, 2002) Improvement in conductivity of LTO by doping with various cations viz. Mg^{2+}, Al^{3+}, Cr^{3+}, Co^{3+}, Fe^{3+}, Ga^{3+}, Mn^{3+}, Ni^{3+}, Mo^{4+}, Zr^{4+}, V^{5+} and Ta^{5+} in Li or Ti site has been reported as shown in Table 2.2. Incorporation of high electronic conductivity phase in LTO also effectively increase its conductivity. The improvement in electrochemical performance of LTO material by doping can be attributed to the microstructural changes occurred by the dopant in the LTO (Song et al., 2014).

Table 2.2. **Doping of LTO with different cations** (Yi et al., 2010b)

Samples	Doped Cation/Anion	Method of synthesis	Electrochemical performance
$Li_{4-x}Mg_xTi_5O_{12}$ (Chen et al., 2001)	Mg^{2+}	Solid State	Increase the conductivity up to 10^{-2} Scm^{-1}. $Li_{4-x}Mg_xTi_5O_{12}$ (for x=0.25) shows discharge capacity of 135mAhg^{-1} at 0.5C rate and 63 mAhg^{-1} at 17C rate.
$Li_{1.3}Ni_{0.1}Ti_{1.6}O_4$ (Robertson, Trevino, Tukamoto, & Irvine, 1999)	Ni^{3+}	Solid State	$Li_{1.3}Ni_{0.1}Ti_{1.6}O_4$ shows high discharge capacity up to 15 cycles compared to LTO at 0.1C rate but due to continuous capacity fading the performance degrades.
$Li_{4-x}Al_xTi_5O_{12}$ (x = 0, 0.05, 0.1 and 0.2) (Zhao et al., 2008)	Al^{3+}	Solid State	Doping of Al decreases the discharge capacity of LTO but enhances the high rate performance. The fading in capacity at 3C rate is controlled by Al

			doping and cycling stability is enhanced.
$Li_{(4-x)/3}Ti_{(5-2x)/3}Cr_xO_4$ (Martın, Lo, Pico, & Veiga, 2007)	Cr^{3+}	Ceramic technique	$Li_{(4-x)/3}Ti_{(5-2x)/3}Cr_xO_4$ with (x=0.7) shows highest discharge capacity which corresponds to the similar contribution of electronic and ionic conductivity to the total electrical conductivity.
$Li_{3.967}M_{0.1}Ti_{4.933}O_{12}$ (M=Mn, Ni, Co) and $Li_{(4-x/3)}Cr_xTi_{(5-2x/3)}O_{12}$(x=0.1, 0.3, 0.6, 0.9, 1.5) (Hao, Lai, & Lu, 2007)	Co^{3+}, Ni^{3+}, Cr^{3+}, Mn^{3+}	Sol-gel	The doping of Mn^{3+}, Ni^{3+} and Cr^{3+} increase the capacity of LTO. The doping of Co^{3+} decrease the initial capacity of LTO. $Li_{3.967}Mn_{0.1}Ti_{4.933}O_{12}$ has the highest initial discharge capacity and is maintained even after 30 cycles. Improvement in reversible capacity as well as cyclic stability of LTO can be achieved by doping of Cr^{3+} in appropriate amount.
$Li_{3.95}M_{0.15}Ti_{4.9}O_{12}$ (M = Al, Ca,Co) and $Li_{3.9}Mg_{0.1}Al_{0.15}Ti_{4.85}O_{12}$ (Huang, Wen, Zhu, & Lin, 2007)	Mg^{2+}, Ca^{3+}, Co^{3+}, Al^{3+}	Solid State	Doping of Al^{3+} and Mg^{2+} contributes to the increase in electronic conductivity of LTO while Co^{3+}, Ga^{3+} dopants doesn't. Al^{3+} substantially enhances the reversible capacity. Doping with Ga^{3+} increase the discharge capacity but with the capacity fading. Electrochemical performance of LTO is degraded by Co^{3+} and Mg^{2+} dopants.
$Li_4Ti_{5-x}Zr_xO_{12}$ (x = 0, 0.05, 0.1 and 0.2) (Li, Qu, & Yu, 2009)	Zr^{4+}	Solid State	High rate capability of LTO is enhanced by Zr^{4+} doping although at low C rates viz. 0.5C and 1C the doped LTO exhibits low discharge

			capacity compared to undoped LTO. $Li_4Ti_{4.9}Zr_{0.1}O_{12}$ shows superior performance among all the doped samples.
$Li_4Ti_{5-x}Mo_xO_{12}$ $(0.5< x <1.5)$ (Zhong, 2007)	Mo^{4+}	Pechini method	The reduction of LTO band gap by doping with Mo^{4+} at Ti site improves its electronic conductivity and hence the electrochemical performance of the Mo doped LTO material in Li-ion battery and EDLC is enhanced.
$Li_4Ti_{5-x}V_xO_{12}$ $(0< x <0.3)$ (Yi et al., 2009)	V^{5+}	Solid State	The discharge capacity of $Li_4Ti_{4.9}V_{0.1}O_{12}$ is highest among all prepared doped LTO samples in the potential window 0-2V. The discharge capacity of 229 $mAhg^{-1}$ is retained even after 130 cycles. V^{5+} doping enhances the structural stability such that the reversible capacity of LTO is not affected much by the deep discharge up to 0 Volts. Based on the cycling performance, higher discharge capacity with simplest and low cost synthesis route the $Li_4Ti_{4.9}V_{0.1}O_{12}$ is expected to serve better in commercial application.
$Li_4Ti_{4.95}Ta_{0.05}O_{12}$ (Wolfenstine & Allen, 2008)	Ta^{5+}	Solid State	Undoped LTO and $Li_4Ti_{4.95}Ta_{0.05}O_{12}$ shows similar ionic conductivity when calcined in the same oxidizing atmosphere. In case of calcination done in a reducing atmosphere LTO and $Li_4Ti_{4.95}Ta_{0.05}O_{12}$ have electronic

			conductivity values of $\sim 3 \times 10^{-5}$ and $\sim 1 \times 10^{-3}$ S cm^{-1} respectively.

V is one of the most suitable dopants for LTO as it does not alter its phase and lattice parameters (Kubiak et al., 2003; Yi et al., 2009, 2010; Yu et al., 2011). This is probably due to similar ionic radii of Ti^{4+} and V^{5+}. Moreover, due to abundance of V the cost of doped material does not escalate. Bandyopadhyay et al. reports the benefits of V doping in tin oxide as sulphur dioxide sensor (Das et al., 2008). Thakur et al. demonstrated the enhancement in properties of Li-Zn-Ti ferrites by V^{5+} doping (Maisnam et al. 2005). T.F. Yi et al. have synthesized V doped LTO in air by solid state method which shows doping with V enhances stabilization of structure even if the electrode discharges up to 0 volts (Yi et al., 2009). The characteristics obtained by him is shown in Figure 2.5. Z.Yu.et al. synthesized V doped LTO in nitrogen atmosphere using solid state method and the conductivity enhances due to coexistence of V^{5+} and Ti^{3+} (Yu et al., 2011). It is understood that both doping and synthesis in reducing atmosphere increase the conductivity of the material and the probable cause for such increase is the reduction of Ti^{4+} to Ti^{3+} (Yi et al., 2009, 2010a; Yu et al., 2011).
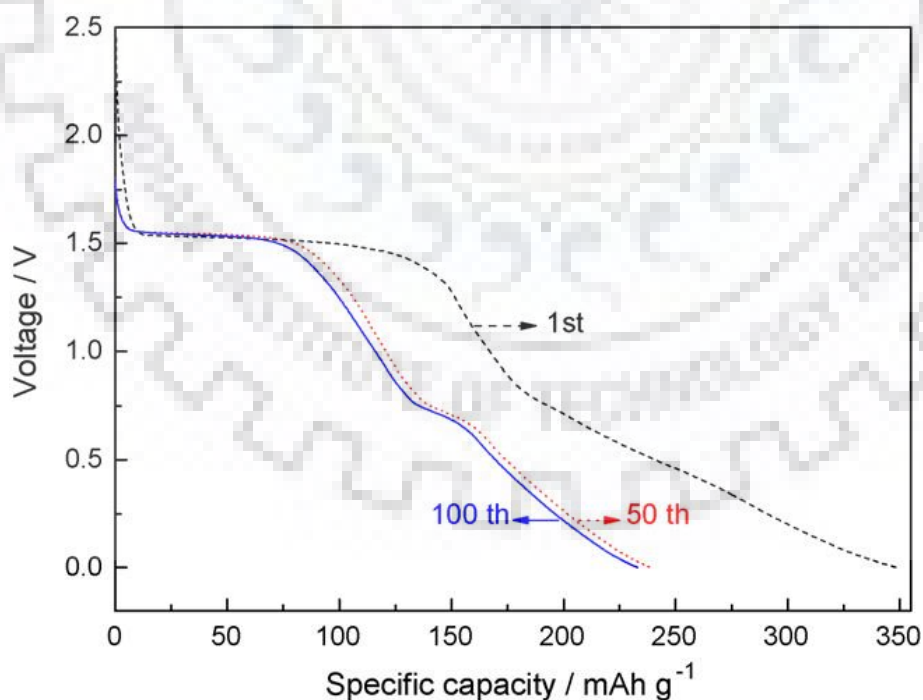
Figure 2.5. Discharge behaviours of Li$_4$V$_{0.1}$Ti$_{4.9}$O$_{12}$ (Yi et al., 2009)

2.2 Supercapacitor

Supercapacitor is an electrochemical energy storage device which stores the electric charge on the interface of electrode and electrolyte. It consists of two electrodes having high surface area immersed in an organic electrolyte. The charge builds up in the form of double layer as shown in Figure 2.6, hence called electrochemical double layer capacitor. The charge-discharge phenomenon is limited to surface of the electrodes, therefore it allows fast charging and discharging leading to become a high specific power device. However, the whole volume of the electrodes is not utilized for storage of charge like lithium ion battery so the specific energy of the device is quite low compared to that of lithium ion battery. The supercapacitor with carbon electrodes using sulfuric acid as electrolyte was first introduced in 1957 by Becker (Becker, 1957). The first supercapacitor is commercialized by NEC (Japan) in 1978 (Simon & Gogotsi, 2008).
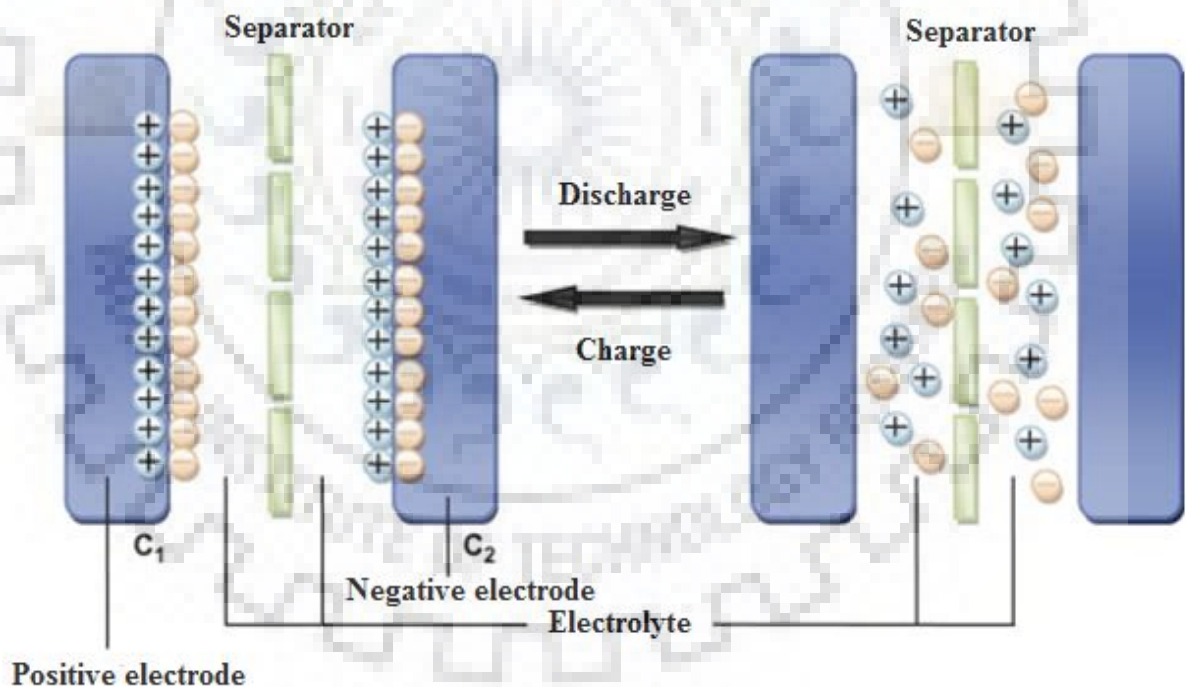
Figure 2.6. Charged and discharged states of supercapacitor

The charged and discharge states of a supercapacitor shown in Figure 2.6. Supercapacitors are considered to have the highest specific power among the rechargeable

electrochemical devices which is about 10 KW/Kg and also have low specific energy of about 10Wh/Kg.

2.3 Need of Hybridization

There is a demand of a device having high specific energy as well as high specific power to fulfill the requirements of many applications. Neither supercapacitor nor lithium ion battery alone has the capability to fulfill that need. In case of lithium ion battery the whole volume of the active material is utilized for storage of charge which results in high specific energy compared to that of supercapacitor. However, charging and discharging phenomena include the diffusion of Li ion inside the volume of active material which is very slow process and therefore specific power of the lithium ion battery is significantly lower than that of supercapacitor.

Hence one can say that lithium Ion battery has high specific energy but low specific power and supercapacitor has high specific power but low specific energy. Hybridization of lithium ion battery and supercapacitor is required if both high specific energy and high specific power are desired in a single device. The feasibility of the hybridization of the two devices is determined by comparing the performance parameters of the devices. The performance parameters of lithium ion battery and supercapacitor are compared in the Table 2.3.

Table 2.3 Performance parameters comparison of lithium ion battery and supercapacitor

Performance Parameters	Supercapacitor	Lithium-ion Battery
Charge time	1–10 seconds	10–60 minutes
Cycle life	1 million or higher	500 and higher
Cell voltage	2.3 to 2.75V	3.6 to 3.7V
Specific energy (Wh/kg)	5 (typical)	100–200
Specific power (W/kg)	Up to 10,000	1,000 to 3,000
Service life (in vehicle)	10 to 15 years	5 to 10 years
Operating temperature	–40 to 65°C	0 to 45°C

The lithium ion battery and supercapacitor also show similar technical aspects. In both systems the process of charging and discharging occurs in nearly same potential ranges. Both the systems can perform in an organic electrolyte. These aspects confirm the feasibility for the practical hybridization of lithium ion battery and supercapacitor. The hybridization of supercapacitor and lithium ion battery has been pursued from the last few decades with a view of combining the high specific energy of the lithium ion battery with the high specific power of the supercapacitor.

2.4 Lithium ion battery – supercapacitor hybrid
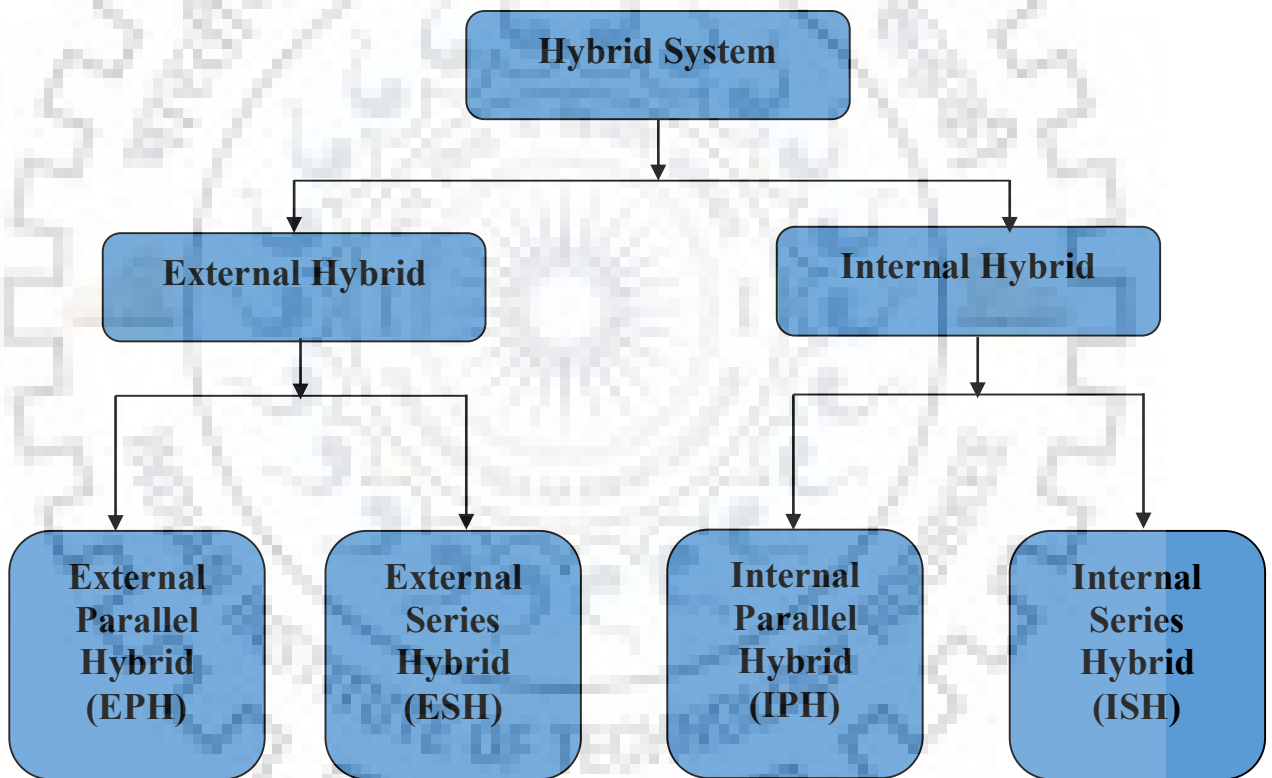
Figure 2.7. Schematic of possible approaches to the hybridization of supercapacitor and lithium ion battery

There are many approaches followed by researchers for the hybridization of supercapacitor and lithium ion battery. All the approaches can be broadly classified into external and internal categories with series and parallel configurations (Cericola & Kötz, 2012) as shown in the Figure 2.7. In external hybrid, the already available lithium ion battery and supercapacitor

are hard wire connected. When the two devices are connected in series configuration, the hybrid system is called external series hybrid and when connected in parallel configuration then the same is called external parallel hybrid. Same type of analogy can be approached at the internal level within single device which can be designated as the internal series and the internal parallel hybrid. All the four approaches followed by researchers are presented in the following sections.

2.4.1 External hybrid

2.4.1.1 Series configuration

In the external series configuration of lithium ion battery and supercapacitor the two devices connected such that the voltages of individual devices get added up to give rise of the hybrid system voltage. A. Burke followed this possible approach (Burke 2008) stating that the current will be the same for both lithium ion battery and supercapacitor, therefore the charge stored in the battery will be limited by supercapacitor as the maximum set voltage reached by the capacitor very soon. Hence in series configuration the overall specific energy of the hybrid system is defined by the device having low specific energy. Similarly the specific power of the hybrid system is defined by device having low specific power. Due to this reason this approach of lithium ion battery supercapacitor hybrid is not intensely followed by the researchers.

2.4.1.2 Parallel configuration

The external parallel configuration was followed by several researchers to improve the high rate performance of lithium ion battery. Holland et al. tested the parallel combination of lithium ion battery of 1.2 Ah and supercapacitor for pulsed applications (Holland, Weidner, Dougal, & White, 2002). The issue of voltage mismatch was resolved by connecting two series connected supercapacitors in parallel to the battery which results in low specific power and energy of the hybrid compared to the lithium ion battery itself. The same issue of voltage mismatch is observed by Sikha and Popov while investigating external parallel hybrid of lithium ion battery and supercapacitor (Sikha & Popov, 2004). Dougal et al. presents first model for external parallel configuration of lithium ion battery and supercapacitor in 2002 (Dougal, Member, Liu, & White, 2002). The optimization of voltage mismatch and current sharing issues between lithium ion battery and supercapacitor in external parallel hybrid configuration by the use of extra electronic circuitry was reviewed by Kuperman and Aharon (Kuperman & Aharon,

2011). The main advantage of parallel configuration is that for pulsed applications the capacitor can accepts and release high current pulses while charging and discharging and relieve the lithium ion battery from high current pulses effect which indirectly reduces the stress of lithium ion battery and increases the life of it.

The specific properties of the external parallel hybrid swings between the supercapacitor and lithium ion battery limit values in accordance with the relative size of battery and supercapacitor. Thus the specific energy of the hybrid system is greater than that of the supercapacitor and the specific power is greater than that of lithium ion battery. It was also demonstrated that for pulsed applications the external parallel hybrid configuration outperforms the lithium ion battery and supercapacitor solely in terms of specific energy and specific power.

2.4.2 Internal Hybrid

2.4.2.1 Series configuration
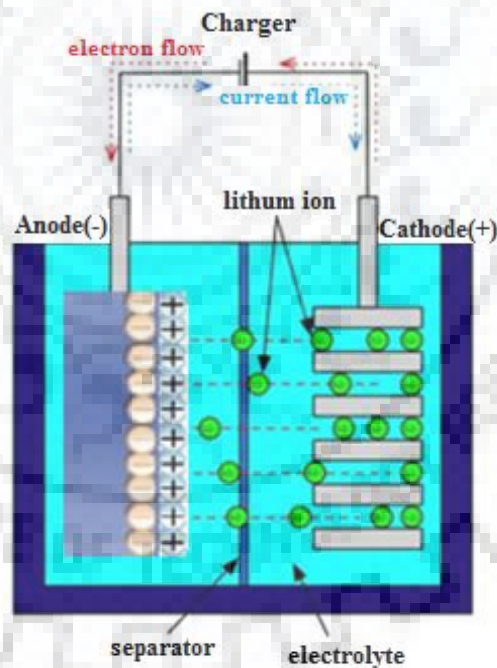
Figure 2.8. Electrode arrangement in internal series hybrid configuration

The internal series hybrid consists of two electrodes with different charge storage and release mechanism immersed in the same electrolyte. One electrode follow the faradaic reaction to store the charge like lithium ion battery material and the other electrode stores charge in the form of electrochemical double layer as shown in Figure 2.8. The faradaic material can be chosen

as anode or cathode. Due to different electrodes this hybrid system is also called asymmetric capacitor. Cericola et al. reviewed this widely investigated approach of the internal series hybrid configuration (Cericola & Kötz, 2012).
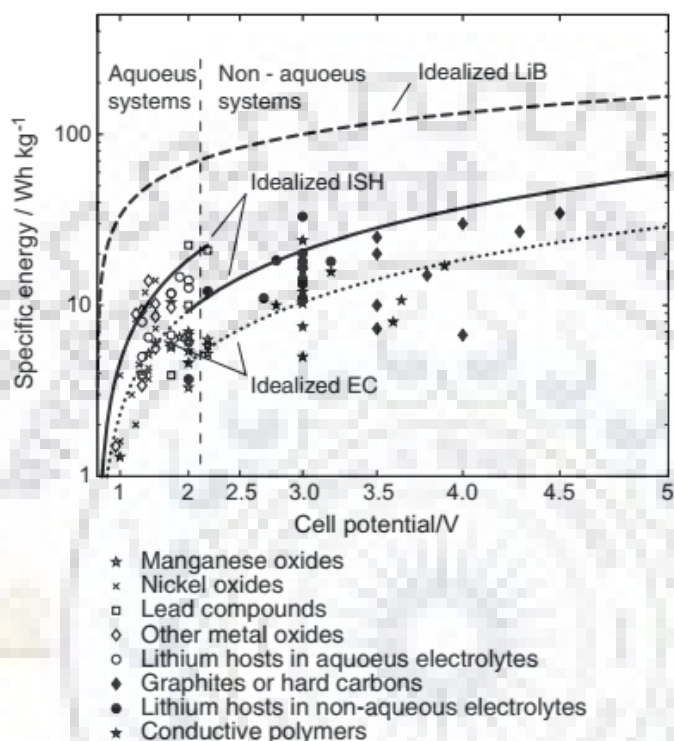
Figure 2.9 Comparison of internal series hybrid configuration using one electrode as activated carbon with different faradaic electrodes (Cericola & Kötz, 2012)

He categorized the internal series hybrid system into metal oxides with aqueous electrolyte based (Brousse et al., 2007; C. Hu & Tsou, 2002a, 2002b; Khomenko, Raymundo-Pi˜nero, & B´eguin, 2006; Qu et al., 2010; Qu, Shi, Tian, et al., 2009; Roberts & Slade, 2010; Yuan, Wang, Wang, & Hu, 2010), nickel oxide and hydroxides based (Duffy et al., 2008; Ganesh, Pitchumani, & Lakshminarayanan, 2006; Nohara et al., 2006; Wang, Li, & Cheng, 2008; Xiao-feng, Dian-bo, & Zheng, 2006; Yuan, Zhang, Wu, & Gao, 2006; Zihong & Anbao, 2009), lead compounds based (Algharaibeh, Liu, & Pickup, 2009; Chen, Lai, Hao, Zhao, & Ji, 2009; Liang, Li, & Zhang, 2008; Moseley, Nelson, & Hollenkamp, 2006; Perret, Khani, Brousse, Bélanger, & Guay, 2011; Qu, Shi, Li, et al., 2009; Wang, Gao, & Hu, 2010; Wang, Wang, & Xia, 2005; Yu, Gao, Zhao, & Wang, 2009), lithium ion host in aqueous electrolyte based (Hao, Lai, Wang, Xu, & Chu, 2010; Luo & Xia, 2009; Mosqueda et al., 2010; Wang & Xia, 2005; Yuan & Zhang, 2006; Zhao et al., 2009), lithium ion host in organic electrolyte based (Khomenko, 2008; Konno,

Kasashima, & Azumi, 2009; Wang & Yoshio, 2006, 2008a, 2008b, 2010; Wang et al., 2007), non-carbon materials in organic electrolytes based (Brousse, Taberna, & Simon, 2006; Chen et al., 2005; Karthikeyan et al., 2010; Liu, He, Li, Liu, & Li, 2006; Naoi, Ishimoto, Isobe, & Aoyagi, 2010; Pasquier, Plitz, Menocal, & Amatucci, 2003; Rao & Rambabu, 2010; Wang, Zhang, Yu, & Qu, 2005; Yoon, Bang, Prakash, & Sun, 2008) and conductive polymer electrode based (Arbizzani, Mastragostino, & Soavi, 2001; Arbizzani et al., 2008; Arbizzani, Beninati, Lazzari, Soavi, & Mastragostino, 2007; Balducci et al., 2005; Balducci, Bardi, Caporali, Mastragostino, & Soavi, 2004; Hung, Chang, Lee, Hu, & Lin, 2010; Mastragostino & Soavi, 2007; Snook, Kao, & Best, 2011; Sun et al., 2004). The Figure 2.9 shows the comparison of internal series hybrid configuration using one electrode as activated carbon with different faradaic electrodes. It also shows comparison of idealized internal series hybrid (ISH) with idealized lithium ion battery (LIB) and idealized supercapacitor (EC).

2.4.2.2 Parallel configuration

The hybrid system in which each electrode consists of lithium ion battery material as well as supercapacitor material is known internal parallel hybrid. This dual material electrode is called as a bimaterial electrode. In a bimaterial electrode the storage of charge occurs via two different charging mechanisms, faradaic as well as electrochemical double layer.

Table 2.4: Internal parallel hybrid of lithium ion battery and supercapacitor with different electrode materials

Author and year	Battery material	Superca-pacitor material	Results	Comments
(Cericola et al., 2011)	$Li_4Ti_5O_{12}$, $LiMn_2O_4$	activated carbon	Specific energy between 53 and 71 $Whkg^{-1}$ and a specific power between 27 and 12 $kWkg^{-1}$	Superior behaviour of IPH over ISH is established.

(Lam and Louey, 2008)	Pb for lead-acid battery	activated carbon	A specific energy of up to 30 Wh kg^{-1} and higher power capability than VRLA batteries	Patented as "ultrabattery"
(Pasqueir et.al, 2004)	LiCoO2	activated carbon	Good rate capability and a specific energy of 40 Wh kg^{-1}	Positive bi-material electrode only
(Hu et al, 2007)	LiFePO4	activated carbon	Specific charge increases from 28 to 40 mAh g^{-1} at low discharge rates but drops to 15 mAh g^{-1} at moderately high discharge rates.	Positive bi-material electrode only
(Hu et al, 2009)	LiMn$_2$O$_4$	activated carbon	specific energy of the device varied from 9.8 to 11 Wh kg^{-1}	Positive bi-material electrode only

The hybrid systems with only one bimaterial electrode and the other electrode of either lithium ion battery material or supercapacitor material also comes under the category of internal parallel hybrid. The internal parallel hybrid configuration was followed by very few researchers and is summarized in the Table 2.4. One mathematical model of the electrode in which both faradaic and electrochemical double layer charging mechanism occurs was presented by Lin et al (Lin, Ritter, Popov, & White, 1999). The authors' focus was on the faradaic reaction between RuO_2 nanoparticles and electrolyte and also the double layer formation on the surface of the nanoparticles itself. They observed that the specific energy of the supercapacitor can be increased by faradic process.

2.5 Bimaterial electrodes designs for the internal parallel hybrid

The bimaterial electrodes of lithium ion battery and supercapacitor materials can be designed using several patterns. Bai et al. patented the various design patterns of bimaterial electrodes as shown in Figure 2.10. The authors designated them as high energy and high power hybrid

electrode (US patent 5744258) (Bai, Changming, & Thomas, 1998). The bimaterial designs shown in figure consists of current collector (aluminium foil for positive bimaterial electrode and copper foil for negative bimaterial electrode) indicated by 40, lithium ion battery material (anode material for negative bimaterial electrode and cathode material for positive bimaterial electrode) indicated by 42 and supercapacitor material (stores charge in the form of double layer) indicated as 44.
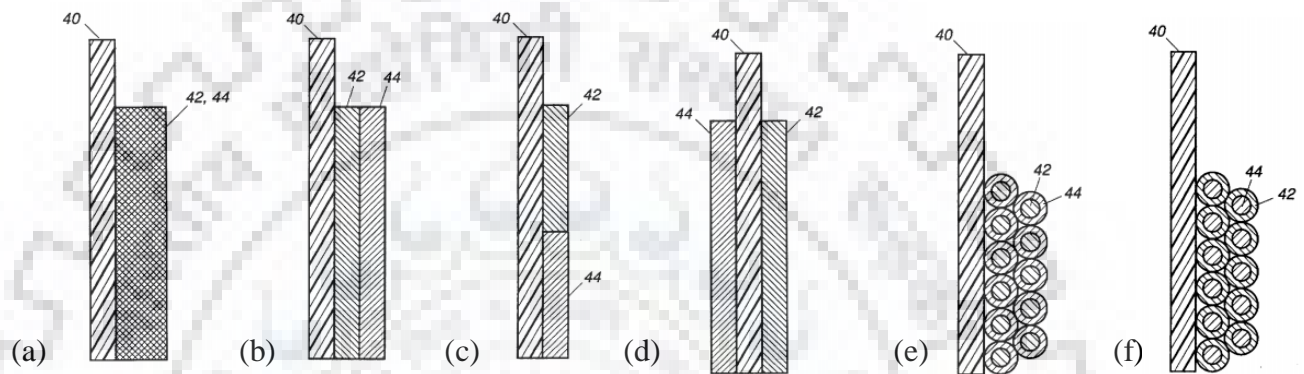
Figure 2.10. Bimaterial electrode designs with battery material (42) and supercapacitor material (44) on current collector (40) (Bai et al., 1998)

(**a**) The active materials of lithium ion battery and supercapacitor are mixed properly to form a single electrode material. This one is the easiest design for the preparation of bi-material electrodes.

(**b**) Separate layers for active materials of lithium ion battery and supercapacitor are pasted on the current collector electrodes one by one. In this particular case any of the active material of lithium ion battery and supercapacitor is sandwiched between the other active material and the current collector. Only one of the active materials can be in the direct contact of current collector.

(**c**) In this case both the active materials are in direct contact with the current collector but the contact area between layers and also with current collector is reduced.

(**d**) This design makes the active materials of lithium ion battery and supercapacitor apart. Both are pasted on the opposite sides of the current collector.

(**e & f**) This core - shell design also makes only one of the active materials can be in the direct contact of current collector. The disadvantage of this design is that the charge carriers has to cross through one active material to reach the other.

2.6 Objective and problem formulation

In this work a different approach is applied in making the internal parallel hybrid of lithium ion battery and super capacitor. Instead of replacing one battery electrode with supercapacitor electrode or mixing of battery and supercapacitor materials for making a bimaterial electrode, a novel three terminal internal parallel hybrid system of lithium ion battery and supercapacitor is proposed and studied. The schematic diagram of the system is shown in Figure 2.11.
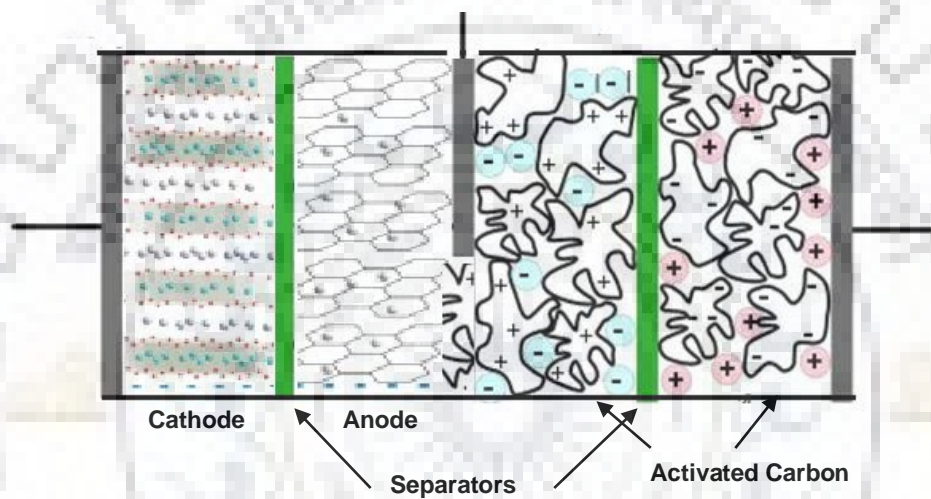
Figure 2.11. Proposed design of lithium ion battery-supercapacitor internal parallel hybrid

The hybrid system consists of a bimaterial electrode having battery material and supercapacitor material sharing the common collector (copper foil) on either sides such that the active materials of the bimaterial electrode are also in contact with each other unlike the non-touching electrodes shown in Figure 2.10(d). A supercapacitor electrode facing the supercapacitor side of the bimaterial electrode and a battery electrode (cathode) facing the battery side of the bimaterial electrode collectively make the three terminal hybrid system. The battery material chosen for this work is spinel lithium titanate LTO and activated carbon as supercapacitor material.

The objective of the thesis is to improve LTO characteristics with

(i) High rate performance by increasing the surface area through making it nanoporous and

(ii) Increase the lithium ion diffusion coefficient and conductivity by means of doping to enhance the performance of the proposed lithium ion battery and supercapacitor internal parallel hybrid.

Experimental Techniques

EXPERIMENTAL TECHNIQUES

3.1 Introduction

The purpose of the present work is to prepare and characterize the LTO material with improved properties to be used as battery material in the bimaterial electrodes based internal parallel hybrid system of lithium ion battery and supercapacitor. Primarily LTO is synthesized following sol-gel method and the prepared powder of LTO is characterized by X-ray diffraction (XRD) method for phase analysis. Few more samples of LTO with change in stoichiometric ratio of precursor elements are prepared followed by XRD analysis till the pure phase LTO is achieved. Subsequently nanoporous LTO and vanadium doped LTO are synthesized following sol-gel method. Characterization of all the synthesized powder samples are performed using powder XRD, Field emission-scanning electron microscopy (FE-SEM), Transmission electron microscopy (TEM), X-ray photoelectron spectroscopy (XPS), and Brunauer–Emmett–Teller (BET) techniques. Electrochemical impedance spectroscopy (EIS) is performed on the electrodes prepared from all the synthesized powder materials separately inside a Teflon cell assembly under the inert gas atmosphere using lithium as counter electrode.

The bimaterial electrodes are prepared according to the design of hybrid system under investigation with LTO, nanoporous LTO and vanadium doped LTO powders separately as battery material and activated carbon (AC) as supercapacitor material for each cell assembly. Galvanostatic charging discharging and cyclic voltammetry tests are performed on cell assemblies fabricated from the prepared electrodes separately.

The carbon nano-beads (CNBs) which are used to prepare the nanoporous LTO are synthesized by using chemical vapour deposition (CVD) process. Vanadium doped LTO is prepared by introducing ammonium metavendate at precursor level during sol-gel process. The XRD analysis of prepared samples is done to confirm their phase purity. Morphology of the prepared powder samples is observed by FE-SEM. TEM of CNBs and LTO powder particles is performed to estimate the particle size. Further, confirmation of amorphous nature of CNBs is done by SAED pattern obtained by TEM. Oxidation state of vanadium in prepared samples of vanadium doped LTO is determined by XPS. In addition, the transition of oxidation state from 4+ to 3+ of titanium is also observed by XPS. EIS is done for conductivity and lithium ion

diffusion coefficient measurements on doped samples. For surface area measurement of porous samples BET analysis is performed.

The flow chart of steps sequentially followed to complete the experimental procedure is shown in Figure 3.1
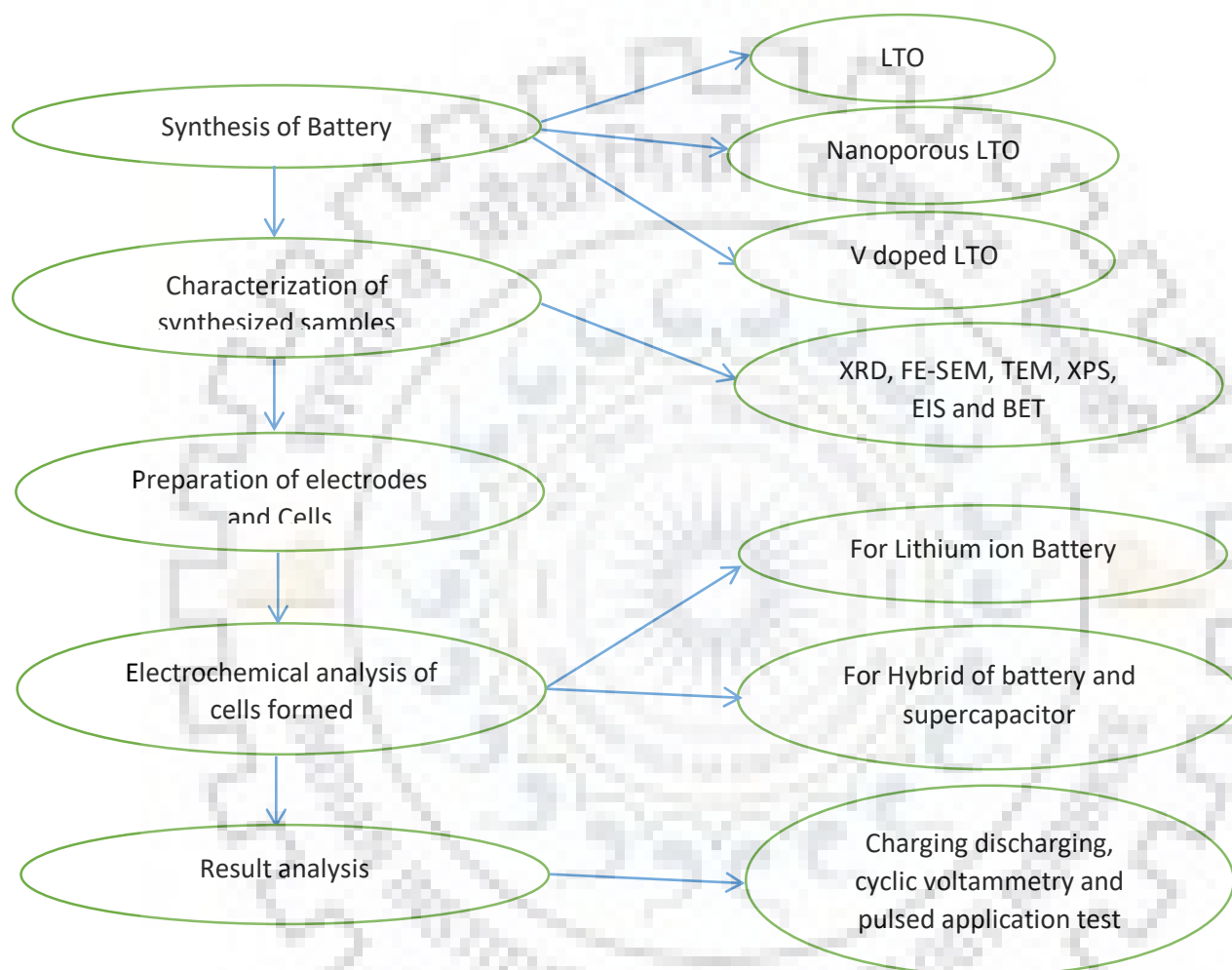
Figure 3.1: Flow chart representing the steps followed to complete the experimental procedure

3.2 Sample Preparation

The LTO, nanoporous LTO and vanadium doped LTO are all synthesized by sol-gel route. The CNBs are prepared by CVD process which are further used as pore former in the synthesis of nanoporous LTO. The preparation of gel is done at room temperature which is then

dried at 80°C followed by calcination at 800°C in both ambient and argon atmosphere to obtain the final ceramic powder samples.

3.2.1 Synthesis of LTO using sol-gel process

Sol-gel process can be defined as a "wet chemical technique" which links the colloidal particles after their agglomeration to form a network (gel). Sol-gel has been considered a useful self-assembly process for formation of nanomaterials.

The concept behind sol-gel synthesis is to "dissolve" the microparticles or molecules in a solution in order to procure it as a solid under controlled environment. This method prevents the issues caused by co-precipitation, which might be the result of a gelation reaction. It enables proper mixing at an atomic level and results in lesser size particles, which promotes higher sinterability.
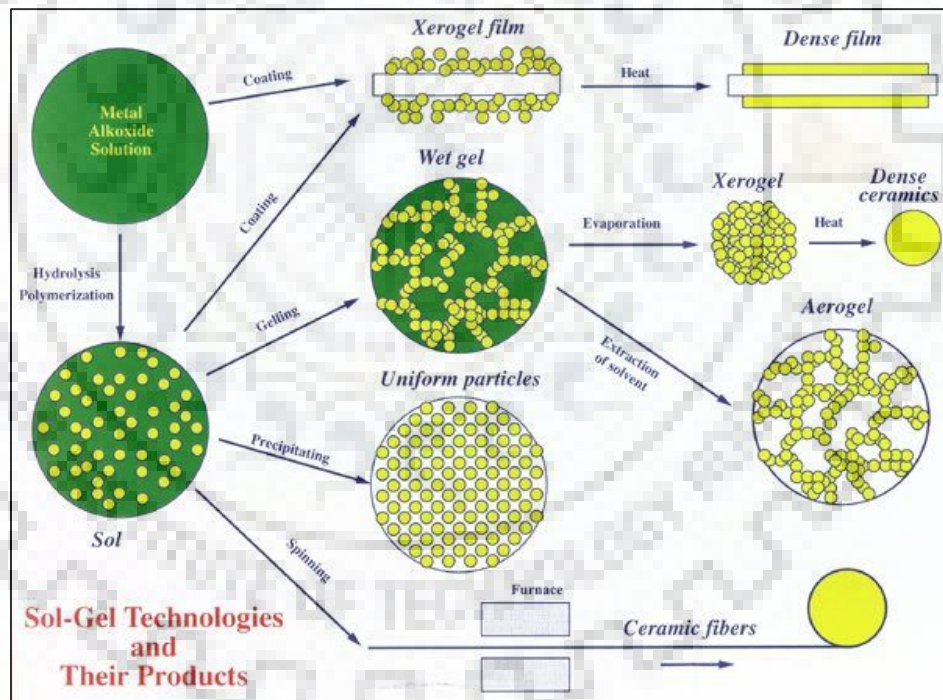
Figure 3.2: Preparation mechanisms of different structures using sol-gel method

Sol-gel synthesis can also be used to produce materials with different structures such as thin fibers, porous structures, thin films, dense powders etc. The types of gel are differentiated by the process of drying. If the gel is dried by evaporation in air, it will undergo shrinkage by the capillary forces, the gel network will collapse, which results in formation of xerogel. If the drying

is performed very slowly under supercritical conditions, the solid matrix may be retained and a gel with large pores might be formed which is called an aerogel.

LTO was prepared by sol-gel process using lithium acetate dihydrate ($C_2H_3LiO_2.2H_2O$, 99%, Loba Chemie), titanium-butoxide ($C_{16}H_{36}O_4Ti$, 99+%, Alfa Aesar) as sources of Li and Ti respectively. Tetrabutyl-titanate is dissolved in 50ml of iso-propyl alcohol to make solution S1and lithium acetate is dissolved in a 50ml mixture of isopropyl alcohol, acetic acid and de-ionized water to make solution S2. The S2 is added drop wise in S1 with vigorous stirring as shown in Figure 3.3. After about 6 hours the gel formation takes place. The gel was dried in vacuum oven at 80°C for 12 hours to obtain the gel in powder form followed by calcination at 800°C for 10 hours in air. The powder formed was white in colour.
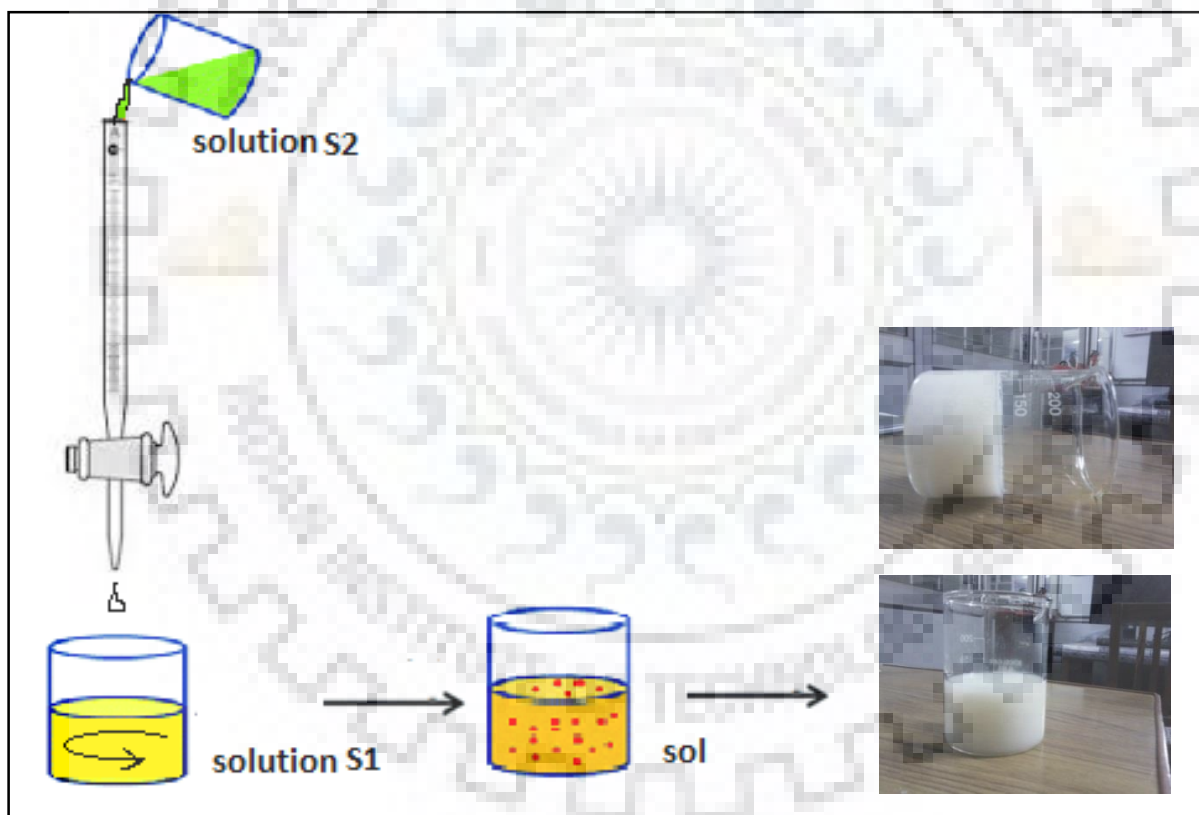
Figure 3.3: Schematic diagram for synthesis of LTO by sol-gel method

3.2.2 Synthesis of CNBs using chemical vapour deposition (CVD)

CVD is a widely used technique in the semiconductor industry, involving the semiconductor device fabrication process, for deposition of various films such as epitaxial,

amorphous and polycrystalline silicon, silicon germanium, silicon dioxide, tungsten, silicon oxynitride silicon nitride, titanium nitride and bunch of high-k dielectrics. CVD systems are based on four major factors: temperature, time, pressure, and surface specificity.

CVD involves the reaction or deposition of a volatile chemical into the desired solid film. In each process, there are couple of reaction paths that lead to conversion of vapours to a solid. Reactors are designed in order to restrict the reaction to a particular place and time within the chamber (typically on the substrate), and not everywhere else. In a typical CVD process, one or more volatile precursors are exposed to the substrate, which either react or decompose on the surface of the substrate to complete the desired deposition. Volatile byproducts are also produced frequently, which have to be removed by proper gas flow through the reaction chamber. These byproducts or particles can also deposit onto the substrates, coat the chamber walls or clog the exhaust openings. CVD is an established method for synthesis of carbon nanotubes (CNT). Silva et al. demonstrates that the photo-thermal CVD technique can provide control over the CNT growth, excellent quality and fast growth rates (Chen, Stolojan, & Silva, 2015).
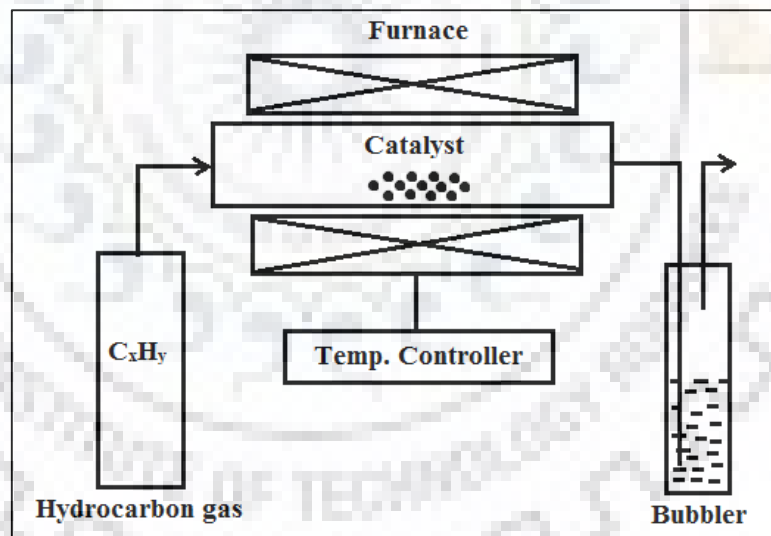
Figure 3.4: The schematic diagram of CVD setup for synthesis of carbon nano beads.

The carbon nanobeads (CNBs) are synthesized by adopting chemical vapour deposition (CVD) method. The schematic diagram of setup is shown in Figure 3.4. The acetylene gas was passed onto an alumina boat as substrate in a horizontal tubular furnace heated to a temperature of 650°C at atmospheric pressure. The flow rate of acetylene gas was maintained at 40 sccm for about 10 seconds.

3.2.3 Synthesis of nanoporous LTO using CNBs as pore former

Nanoporous LTO has been synthesized by sol-gel method using 2 wt. % of CNBs incorporated at precursor level during the synthesis of LTO which is explained in sec 3.2.1. The nanoporous structure is formed due to removal of CNBs in the form of CO_2 at the calcination temperature of $800^{\circ}C$ named as LTO-P.

3.2.4 Synthesis of vanadium doped LTO

Vanadium doped LTO samples are prepared by sol-gel process using lithium acetate dihydrate, titanium-butoxide and ammonium metavanadate (NH_4VO_3, 99+%, Sigma Aldrich) as sources of Li, Ti and V respectively. Ammonium metavanadate was added in a solution containing titanium butoxide dissolved in isopropyl alcohol (solution S1 in Figure 3.3). The process followed after this is same as described in section 3.2.1. Vanadium doped LTO powder is synthesized in three different compositions according to stoichiometric formula $Li_4Ti_{5-x}V_xO_{12}$ (x = 0.05, 0.1 and 0.15) named as VLTO-05, VLTO-10 and VLTO-15 for x = 0.05, 0.1 and 0.15 respectively. The above experiment was repeated for the same compositions with the dried gel calcined in argon atmosphere and were named as VLTO-05AR, VLTO-10AR and VLTO-15AR for x = 0.05, 0.1 and 0.15 respectively.

3.3 Characterization Techniques

3.3.1 X-Ray Diffraction (XRD)

X-ray powder diffraction (XRD) is a widely known non-destructive analytical technique for characterizing crystalline materials, providing information on crystal structure, texture, phase, crystallinity etc. The information obtained can be used to calculate unit cell dimensions.

3.3.1.1 Indexing of XRD Pattern

From the XRD pattern a table of θ, $\sin^2\theta$ and ($\sin^2\theta/\sin^2\theta_m$) is generated.

• If all the diffraction lines are kept under consideration, then the experimental numerical values of $\sin^2\theta$ should form a relation to the values of h, k and l for the specific crystal structure.
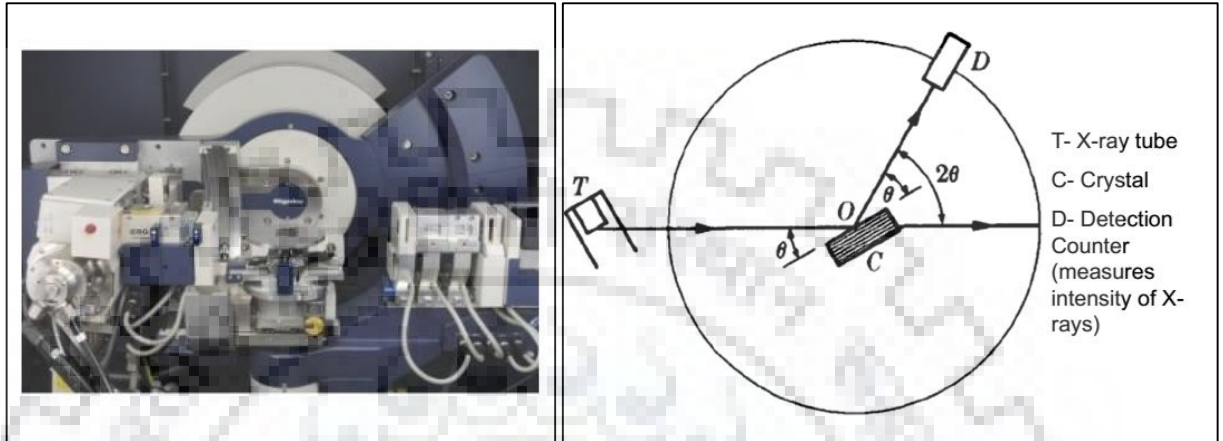
Figure 3.5: Image and schematic diagram of X-Ray diffractometer

• To obtain whole integer values, the values of $\sin^2\theta$ are multiplied by some constant numerical value to obtain all the $h^2 + k^2 + l^2$ values.

According to Bragg's equation $\qquad n\lambda = 2d \sin\theta \qquad$ …….. (3.1)
where n is a positive integer and λ is the wavelength of incident wave.

The equation for interplanar spacing, 'd', for cubic crystals is given by:

$$d_{hkl} = \frac{a}{\sqrt{h^2+k^2+l^2}} \qquad \text{…….. (3.2)}$$

where 'a' denotes the lattice parameter.
This gives:-

$$\sin^2\theta = \frac{\lambda^2}{4a^2} (h^2 + k^2 + l^2) \qquad \text{…….. (3.3)}$$

• The values of $h^2 + k^2 + l^2$ integers are then equated to their hkl values.

• Lattice parameter 'a' can be calculated for each line. Therefore, to achieve greater accuracy, the lattice parameter value is averaged over all the diffraction lines.

3.3.1.2 Quantitative analysis by relative intensity ratio (RIR) method using PDXL2

After the analysis of obtained XRD pattern, if more than one phase are observed then by means of quantitative analysis the weight percentage of the phases present can be achieved. In the PDXL2 XRD-analysis software, RIR is one of the quantitative analysis methods. The working principle of the method is as follows:

If the RIR value, R_i, is given, the weight ratio can be calculated from the integrated intensity of the highest peak (Hubbard et al., 1976). The RIR value R_i of a substance is defined as the ratio of the highest peak intensity I_i^{max} of the substance to that of corundum (Al_2O_3) when mixed with corundum at a weight ratio of 1:1. When the weight ratio of the substance and corundum is $W_i:W_c$, the following formula holds:

$$\frac{W_i}{W_c} = \frac{1}{R_i} \frac{I_i^{max}}{I_c^{max}} \qquad \text{........ (3.4)}$$

This formula provides the weight ratio, W_i, in terms of the RIR value R_i of the substance i and its highest peak intensity I_i^{max} as expressed in eq.3.4

$$W_i \propto \frac{I_i^{max}}{R_i} \qquad \text{........ (3.5)}$$

3.3.2 Field Emission-Scanning Electron Microscopy (FE-SEM)

The Field emission scanning electron microscopy (FE-SEM) is a technique in which high magnification and high-resolution imaging of sample surfaces is done to study its morphology. Chemical compositional analysis can also be obtained using an Energy dispersive X-ray spectrometer (EDS) along with FESEM.

3.3.2.1 Working principle of FE-SEM

The beam-specimen interaction is shown in figure 3.6. Secondary and back-scattered electrons are used for image analysis and characteristic X-rays are used for EDS. The images taken from FE-SEM (Carl Zeiss Ultra Plus) are used to study the morphology of CNBs, LTO, nanoporous LTO and vanadium doped LTO prepared in ambient and argon atmosphere. Average pore size estimation of nanoporous LTO is also done by FE-SEM images.
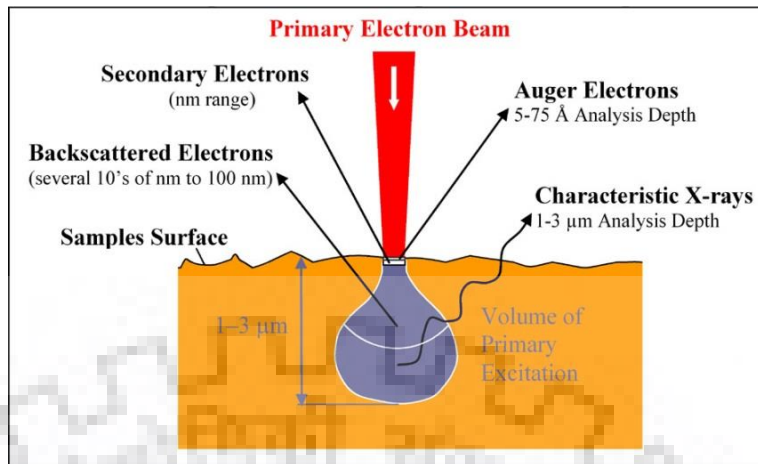
Figure 3.6: Electron beam – specimen interaction in FE-SEM

3.3.3 Transmission electron microscopy (TEM)

Working principle of TEM is mostly same in TEM as of the light microscope. TEM utilizes electrons to produce image instead of light. Lower wavelength of electrons allows for much higher resolution than what is possible with light microscope.
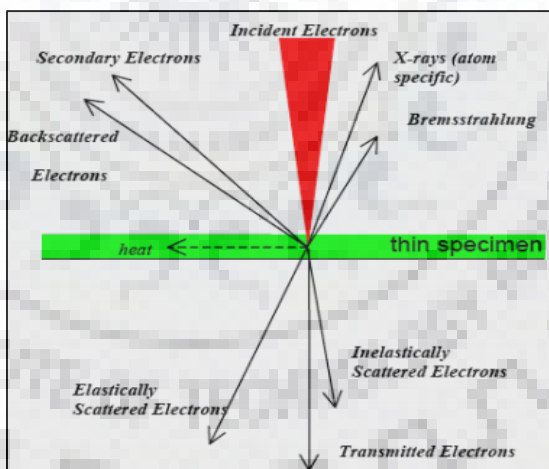
Figure 3.7: Electron beam – thin specimen interaction in TEM

Electrons accelerated to defined energy behave as a wave. Objects of the order of 10^{-10}m are visible. In this technique, high energy electrons are focused into a beam and is transmitted through the sample.

The working of TEM (FEI Technai G^2-20 S-Twin) in diffraction mode for getting SAED pattern and image mode for particle size determination is explained in the Figure 3.8. The

prepared powder samples were placed on the copper grid after ultra-sonication for de-agglomeration and dried before examination under the TEM.
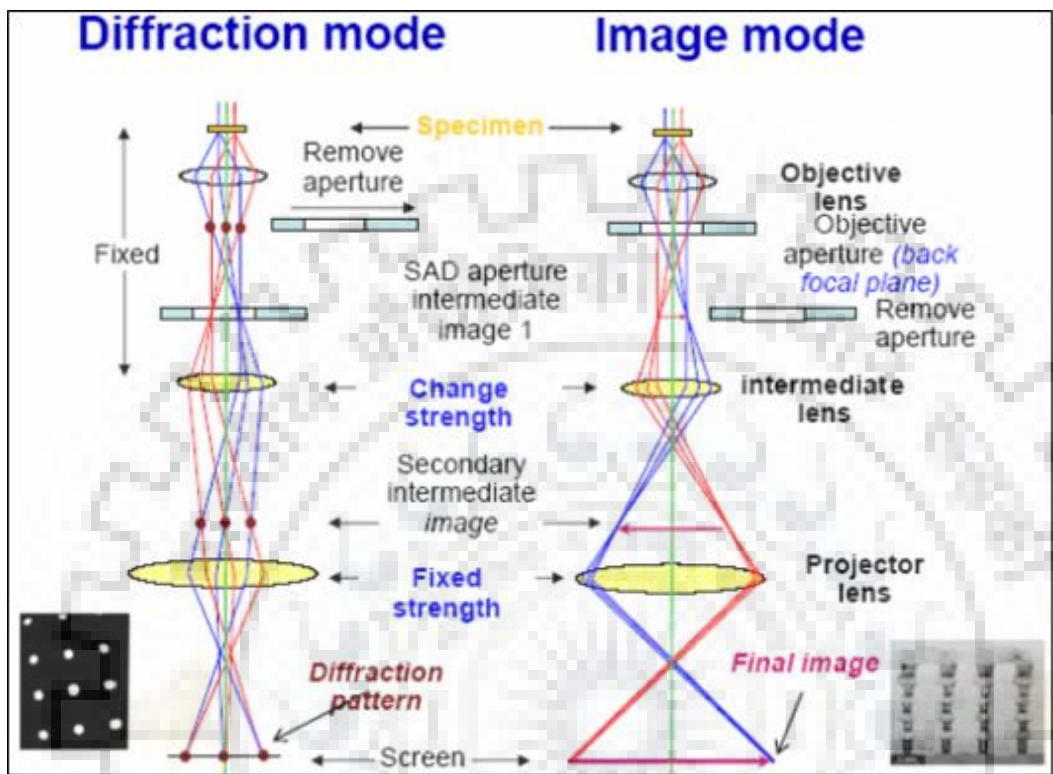
Figure 3.8: Diffraction mode and image mode operation ray diagram

3.3.4 X-ray photoelectron spectroscopy (XPS)

X-ray photoelectron spectroscopy (XPS) is a non-destructive surface analysis technique which is most widely used. It has been also known as Electron spectroscopy for chemical analysis (ESCA). It can be used for a variety of materials for their quantitative information and their chemical characteristics. Such techniques are useful for materials whose surface or film plays a critical role in their applications. XPS is performed by exciting the sample surface by a beam of mono-energetic X-rays which causes photoelectrons to be emitted. Electron energy analysis by the instrument can study the energy of the photo-electron emitted and deduce its respective elemental and chemical identity with quantitative results. XPS requires high or ultra-high vacuum conditions (P $=10^{-8}$ to 10^{-9} mbar).

The de-convolution of XPS peaks is performed using XPS peak4.1 software for quantitative analysis of oxidation states of vanadium.
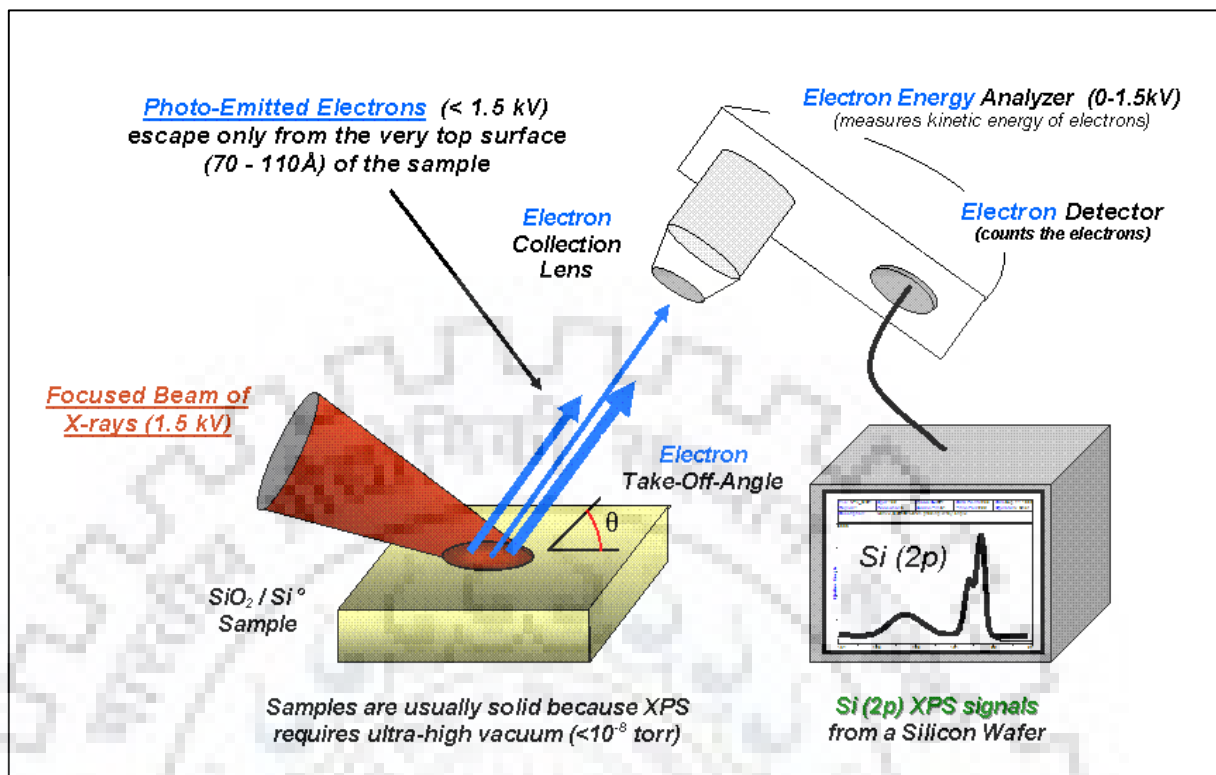
Figure 3.9: Basic components of a monochromatic XPS system

3.3.5 Electrochemical Impedance Spectroscopy

Electrochemical Impedance Spectroscopy (EIS) is a widely used technique to investigate electrochemical systems. EIS provides several information such as thickness of electrically-active grain boundaries, and conduction mechanism at grain and grain boundaries (Biendicho & West, 2012). Generally, a sinusoidal alternate voltage excitation signal of amplitude 5 mV is applied to the system under study during an EIS experiment and the alternate voltage response is measured. The Nyquist plot of the EIS measurement is the plot of imaginary vs real parts of the complex impedance of the cell at different frequencies of measurement. The plot consists of a semicircle or depressed semicircle starting from high frequency to intermediate frequency and a straight line in the low frequency region. The profiles of impedance spectra can be explained by equivalent circuit of the Nyquist plot shown in the inset of Figure. 3.10 (Mukherjee et al., 2013). The high frequency intercept (Figure. 3.10) on Z_{real} axis corresponds to resistance (R_s) of the electrochemical cell, offered by the separator, electrolyte and at interface of electrode and current collector (Mahajan, Thakur, Prakash, & Sreenivas, 2011). Medium frequency intercept on real impedance axis corresponds to R_{ct}.
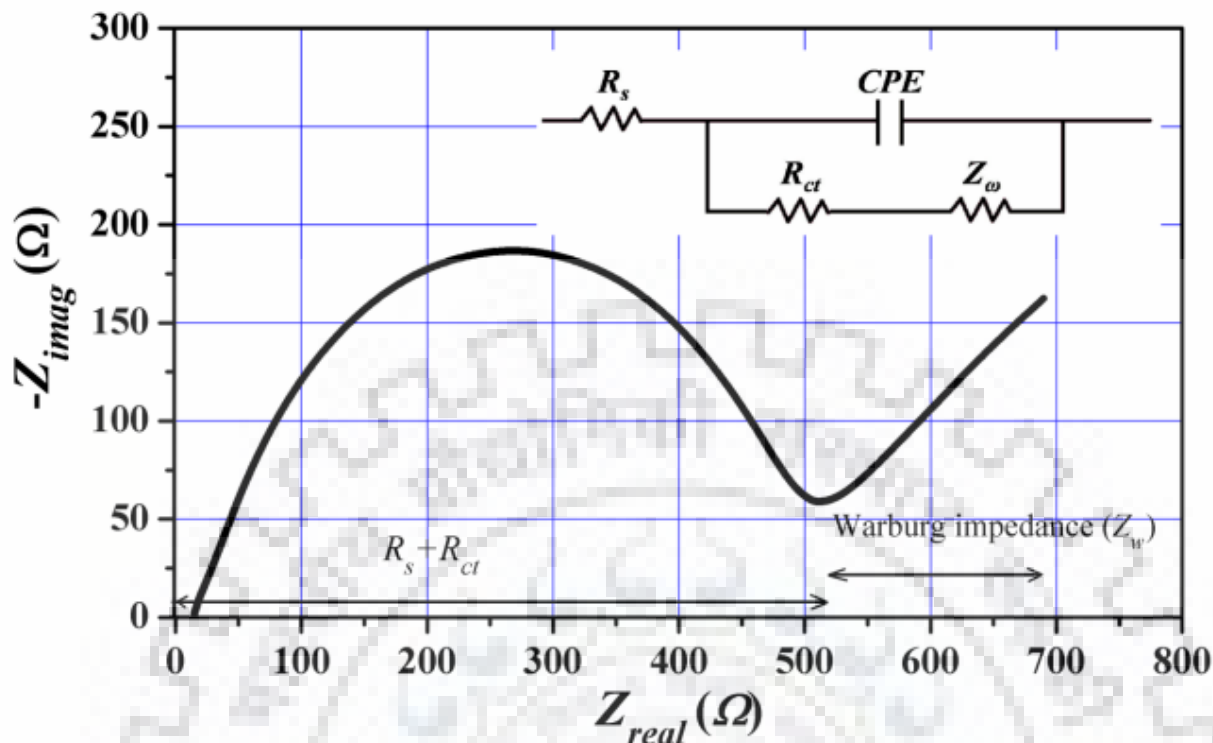
Figure. 3.10: Nyquist plot of EIS measurement of a LTO sample

The R_{ct} is attributed to charge transfer resistance offered during the electrochemical reaction of cell which is associated with the electrode / electrolyte interface and particle / particle contact resistance during the electrochemical reaction of the cell. The straight line starting from the edge of medium frequency side of semicircle to low frequency region corresponds to Warburg impedance (Z_ω) which reflects the Li-ion diffusion in the electrode. R_{ct} represents all Faradic reactions that occur on the electrode surface. These reactions can be reversible or irreversible. In contrast, constant phase element (CPE) describes non faradic charge storage mechanisms and is angle made by the straight line with X-axis in the Warburg region of Nyquist plot. The Nyquist plot can be simplified by using the model of electronic equivalent circuit. The electronic equivalent circuit has R_s in series with a parallel combination of *CPE* and R_{ct} in series with Z_ω.

All the EIS analyses of the cells were carried out on the electrochemical workstation (Gamry Instruments, INTERFACE 1000) over the frequency range 0.1 Hz to 1 MHz and at a voltage amplitude of 0.5 mV.

3.3.6 Brunauer–Emmett–Teller (BET)

In 1938, Stephen Brunauer, Paul Emmett and Edward Teller published their first article explaining the BET theory in the Journal of the American Chemical Society. BET theory explains how the specific surface area may be calculated by physically adsorbing a gas onto the sample substrate surface. After adsorption of gas, the amount of adsorbate gas is calculated, which is usually done at liquid nitrogen temperature. Physical adsorption results due to weak Van der Waals forces between gas and substrate surface. The BET surface area result is obtained with units of m^2/g.

The Micromeritics ASAP 2020 instrument is used to determine the BET surface area. This instrument includes variety of automated gas sorption techniques into a single table-top instrument. The system provides high-quality isotherms of surface area, porosity, chemisorption and physisorption.

Figure 3.11: Image of Micromeritics system for BET surface area measurement

3.4 Electrochemical Analysis

The electrochemical analysis includes the study of charging-discharging, cyclic voltammetry etc. of prepared electrodes comprised in the cell assembly inside the Glove Box under the inert gas atmosphere. The Glove box MB 200G, MBRAUN, Germany is maintained

at a level of < 0.1 ppm for both O_2 and moisture. The cells assembly is electrically connected to an electrochemical analyzer. The BT-2000, Arbin Instruments, USA is used as electrochemical analyzer controlled by MITS Pro software. Using the MITS Pro software, one can make program for testing the prepared cell.

3.4.1 Preparation of Electrodes

The electrodes are prepared using the following steps:

- In the present work, LTO is used as a battery material, AC as a supercapacitor material and combination of both LTO and AC for a hybrid systems.
- The slurry was prepared by mixture of active material (LTO or AC), conducting agent acetylene black and polyvinylidene fluoride (PVDF) as a binder in the weight ratio of 80:10:10.
- N-methyl-2 pyrrolidone (NMP) was used as a solvent.
- The slurry of each material was pasted onto Cu and Al foils for anode and cathode respectively
- Electrode was first dried at 80°C in air, pressed and then further dried in vacuum at 80°C for 4 hours.
- Electrodes formed were punched into discs with a diameter of 10 mm for further analysis.

3.4.2 Formation of Cell Assembly

The cell assemblies using cylindrical Teflon cells shown in Figure 3.12 are formed for lithium ion battery, supercapacitor and hybrid of lithium ion battery and supercapacitor inside argon filled Glove box at < 0.1ppm of O_2 and H_2O. A separator of polypropylene (Cellguard) for the separation of electrodes and 1M $LiPF_6$ + EC: DEC (1:1, by volume) as electrolyte used.

- Cell assembly for Li-ion battery consists of Li metal as anode and LTO as cathode.
- Cell assembly for supercapacitor consists of activated carbon both as anode and cathode.
- Cell assembly for hybrid of lithium ion battery and supercapacitor is a three electrode system consisting of Li metal and LTO as battery electrode materials and activated carbon as supercapacitor electrode material. The hybrid system is shown in Figure 3.13.

Figure 3.12: Teflon Cell Assembly

Figure 3.13: Three terminal hybrid system cell assembly

3.4.3 Electrochemical Testing

The charge-discharge behaviours of the lithium ion battery cells, supercapacitor cells and hybrid cells are studied at different C-rates viz. 0.1C, 0.2C, 0.5C, 1C, 2C and 5C where 1C = 175mAhg^{-1} (theoretical capacity of LTO). The cyclic voltammetry is performed at a rate of 0.1mV/sec for all the prepared cells. The pulse application test is performed on LTO based battery, AC based supercapacitor and all bimaterial electrodes based hybrid systems using three pulse patterns of 0.1C-1C, 0.5C-5C and 1C-10C.

Li$_4$Ti$_5$O$_{12}$ and Nanoporous Li$_4$Ti$_5$O$_{12}$

$Li_4Ti_5O_{12}$ and Nanoporous $Li_4Ti_5O_{12}$

Occurrence of rutile TiO_2 phase in the compound $Li_4Ti_5O_{12}$ (LTO) is due to Li evaporation during high temperature calcination at 800°C - 950°C and is independent of synthesis method (Shin et al., 2012). Pure LTO phase is desired as rutile TiO_2 does not contribute in lithium intake while charging at room temperature due to its unique primitive tetragonal packing. The cation radius of octahedral sites is 0.40 Å but the Li^+ radius is 0.68 Å (Christiansen et al., 1988). Christiansen et al. compare Li insertion in these three titanium dioxides. The investigations are based on electrochemical measurements on cells with either organic liquid electrolyte operated at ambient temperature or with polymer electrolyte (120°C). Figure 4.1 shows that anatase TiO_2 [TiO_2 (A)] and brookite TiO_2 [TiO_2 (B)] have lithium intake capacity at both 25°C and 120°C but rutile TiO_2 [TiO_2 (R)] shows intake of Li ion only at 120°C.
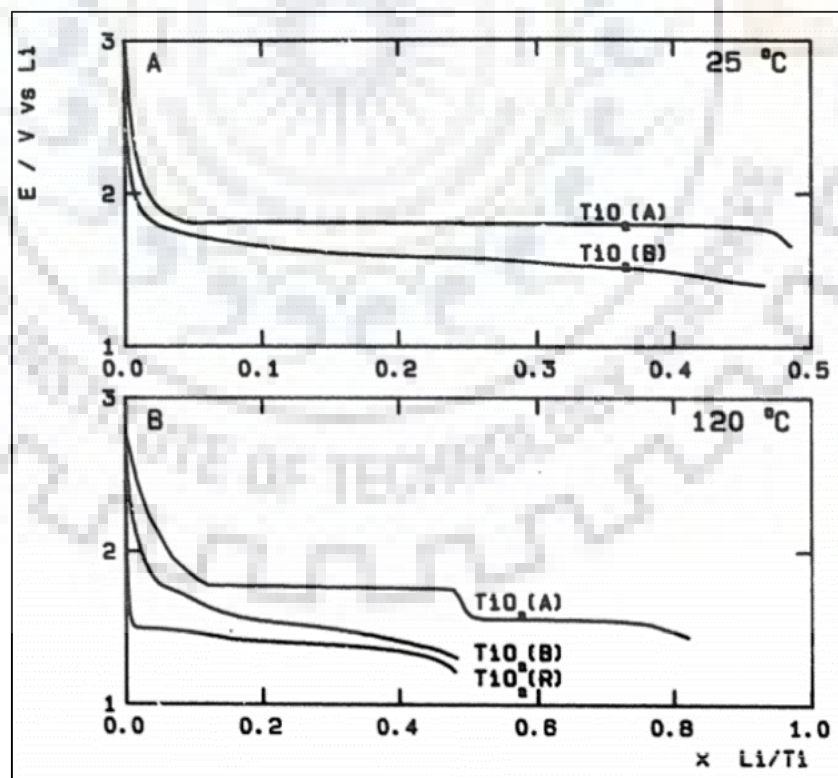
Figure 4.1. Constant current discharges for Li_xTiO_2 at 25 and 120°C

(Christiansen et al., 1988)

This chapter presents the results and discussion on synthesis and characterization of phase pure LTO. Impurity phase having developed with synthesis of compound LTO considering the stoichiometric ratio Li: Ti = 4:5 was found to be of Rutile TiO_2 after XRD analysis. These phases were quantitatively analyzed following Relative Intensity Ratio (RIR) method using PDXL software. After having obtained the impurity phase content theoretical estimates were made to determine the excess Li required to get TiO_2 impure phase free LTO. Based on theoretical estimates three different compositions namely $Li_{4+x}Ti_5O_{12}$ (x = 0.2, 0.4 and 0.6) were selected to synthesize the compound close to the theoretical estimates using sol-gel route (described in chapter 3). Electrochemical analysis of the samples prepared in all three compositions were performed. Morphological feature of LTO with highest level of purity is performed using TEM.

This chapter also describes results and discussion on synthesis and characterization of nanoporous LTO (LTO-P) formed using carbon nano beads (CNBs) as pore former. CNBs were synthesized separately using CVD process and added at precursor level LTO synthesis. The nanoporous structure is formed due to removal of CNBs in the form of CO_2 at the calcination temperature of $800^{\circ}C$. The surface area of the LTO-P powder was measured following BET method. SEM micrographs of LTO-P were taken to estimate the average pore size in the powder. The electrochemical analysis of LTO and LTO-P was also conducted.

4.1 LTO with phase purity

4.1.1 XRD analysis of LTO with stoichiometric ratio Li: Ti = 4:5

Figure 4.2 shows the XRD pattern of the LTO powder and the pattern has been analyzed by Xpert High Score plus. The pattern is found in accordance with JCPDS file no. 00-049-0207 for major phase and with JCPDS file no. 01-083-2242 for impurity phase of rutile TiO_2. Similar observations were also made by researchers while preparing LTO using sol-gel process (C. Chen et al., 2003). The relative intensity levels particularly for the rutile TiO_2 peaks as present in XRD pattern are shown in Table 4.1. All the high intensity peaks corresponding to JCPDS 01-083-2242 of rutile TiO_2 are present in the pattern. Therefore the XRD pattern confirms $Li_4Ti_5O_{12}$ – TiO_2 dual phase.
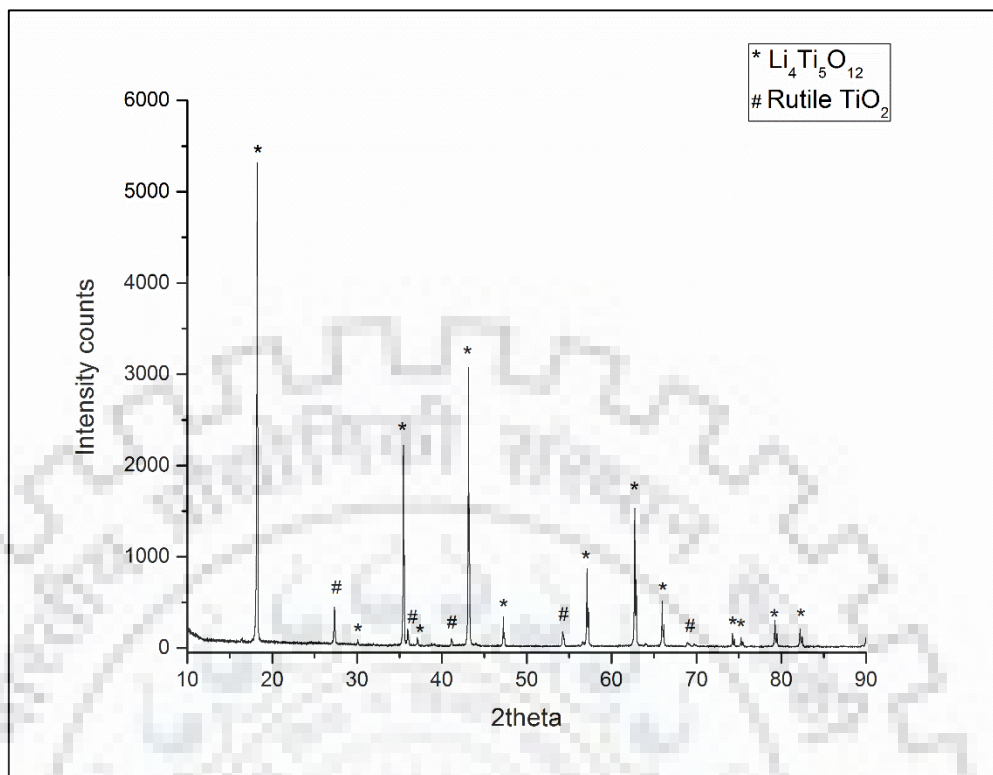
Figure 4.2. XRD pattern of $Li_4Ti_5O_{12}$ powder with Li:Ti=4:5

Table 4.1 Relative Intensity of rutile TiO_2 peaks w.r.t. LTO peaks

2Theta	Relative Intensity	Intensity [%] according to JCPDS 01-083-2242
27.459	7.54%	100
36.077	2.60%	30.7
41.245	1.10%	10.8
54.344	2.15%	41.4
69.784	1.43%	14.3

4.1.2. Impurity phase in LTO

Synthesis of LTO includes calcination of dried gel at 800°C due to which evaporation of Li takes place and undesired rutile TiO_2 appears in the resultant compound. Such impurity TiO_2 phase can be eliminated by adding excess Li than stoichiometric amount required at precursor level. Addition of excess Li in order to subside the impurity phase in LTO was reported by

researchers. However no reports on optimum excess amount of Li was asserted. The following gives the examples of variability of excess Li content used by different researchers in attempts to synthesize phase pure LTO compound.

Yu et al. added 5wt% excess lithium carbonate to compensate Li loss during hyper thermal synthesis (Yu et al., 2011). J. Wolfenstine et al. added 3wt% excess lithium carbonate to compensate Li loss during synthesis by solid state method (Wolfenstine & Allen, 2008). C. Lin et al. added 3mol% excess lithium carbonate to compensate Li loss during synthesis by solid state method (Lin et al., 2014). Q. Zhang et al. added 5wt% excess lithium acetate to compensate Li loss during synthesis by sol-gel method (Zhang & Li, 2013). R. P. Maloney et al. reports a Li:Ti precursor ratio of 10:5 to compensate Li loss during synthesis of aerogel of LTO by sol-gel method (Maloney, Kim, & Sakamoto, 2012). The requirement of optimum quantity of excess Li content for phase pure LTO, the estimate was made following the steps given below:

(i) Quantitative analysis of two phases present in LTO.

(ii) Theoretical estimate of excess moles of Li_2O give rise to excess lithium precursor weight.

(iii) Samples preparation with varying quantities of excess Li content as obtained from theoretical estimations.

(iv) Constructing of relative intensity of XRD impurity peaks with the excess lithium content.

(v) Comparing theoretical estimate with experimental observations.

4.1.3 Quantitative analysis by RIR method

RIR method is followed to do the quantitative analysis using PDXL2 software. The XRD pattern data file of LTO compound with .raw extension is loaded in PDXL2 software for matching of the phases present. The JCPDS data file which may have highest score with the compound to match with does not necessarily have RIR value, therefore a suitable compromise between the JCPDs database file having RIR value was to be accepted for quantitative estimations. The wt. % of the different phases were obtained from the selected JCPDS database.

The quantitative analysis results in the composition of two phases as given below:

$Li_4Ti_5O_{12}$	92.2%
Rutile TiO_2	7.8%

4.1.4 Theoretical estimates of excess Li content required

$$5TiO_2 \ + 2\ Li_2O \quad = \quad Li_4Ti_5O_{12}$$

i.e. 5 moles of TiO_2 requires 2 moles of Li_2O to form one mole of $Li_4Ti_5O_{12}$.

5 moles	=	5 x molecular weight of TiO_2
	=	5 x 79.88g
	=	399.4g

399.4g of TiO_2 requires 2 moles of Li_2O

For 4:5 ratio 2.0405g of lithium acetate and 8.5085 g of tetrabutyl titante are used which gives 2.58 g of $Li_4Ti_5O_{12}$ and TiO_2.

So, if the wt. % of TiO_2 is 7.8% then weight of TiO_2 will be (7.8x2.58)/100 = 0.20124g

0.20124 g of TiO_2 requires	=	(2x0.20124)/399.4 moles of Li_2O
	=	0.001008 moles of Li_2O
	=	2 x 0.001008 moles of Lithium acetate
	=	(2 x 0.001008 x 102.01) g of lithium acetate
	=	0.20565g of lithium acetate

Initially 2.0405g of lithium acetate is used. So to get the pure phase $Li_4Ti_5O_{12}$ 0.20565 g is more required.

i.e. (0.20565 x 100)/2.0405   =   **10.07%**

Hence theoretically it is estimated that 10.07 wt. % of excess Li content required to get rid of TiO_2 as impurity phase in the LTO compound. However in view of the experimental considerations the samples were made by taking three different compositions viz. 5wt. %, 10% wt. % and 15 wt. % of excess Li content having 10 wt. % as a central composition. This is due to the fact that the precursor composition as per the theoretical estimates does not necessarily lead to unchanged composition in the synthesized sample. Therefore, samples are prepared by

choosing three different Li excess quantities namely 5 wt. %, 10 wt. % and 15 wt. % resulting in the compositions $Li_{4.2}Ti_5O_{12}$, $Li_{4.4}Ti_5O_{12}$ and $Li_{4.6}Ti_5O_{12}$ respectively.

4.1.6 Analysis of XRD patterns of $Li_{4+x}Ti_5O_{12}$ (x = 0.2, 0.4 and 0.6)

The XRD patterns of $Li_{4+x}Ti_5O_{12}$ (x = 0.2, 0.4 and 0.6) are shown in Figure 4.4. It can be seen that after addition of excess Li, the intensity of impurity peaks of TiO_2 gradually decreases to a vanishingly small level with increase in Li content.
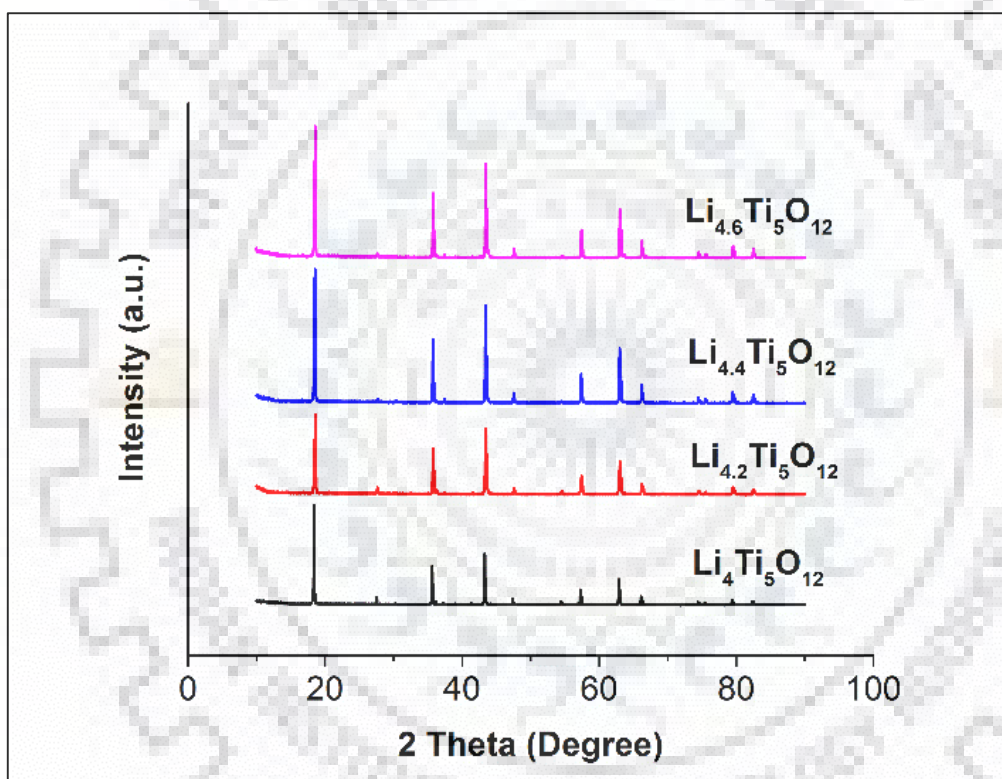
Figure 4.3. XRD patterns of $Li_{4+x}Ti_5O_{12}$ (x = 0.2, 0.4 & 0.6)

The relevant range of XRD patterns showing the intensity reduction of TiO_2 impurity peaks is shown in an enlarged view in Figure 4.4. This can be observed that the intensity of impurity peaks at $2\theta = 36.07$ and 41.24 reduced to a vanishingly small level for the compositions $Li_{4.4}Ti_5O_{12}$ and $Li_{4.6}Ti_5O_{12}$ and the intensity of impurity peaks at $2\theta = 27.46$ and 54.34 reduces up to composition $Li_{4.4}Ti_5O_{12}$ and maintained their existence for higher Li content composition. A new impurity peak at $2\theta = 43.63$ is also observed in the diffraction pattern of $Li_{4.6}Ti_5O_{12}$. This new impurity peak corresponds to a new phase Li_2TiO_3. This new phase having Li : Ti = 2 : 1 comes into existence due to presence of more than required Li content in the precursor.

66
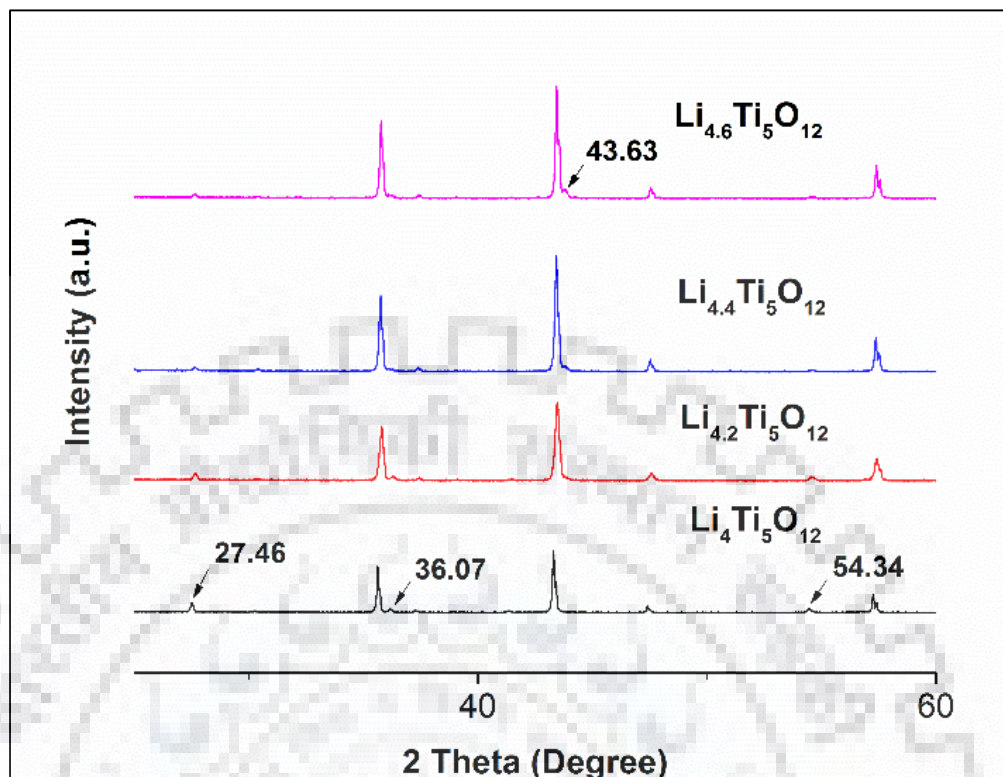
Figure 4.4. Enlarge View of XRD patterns of $Li_{4+x}Ti_5O_{12}$ (x = 0.2, 0.4 & 0.6)

Relative intensities of impurity peaks of TiO_2 are plotted against the excess Li content in $Li_{4+x}Ti_5O_{12}$ as shown in Figure 4.5. This can be clearly seen that the intensity of three impurity peaks of TiO_2 at 2θ = 36.07, 41.24 and 69.04 present in LTO reduced to zero level for the composition $Li_{4.4}Ti_5O_{12}$ and remaining two peaks at 2θ = 27.46 and 54.34 still exists with less than 2% relative intensity. For higher Li excess content composition $Li_{4.6}Ti_5O_{12}$ the intensity of impurity peaks at 2θ = 27.46 and 54.34 rises a bit higher compared to the intensity values for composition $Li_{4.4}Ti_5O_{12}$. On the basis of above analysis it can be concluded that ~10wt% of excess Li is required to achieve LTO phase with minimal impurities. These experimental observations are also in accordance with the theoretical estimate.
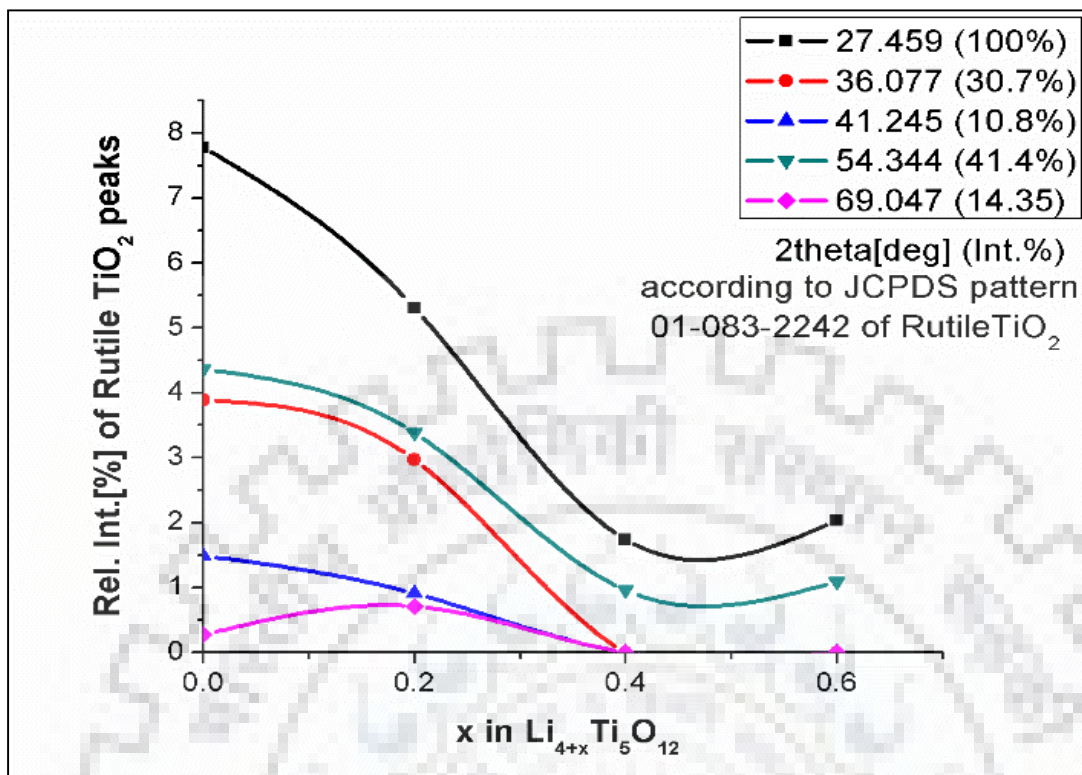
Figure 4.5. Relative intensity of TiO₂ impurity peaks in Li₄₊ₓTi₅O₁₂ (x = 0.2, 0.4 and 0.6)

4.2 Electrochemical Analysis of Li₄₊ₓTi₅O₁₂ (x = 0.2, 0.4 and 0.6)

Electrochemical analysis of all the samples prepared with desired compositions is performed with a view to observe the effect of phase purity in LTO compound on the lithium intake capacity. The fabricated cells of all compositions are subjected to charge-discharge at constant current of 0.1C rate in a potential range from 0-2.5V.

The first charge-discharge behaviors of $Li_{4+x}Ti_5O_{12}$ (x = 0, 0.2, 0.4 and 0.6) are shown in Figure 4.6. The characteristic curves are similar to that reported earlier(Alias, Kufian, Teo, Majid, & Arof, 2009; Yi et al., 2009, 2010a). The primary discharge plateau and second discharge plateau are found to be approximately at 1.55V and 0.68V vs. Li⁺/Li respectively for all the compositions (Wen et al., 2005). The first cycle discharged capacities obtained for $Li_4Ti_5O_{12}$, $Li_{4.2}Ti_5O_{12}$, $Li_{4.4}Ti_5O_{12}$ and $Li_{4.6}Ti_5O_{12}$ for the first cycle are 240 mAhg⁻¹, 289 mAhg⁻¹, 407 mAhg⁻¹ and 237 mAhg⁻¹ respectively. The composition $Li_{4.4}Ti_5O_{12}$ with minimal impurities compared to all other compositions also shows much higher discharge capacity than all other compositions. The discharge capacity of $Li_{4.4}Ti_5O_{12}$ is ~1.7 times higher than $Li_4Ti_5O_{12}$.
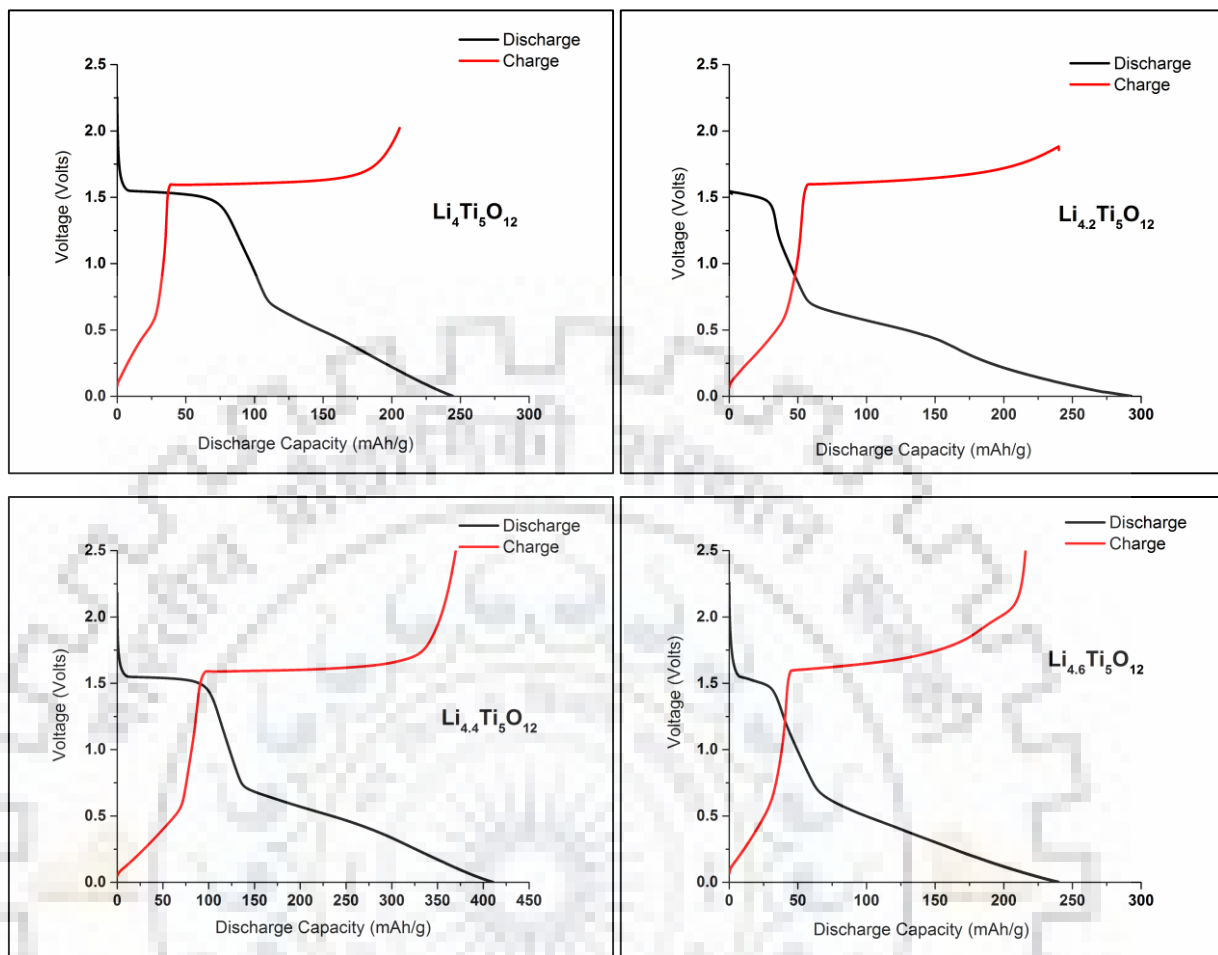
Figure 4.6 First Charge-discharge curves of $Li_{4+x}Ti_5O_{12}$ (x = 0.2, 0.4 and 0.6)

At this point we can say that phase pure component with suitable stoichiometry at the precursor level is very much essential for superior electrochemical characteristics.

$Li_{4.4}Ti_5O_{12}$ cell is further subjected to charge-discharge at different C-rates and the characteristic behaviours obtained are shown in Figure 4.7. The discharge capacities at 0.1, 0.2, 0.5, 1, 2 and 5C are 407 mAhg^{-1}, 323 mAhg^{-1}, 275 mAhg^{-1}, 228 mAhg^{-1}, 163 mAhg^{-1} and 76 mAhg^{-1} respectively.
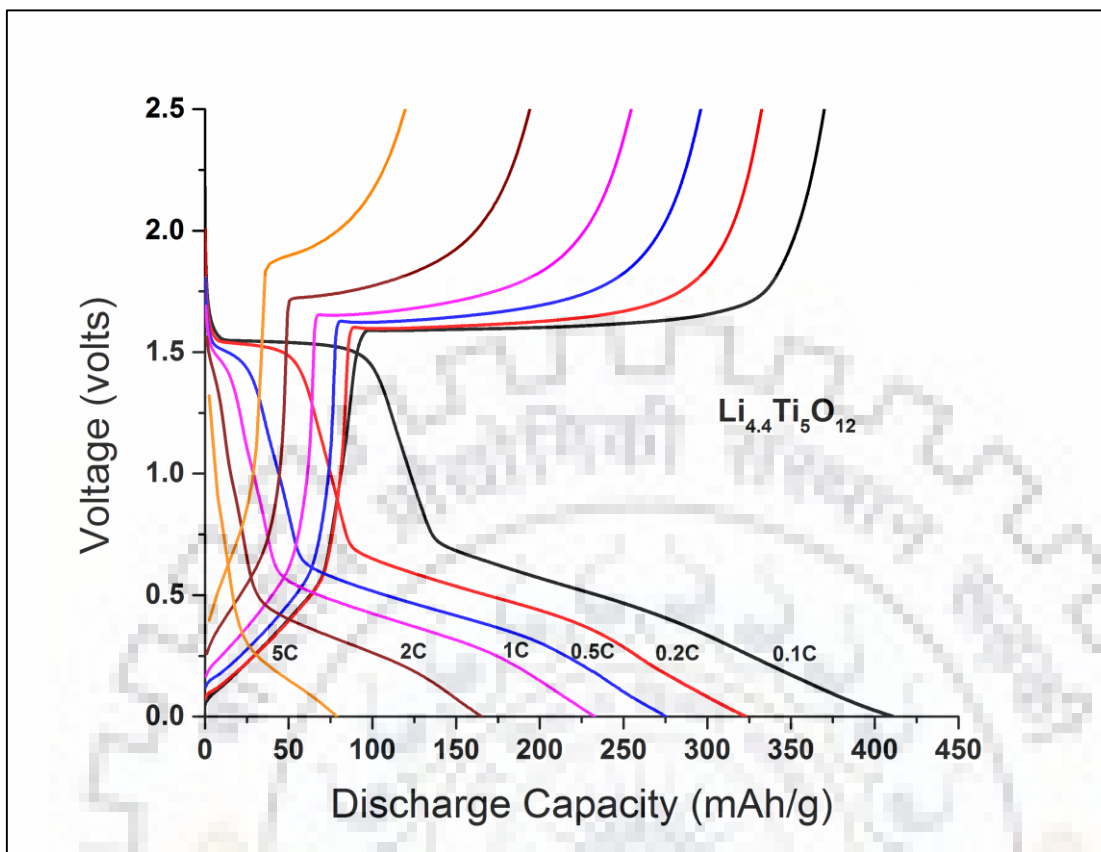
Figure 4.7 First Charge-discharge curves of Li$_{4.4}$Ti$_5$O$_{12}$ at different C-rates

4.3 Morphology of LTO

The particle size is one of the important factors which affects the discharge capacity of the electrode material. The TEM image of as prepared powder of LTO is shown in Figure 4.8. The observed particle size lies in the range 350nm to 400nm. The particles are of almost rounded shape.
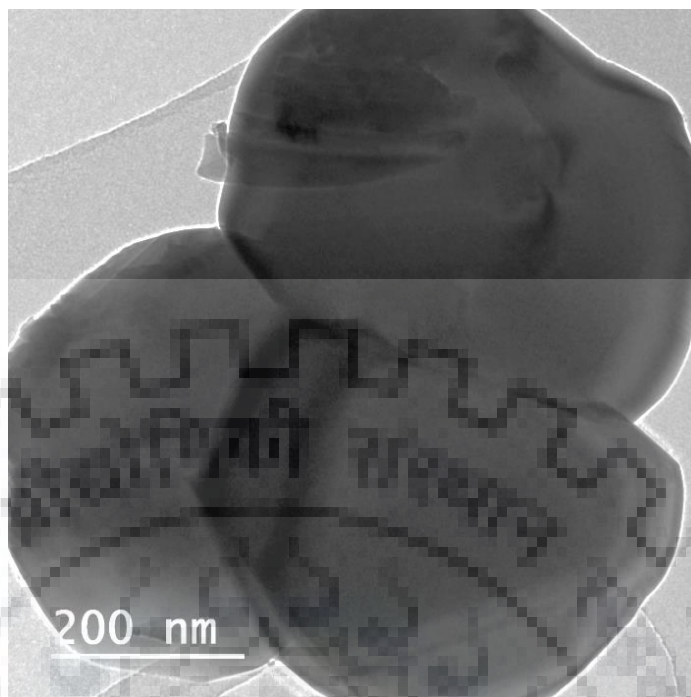
Figure 4.8 TEM image of Li$_{4.4}$Ti$_5$O$_{12}$

4.4 Nanoporous LTO (LTO-P)

The template method is used normally to develop porous structure in the material. Shao et al. prepared nanoporous LTO by using polystyrene spheres as template. The diameter of polystyrene sphere is 350nm which develop the pores of 100nm (Shao et al., 2012). Since the Li$^+$ ion size is much smaller, lower pore size is desirable. So far carbon nanobeads (CNBs) have not been used as template for developing the LTO-P material. The advantage of using CNBs as template is that it has particle size of less than 100nm so as to give rise the pores of less than 100nm in the material. Moreover it is all carbon, if the template is not completely removed even than it helps the material with its conductive properties. LTO-P has been synthesized by sol-gel method using CNBs incorporated at precursor level. CNBs were prepared by chemical vapour deposition (CVD) process using acetylene gas as carbon precursor source.

4.4.1 Morphological study of carbon nano beads

The FE-SEM image of carbon nano beads is shown in Figure 4.9. It can be observed that all the CNBs obtained are of almost uniform size and shape though these beads seem to be present attached to each other. It is confirmed from the TEM image of CNBs that the particle size is about 50-60nm. The SAED pattern confirms the amorphous nature of the carbon.
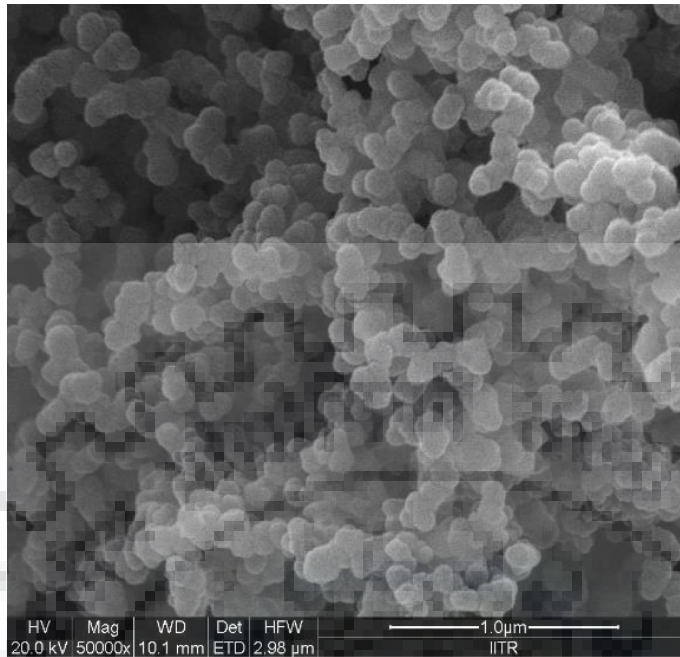
(a)
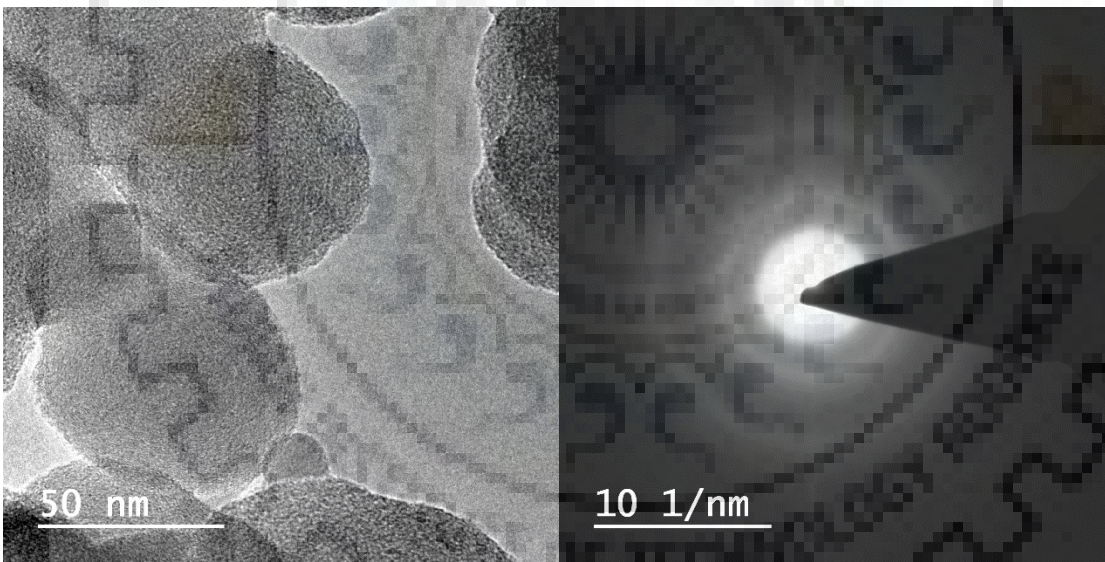
(b)   (c)

Figure 4.9 (a) FE-SEM image (b) TEM image (c) SAED pattern of CNBs

4.4.2 Analysis of XRD patterns of LTO and LTO-P

The XRD patterns are analyzed by Xpert High Score plus. The pattern is in accordance with JCPDS file no. 00-049-0207. It can be observed from the Fig. 4.10 that the XRD patterns of LTO-P and LTO materials are identical implementing that structure of LTO does not get altered with the addition of CNBs.
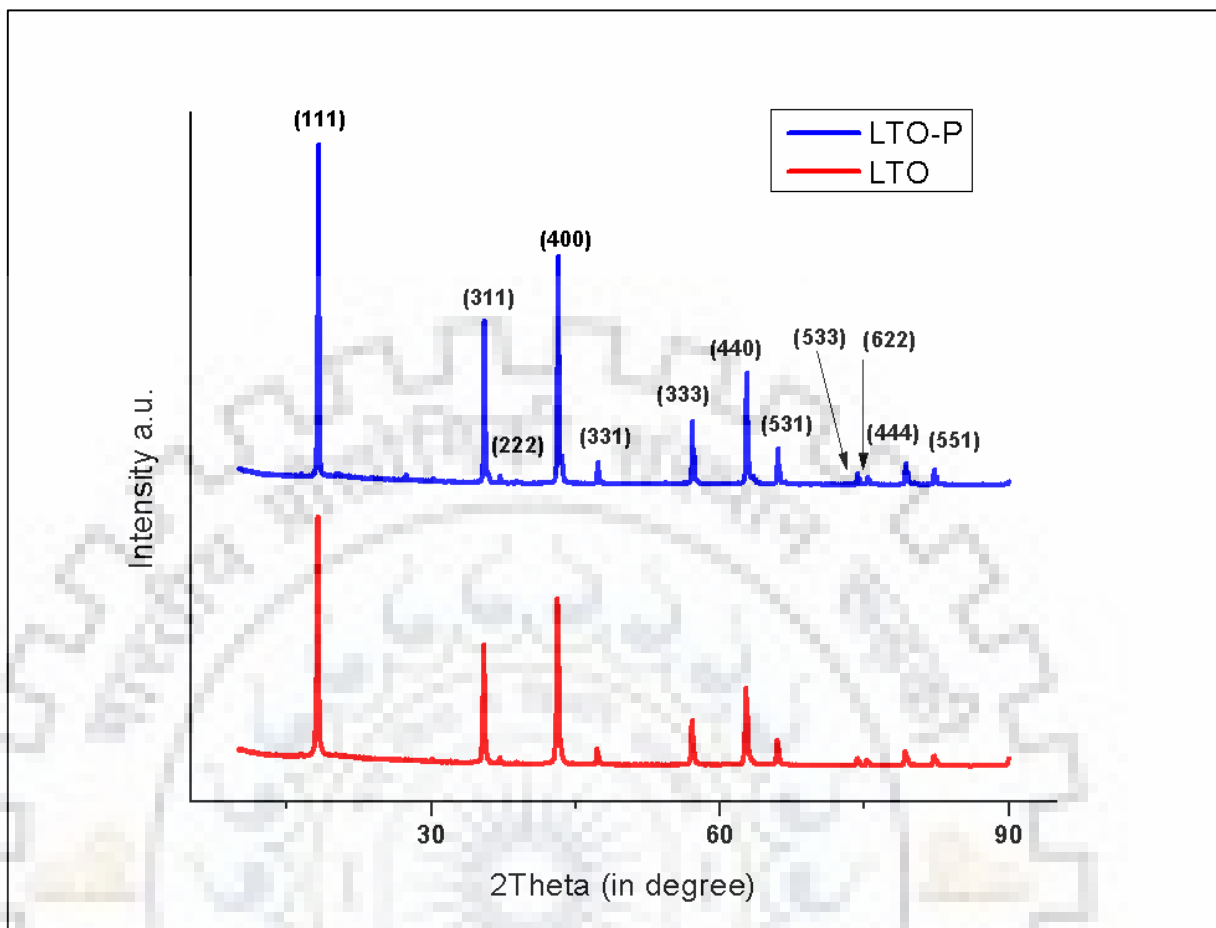
Figure 4.10 X-ray diffraction patterns of LTO-P AND LTO calcined in air at 800°C.

4.4.3 Morphological study of LTO-P

The FE-SEM image of LTO-P is shown in Figure 4.11. Pores on the particle surface are visible in the micrograph. Pore sizes were estimated from the particle micrographs taken at higher magnification as shown in Fig.4.12 and from the measured data average pore size is presented. The Table 4.1 shows that the average pore size of less than 100nm is achieved.
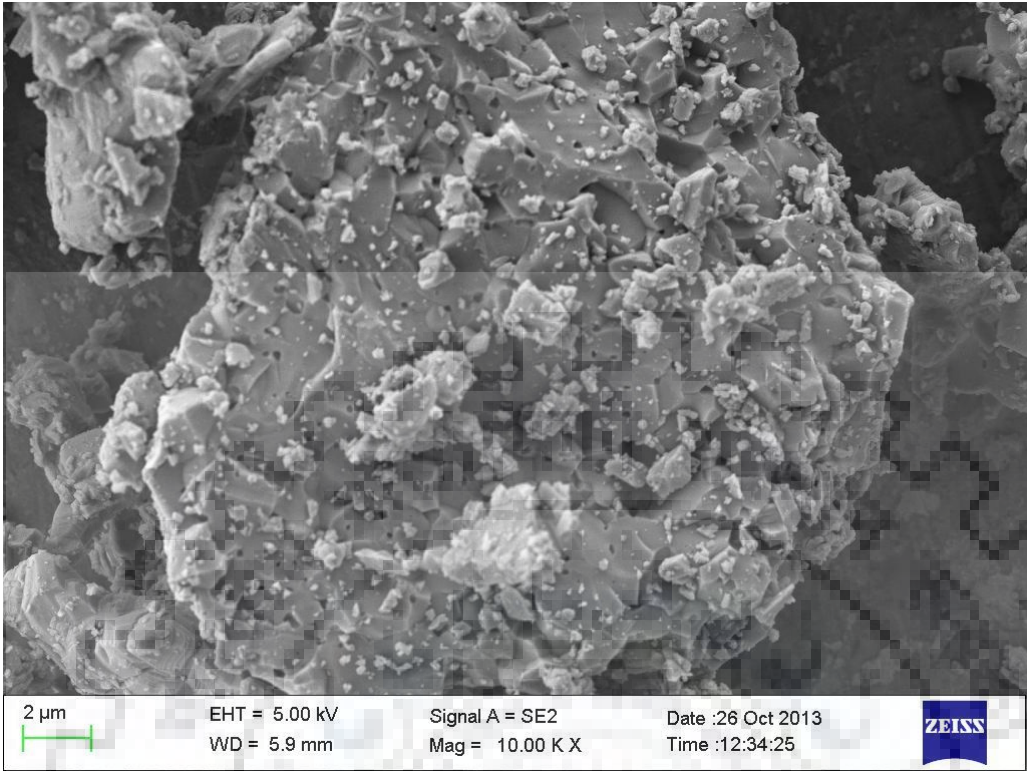
Figure 4.11 FE-SEM image of LTO-P
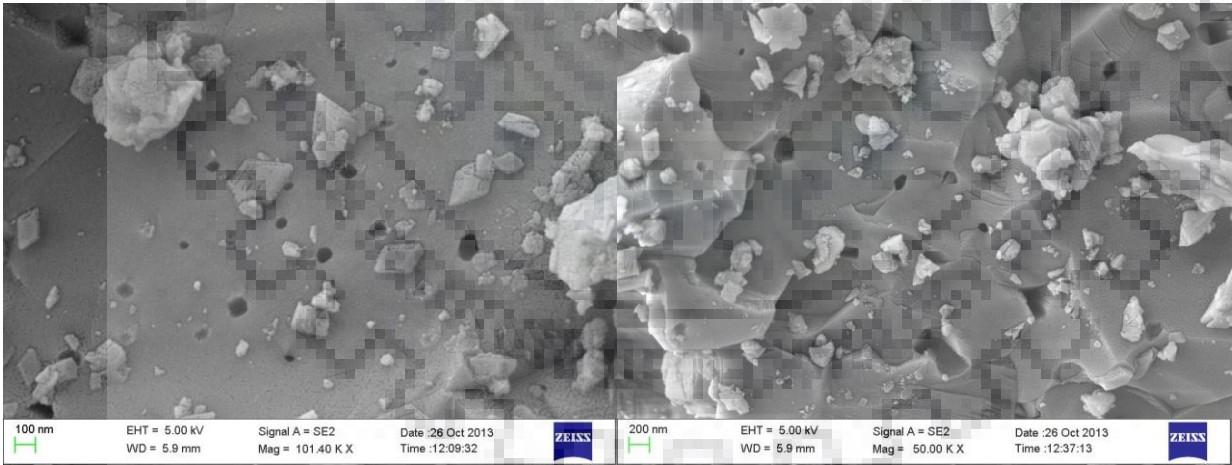
Figure 4.12 FE-SEM images of two different particles of LTO-P at higher magnification

Table 4.2 Measured pore sizes of two different particles shown in Figure 4.12

Pore size (in nm) of different pores									Average pore size
For Figure 4.13(a)									
120	50	75	50	35	70	125	35	35	**66.4**
For Figure 4.13(b)									
50	70	150	150	100	300	200	150	100	**140**

4.4.4 BET of LTO and LTO-P

The obtained surface area of LTO and LTO-P were measured as 1.2485 m²/g and 4.0784 m²/g respectively from BET analysis. It means that the surface area of LTO-P is more than three times greater than the surface area of LTO.

4.4.5 Electrochemical analysis of LTO and LTO-P
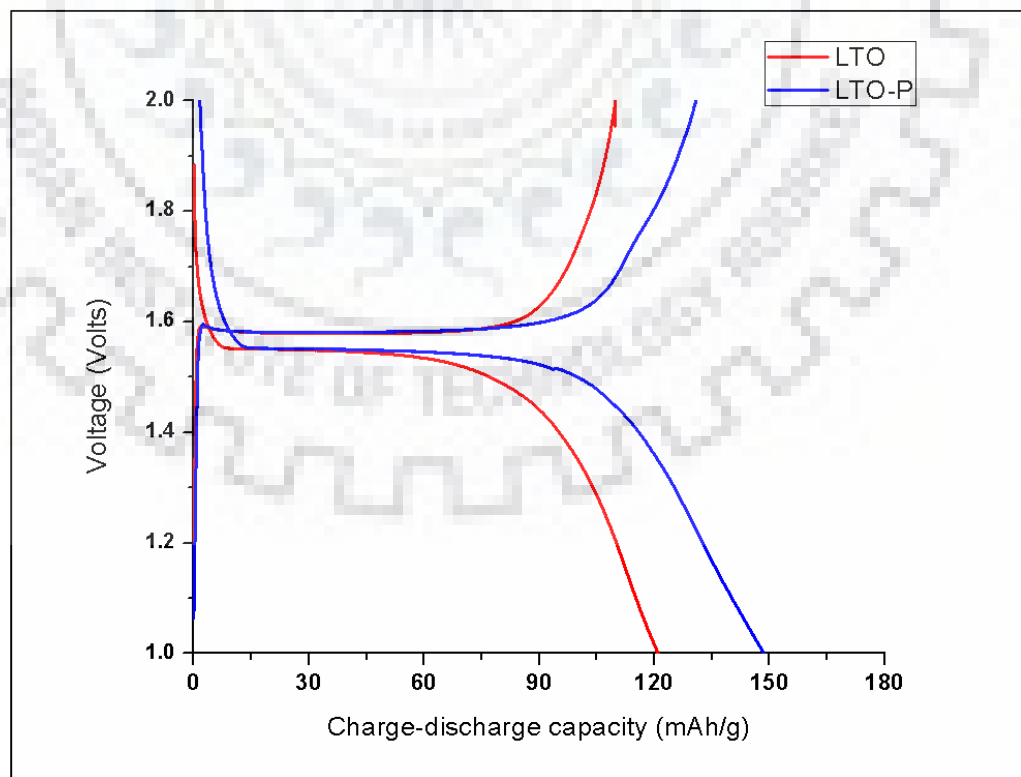
Figure 4.13 Charge-discharge behaviors of LTO & LTO-P at 0.1C rate

The charge-discharge behaviors of LTO and LTO-P at 0.1 C-rate in the potential window 1-2V are shown in Figure 4.13. LTO-P has achieved a discharge capacity of 148mAhg^{-1} which is much higher than the discharge capacity achieved by LTO which is 121mAhg^{-1}. The first discharge plateau is at 1.58 V for both the materials. The difference in the discharge capacity is due to nanoporous structure of LTO-P which increases electrode–electrolyte interaction area. Cyclic voltammetry (CV) is also performed at an input voltage rate of 0.1mV/sec as shown in Figure 4.14. Both the profiles show a pair of reversible redox peaks near the potential of 1.55V vs. Li$^+$/Li, corresponding to Ti$^{3+/4+}$ accompanying Li$^+$-ion insertion and extraction. This indicates that Li$^+$ ions can successfully insert/extract in both the materials. The peak value of the current in the CV of LTO-P is higher than LTO, also the reduction and oxidation peaks are less broaden compared to that of LTO which confirms that the prepared LTO-P material has superior electrochemical performance than LTO. Similar characteristic curves of CV are obtained by Shao et al. for nanoporous LTO (Shao et al., 2012).
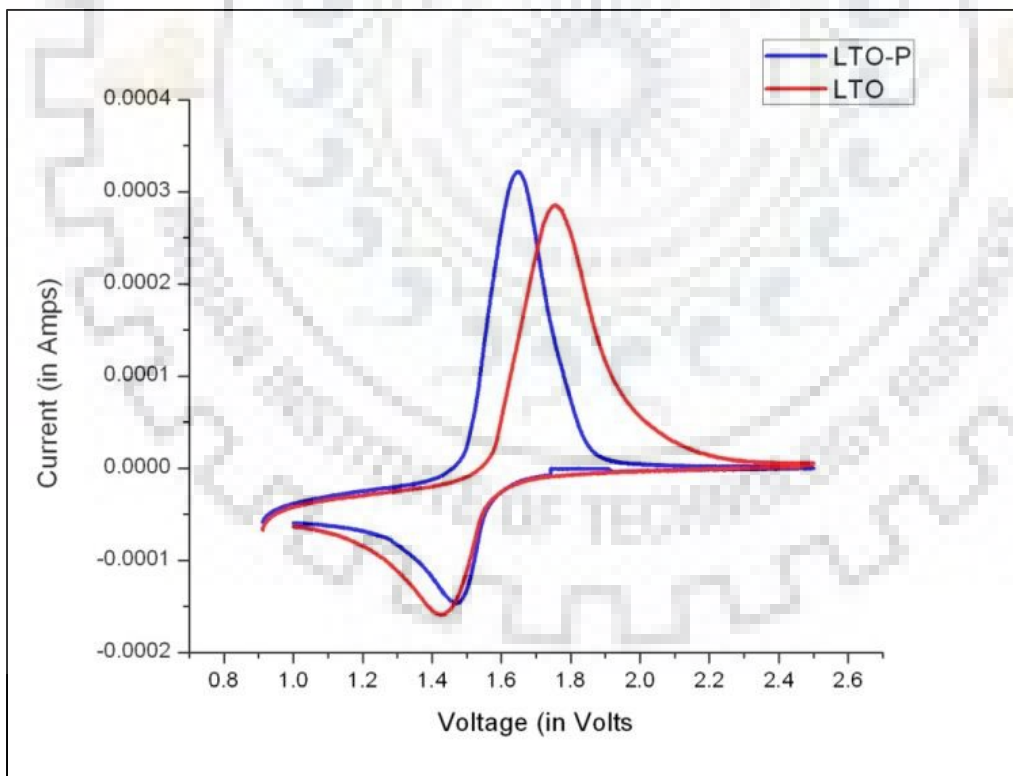
Figure 4.14 Cyclic voltammetry of LTO & LTO-P at 0.1mv/sec

Summary

LTO was synthesized by so-gel process with stoichiometric ratio Li:Ti = 4:5 calcined in air at 800°C. Quantitative analysis of LTO (Li :Ti = 4:5) shows presence of rutile TiO_2 phase as impurity in the LTO compound by 7.8 wt. %. Outcome of theoretical calculations based on quantitative analysis is that 10.07 wt. % of excess Li is required for phase pure LTO. $Li_{4+x}Ti_5O_{12}$ (x = 0.2, 0.4 and 0.6) were synthesized again with 5, 10 and 15wt. % of excess Li respectively. XRD analysis reveals that TiO_2 almost vanished in $Li_{4.4}Ti_5O_{12}$ (10wt. % of excess Li) and a new Li_2TiO_3 phase exists in $Li_{4.6}Ti_5O_{12}$ (15wt % of excess Li). Experimental observations are in accordance with the theoretical estimates.

Nanoporous structure of LTO has been prepared by carbon nano beads as source of pores. Average pore size of less than 100nm (~ 66nm) is observed. Smaller particles (of size less than 500 nm) do not have pores. Structure of LTO does not get altered with the addition of CNBs. LTO-P shows better electrochemical performance than non-porous LTO with discharge capacity of 148mAhg^{-1} compared to 121mAhg^{-1} achieved by LTO. This is due to that the surface area of achieved by nanoporous structure of LTO-P is three times than that of LTO.

Vanadium doped $Li_4Ti_5O_{12}$ for lithium ion battery anode material

Vanadium doped Li$_4$Ti$_5$O$_{12}$ for lithium ion battery anode material

LTO with enhanced properties can replace the conventional carbonaceous anode material of lithium ion battery. Vanadium doped LTO (Li$_4$Ti$_{5-x}$V$_x$O$_{12}$, x = 0, 0.05, 0.1, 0.15) materials are synthesized by sol-gel process followed by calcination of dried gel in air and argon atmosphere separately to examine the role of calcination atmosphere on the oxidation state of V and Ti. The electronic conductivity and electrochemical performance of the synthesized samples as anode of lithium ion battery are analyzed and the results are presented in this chapter. It is understood from the literature review that both doping and synthesis in reducing atmosphere increase the conductivity of the material and the probable cause for such increase is the reduction of Ti^{4+} to Ti^{3+} (Yi et al., 2009, 2010a; Yu et al., 2011). It is still ambiguous that reduction of Ti ion occurs either due to doping or calcination in reducing atmosphere. Detail study on oxidation states of V and Ti is performed to understand the behaviour.

LTO based powders studied in three different compositions viz. Li$_4$Ti$_{5-x}$V$_x$O$_{12}$ where x = 0.05, 0.1 & 0.15 are designated as VLTO-05, VLTO-10 & VLTO-15 for air calcined samples and VLTO-05AR, VLTO-10AR & VLTO-15AR for argon calcined samples respectively. The pristine samples of LTO are also synthesized in air and argon atmosphere and the samples are identified as LTO and LTOAR respectively. The 10% excess Li content is used in making all the samples to keep the TiO$_2$ impurity at level minimum level as discussed in chapter 4.

For electronic conductivity measurements, the powder samples were compacted in the form of cylindrical pellets by hydraulic press followed by heat treatment. Ohmic contacts were developed by applying silver paste onto flat surfaces of pellets for electrical connections.

5.1 XRD analysis of Li$_4$Ti$_{5-x}$V$_x$O$_{12}$ calcined in air and argon atmosphere

The prepared samples were subjected to XRD analysis for phase determination.
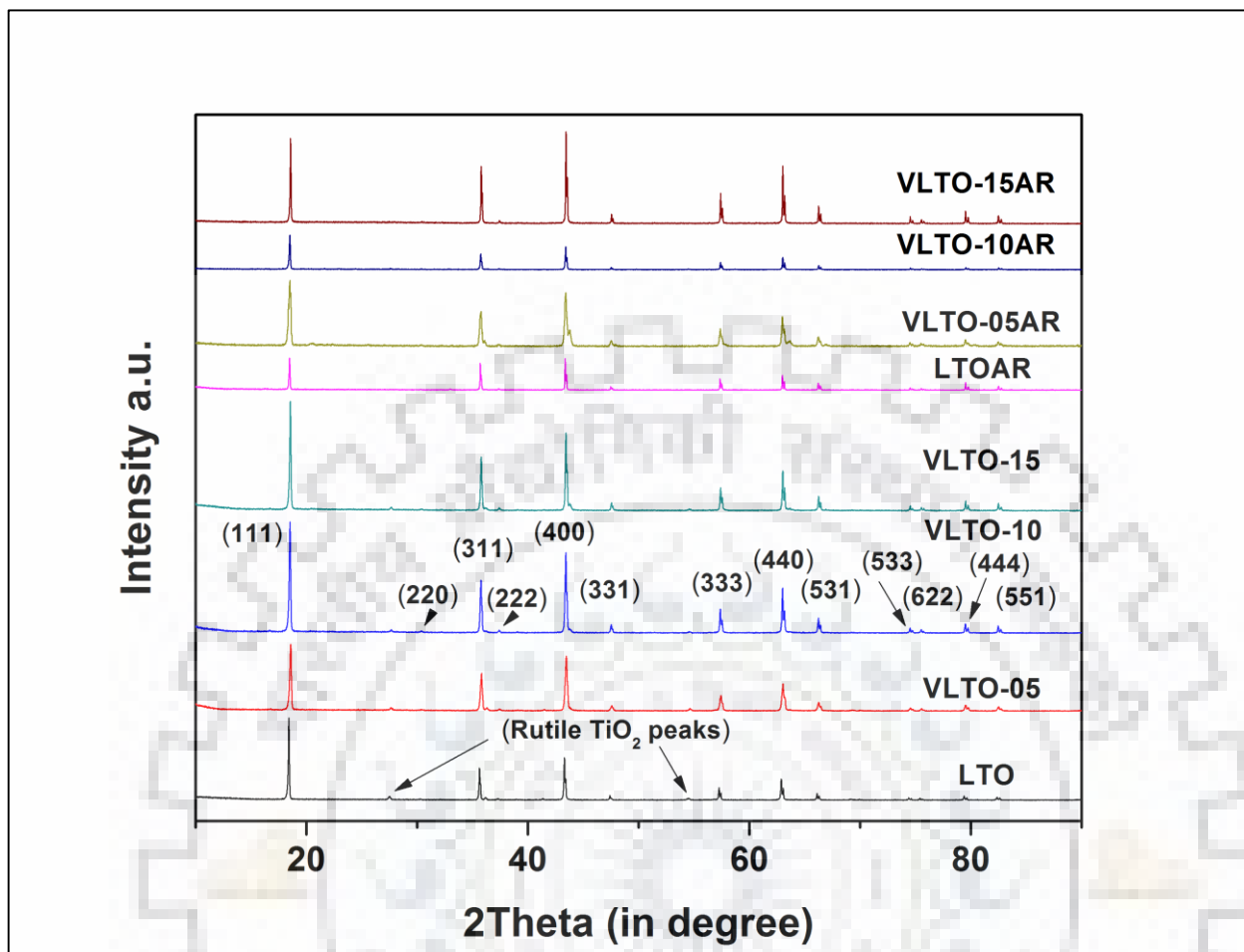
Figure 5.1: XRD patterns of Li$_4$Ti$_{5-x}$V$_x$O$_{12}$ (x = 0, 0.05, 0.1 and 0.15) calcined in air and argon atmosphere

XRD patterns of the different samples are shown in Figure 5.1 and are found in accordance with JCPDS file no. 00-049-0207 of LTO with cubic spinel structure having Fd3m space group. The two weak diffraction peaks at $2\theta = 27.45°$ and $54.34°$ are in accordance with JCPDS file no. 01-083-2242 and correspond to rutile TiO$_2$ phase having intensity less than 2%. These impurity peaks were also observed in the XRD pattern of LTO synthesized with 10% excess Li content (chapter 4). The presence of TiO$_2$ impurity peaks in the XRD pattern of is due to evaporation of Li while calcination at 800°C. In the case of argon calcined samples the TiO$_2$ impurity peaks are absent and this may happen due to the reason that in oxygen deficient atmosphere oxygen vacancies in the LTO lattice structure creates some stress which suppresses the Li evaporation.
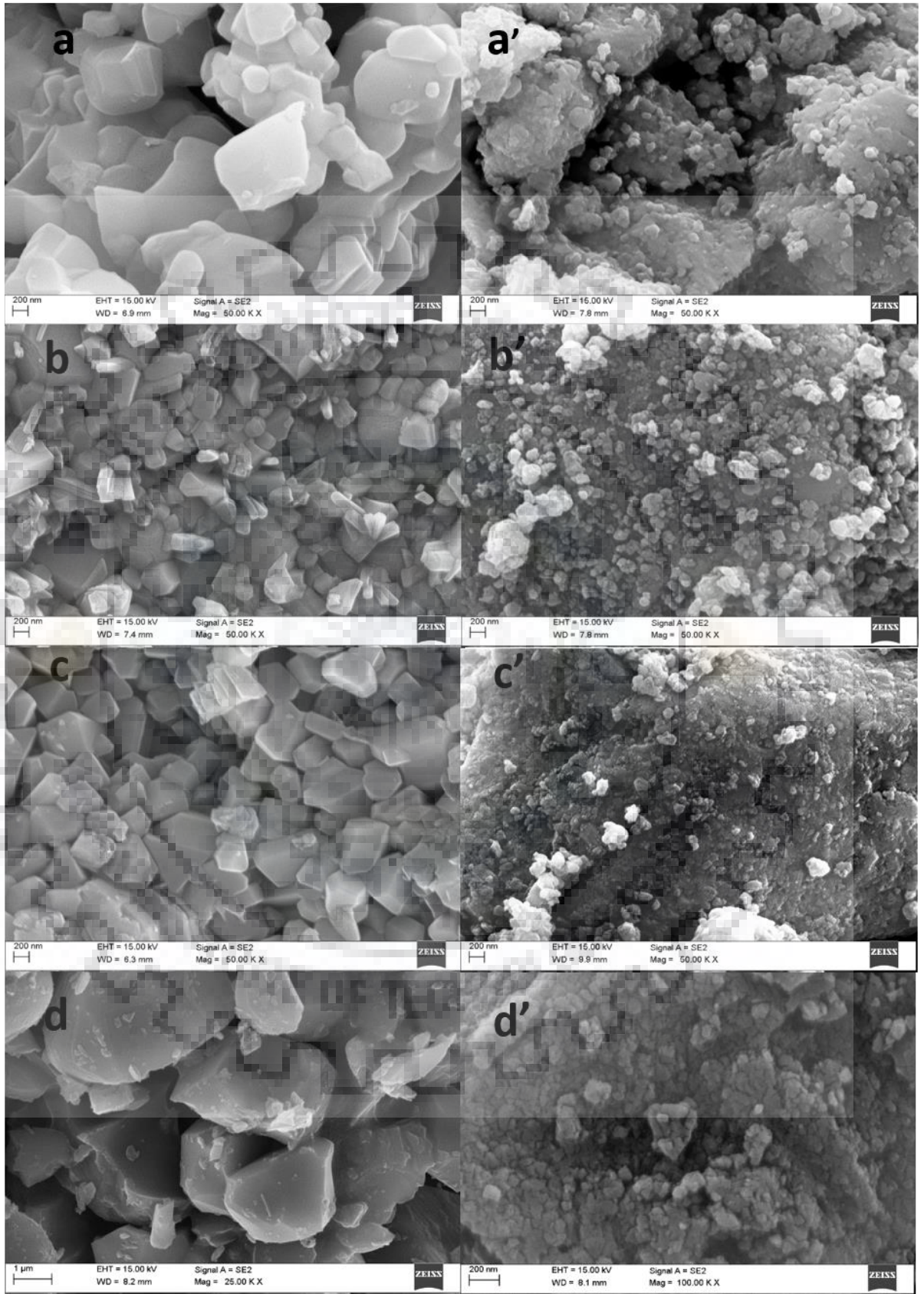
Figure 5.2: FE-SEM images of (a) LTO, (a') LTOAR, (b) VLTO-05, (b') VLTO-05AR, (c) VLTO-10, (c') VLTO-10AR, (d) VLTO-15 and (d') VLTO-15AR

All the samples exhibit similar patterns with no additional peak showing the V containing phase. This observation therefore confirms that V has been able to occupy the empty Ti sites. The major (higher intensity) XRD peaks of the V doped samples are found not undergoing any appreciable angular shift with respect to those of pristine sample, it may be inferred that the lattice parameter of the unit cell of doped compound remains unaltered. This can be attributed to the fact that the difference in ionic radii of V^{5+} (0.54Å), V^{4+} (0.58 Å) and Ti^{4+} (0.60 Å) is not appreciable to cause lattice parameter change. The intensities of XRD peaks of argon calcined samples is low compared to those of air calcined samples which can be attributed to the much smaller particle size of the argon calcined samples. The details related to particle size of the different samples are explained in the next section.

5.2 Morphological studies of $Li_4Ti_{5-x}V_xO_{12}$ calcined in air and argon atmosphere

Morphologies of $Li_4Ti_{5-x}V_xO_{12}$ powder synthesized in air and argon atmosphere are shown in Figure 5.2. The particle size distribution was estimated from the micrographs using Image J software. LTO, VLTO-05, VLTO-10 and VLTO-15 were found to have the particle size in the range of 165 - 915nm, 112 - 478nm, 331 - 577nm and 2919 - 3291nm respectively, showing that VLTO-10 has relatively smaller size variation spread. Moreover, the lowest average particle size was resulted in the case of VLTO-05 and with increase in doping level of V particle size increases. As can be seen from the micrographs in Figure 5.2 (a', b', c', d') that the particle size ranges of the $Li_4Ti_{5-x}V_xO_{12}$ calcined in argon atmosphere is much smaller (< 50nm) than the corresponding compositions of powders calcined in air. The particle shape for all the powders especially for air calcined samples as seen from the micrographs in Figure 5.2 is largely regular.

5.3 XPS analysis for oxidation states of V and Ti

XPS was performed for confirming the oxidation states of V and Ti in the compounds $Li_4Ti_{5-x}V_xO_{12}$. XPS data has been collected after sputter-etching done at low energy level. Survey spectra of LTO, VLTO-05, VLTO-10 and VLTO-15 are shown in Figure 5.3 in which V_{2p} peak is observed in all the V doped LTO samples confirming the presence of V in the doped LTO samples.
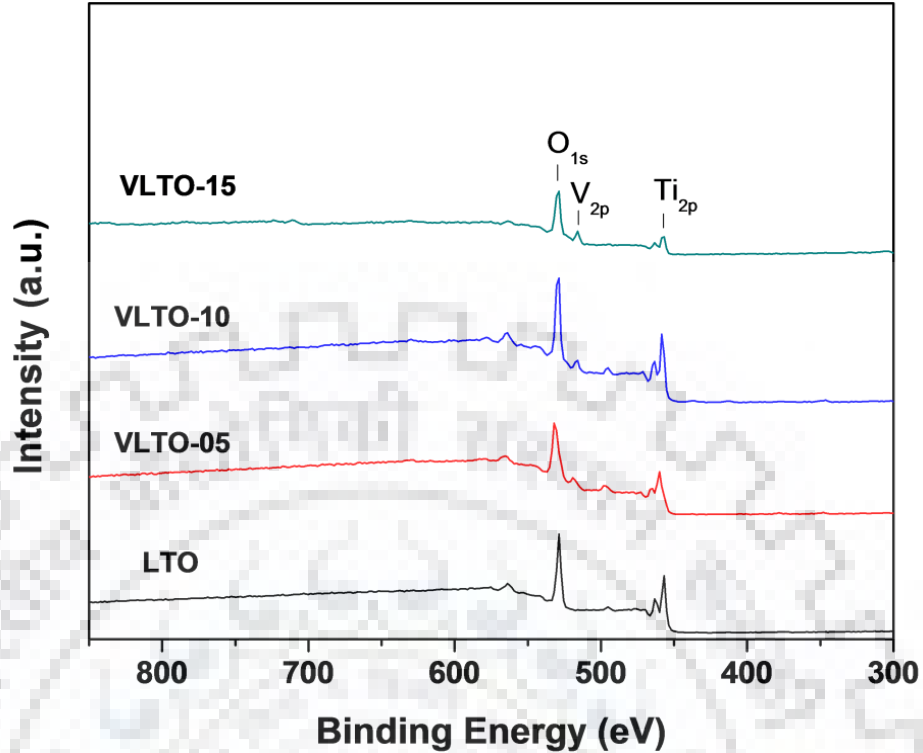
Figure 5.3: Survey spectra of $Li_4Ti_{5-x}V_xO_{12}$ (x = 0, 0.05, 0.1 and 0.15)

To verify the oxidation state of the V, the V_{2p} peaks of $Li_4Ti_{5-x}V_xO_{12}$ calcined in air and argon atmosphere were magnified and de-convoluted using software XPSPEAK4.1 as shown in Figure 5.4. The peaks obtained at binding energies 517.3eV and 516.5eV can be assigned to V^{5+} and V^{4+} respectively (Wanger et al., 1991). V_{2p} peaks of all the V doped LTO samples are also shown in their original forms along with the de-convoluted peaks in the Figure 4.1. All of them have good signal to noise ratio (S/N) except the for the peak of VLTO-10 sample. This may happened due to sudden disturbance occurred in the XPS instrument while recording the data. The proportion of V in two different oxidation states of 5+ and 4+ has been estimated by calculating the area under the deconvoluted peaks.

Table 5.1 represents the peak parameters estimated by software including peak positions, area under curve, FWHM and percentage of V^{5+} and V^{4+} oxidation states. V^{4+} is present in VLTO-10AR and VLTO-15AR as reduction of V takes place during calcination in reduced atmosphere but may be due to very low doping concentration the atomic % of V^{4+} in VLTO-05AR is lower than minimum detection limit of the instrument (Shard, 2014). The presence of V^{4+} in VLTO-15 indicates higher doping concentration leads to reduction of some V^{5+} into V^{4+} even in non-reducing atmosphere.
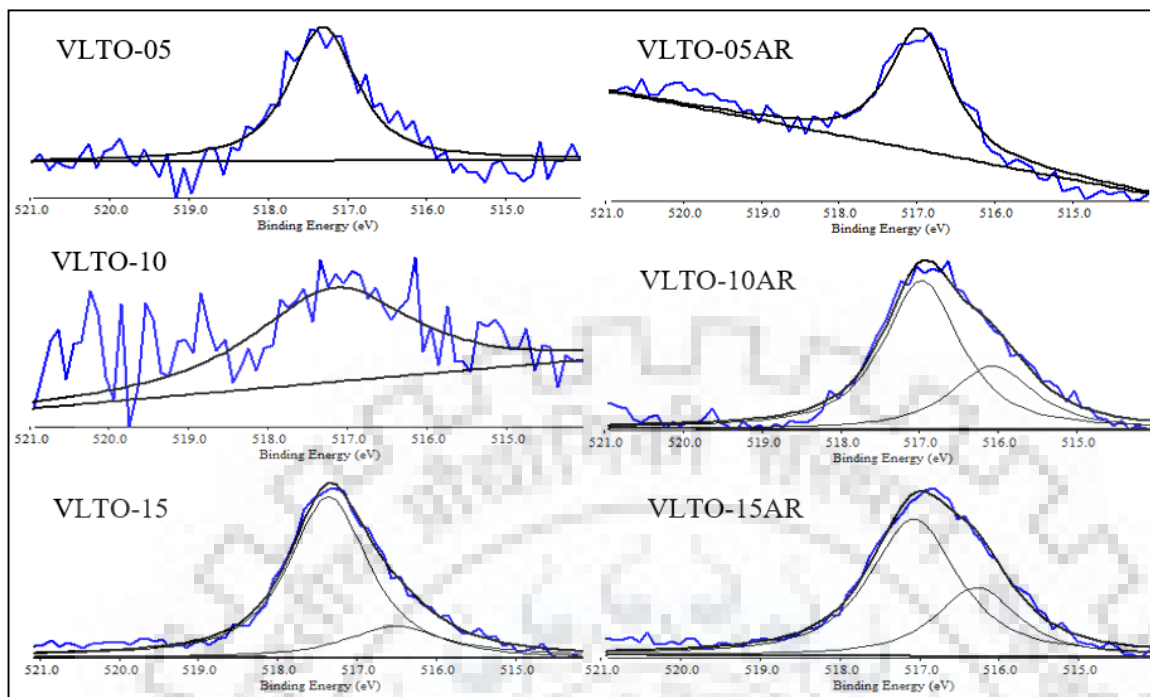
Figure 5.4: Deconvoluted V$_{2P}$ XPS peaks of V doped LTO calcined in air and argon atmosphere

Table 5.1: The V$_{2P}$ XPS peaks parameters of V doped LTO

Sample		Peak Position (eV)	Area (a.u.)	FWHM (eV)	%
(VLTO-05)	V^{5+}	517.307	169.423	1.009	100
(VLTO-10)	V^{5+}	517.019	84.786	1.826	100
(VLTO-15)	V^{5+}	517.354	775.431	1.197	80.5
	V^{4+}	516.509	187.83	1.479	19.5
(VLTO-05AR)	V^{5+}	516.955	499.416	0.967	100
(VLTO-10AR)	V^{5+}	516.97	1036.817	1.174	68.23
	V^{4+}	516.07	482.994	1.276	31.77
(VLTO-15AR)	V^{5+}	517.072	1171.568	1.315	68.13
	V^{4+}	516.281	548.038	1.227	31.87

86
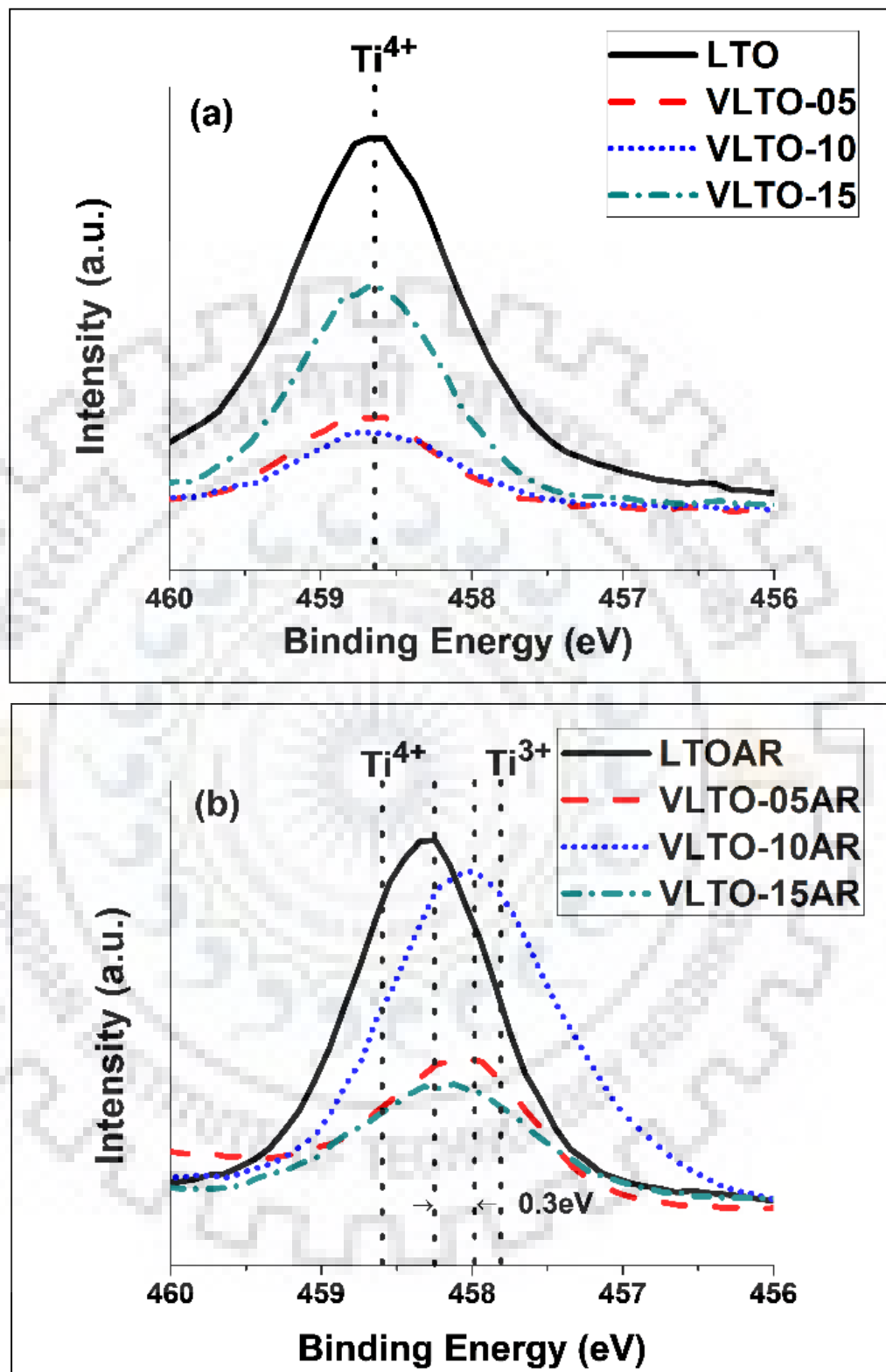
Figure 5.5: Ti 2p$_{3/2}$ XPS peaks of Li$_4$Ti$_{5-x}$V$_x$O$_{12}$ (x = 0, 0.05, 0.1 and 0.15) (a) calcined in air, (b) calcined in argon atmosphere

The Ti 2p$_{3/2}$ XPS peaks of Li$_4$Ti$_{5-x}$V$_x$O$_{12}$ synthesized in air and argon atmosphere were also analyzed to understand the effect of doping and calcination atmosphere on the reduction of Ti^{4+} ions to Ti^{3+} ions. This can be observed from Figure 5.5(a) that Ti 2p$_{3/2}$ peaks of all the air calcined Li$_4$Ti$_{5-x}$V$_x$O$_{12}$ were appeared at the same binding energy corresponding to Ti^{4+} peak showing that V doping in LTO does not reduces Ti^{4+} to Ti^{3+} on calcination of the dried gel in air. Therefore, the additional charge of V^{5+} in air calcined Li$_4$Ti$_{5-x}$V$_x$O$_{12}$ must be compensated by the creation of defects in the lattice structure of LTO.

The Ti 2p$_{3/2}$ peaks of argon calcined Li$_4$Ti$_{5-x}$V$_x$O$_{12}$ were appeared in between the binding energies corresponding to Ti^{4+} peak (458.6 eV) and Ti^{3+} peak (457.8 eV) as shown in Figure 5.5(b) showing Ti ions partially exits in 3+ oxidation state also.

The results are in agreement with the XPS spectra if Ti 2p$_{3/2}$ obtained by Q. Zhang et al. for W doped LTO. The peaks of V doped LTO obtained were shifted more (~ 0.3eV) towards the Ti^{3+} peak as compared to that of pristine LTOAR. Such shift indicates that doping of V in LTO further increases the proportion of Ti ions in 3+ state (Zhang et al., 2013).

5.4 Electrochemical Analysis of Li$_4$Ti$_{5-x}$V$_x$O$_{12}$ calcined in air and argon atmosphere

5.4.1 Electrochemical Impedance Spectroscopy (EIS)

The potentiostatic EIS Nyquist plots of air and argon calcined Li$_4$Ti$_{5-x}$V$_x$O$_{12}$ electrodes with lithium metal as counter electrode in teflon cell assembly are shown in Figure 5.6(a) and (b) respectively. The plots intercepted the real axis at highest frequency correspond to the resistance (R$_s$) of the electrolyte.

There is a semicircle in the intermediate frequency region which is followed by profile portion showing slanted line towards the low frequency region. The Z$_{Real}$ value corresponds to the end of semicircle from where the slanted line starts is designated as R$_{ct}$ which shows lithium ion transfer resistance at electrode-electrolyte interface and particle-particle contact resistance during the electrochemical reaction of the cell. The slanted line corresponds to Warburg impedance (Z$_w$) experienced by lithium ion while diffusing inside the electrode. The electrical circuit shown in Figure 5.6 represents equivalent electrical model of lithium ion cell in which constant phase element (CPE) exhibits non-faradaic charge storage mechanism i.e. capacitance due to deposition of charge on the surface of the electrodes.

The Warburg impedance coefficient σ_w can be obtained from the slope of the linear portion in the plot Z_{Real} vs. $\omega^{-1/2}$ presented in Figure 5.6. The relationship is expressed as

$$Z_{Real} = R_S + R_{ct} + \sigma_w \omega^{-1/2} \qquad \dots (1)$$

D_{Li+} has been calculated following the expression:-

$$D_{Li+} = 0.5 \left(\frac{RT}{AF^2 \sigma_w C}\right)^2 \qquad \dots (2)$$
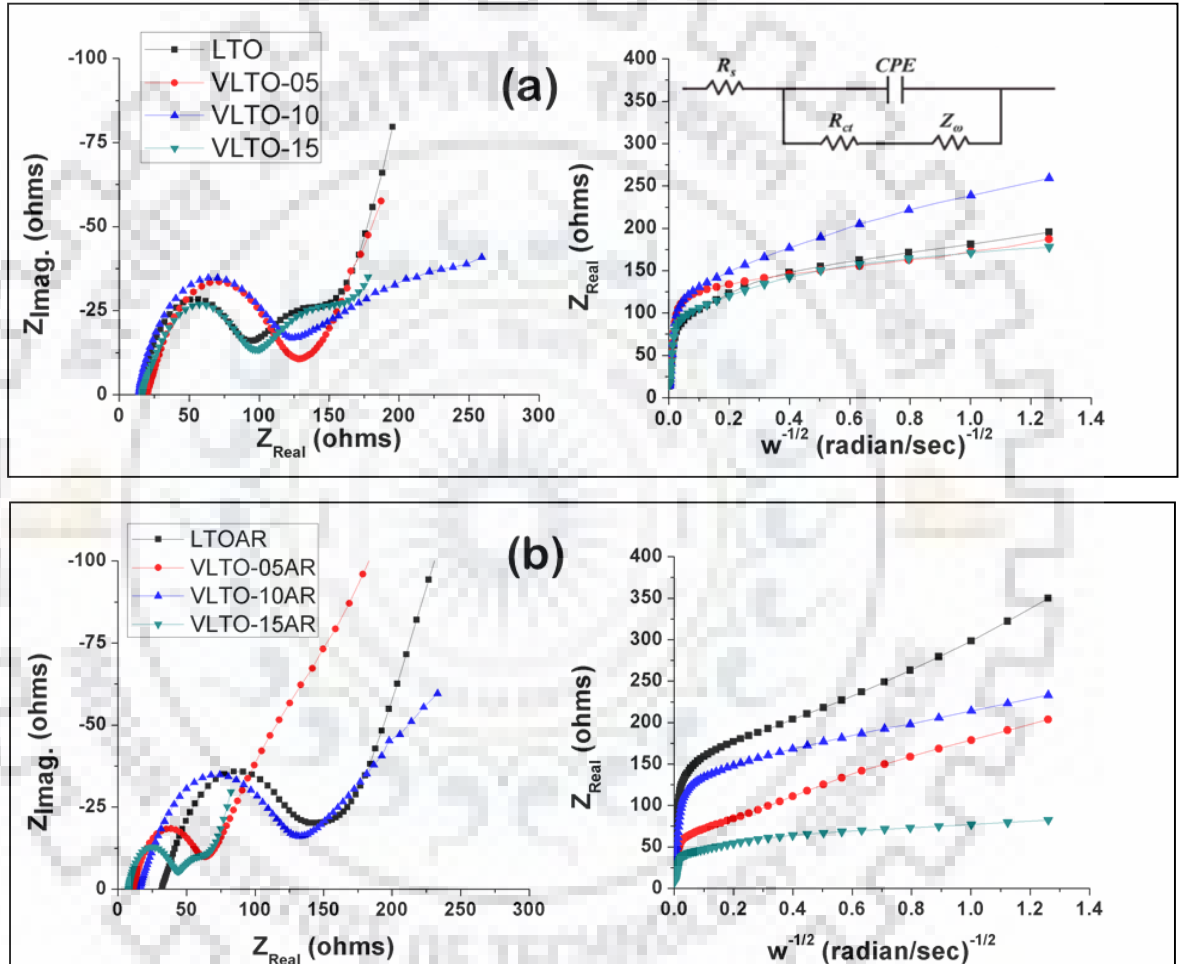
Figure 5.6: EIS Nyquist plots and Z_{Real} vs. $\omega^{-1/2}$ plots of electrodes (assembled in teflon cell) prepared from $Li_4Ti_{5-x}V_xO_{12}$ (a) calcined in air atmosphere (b) calcined in argon atmosphere

where R is the gas constant, T is the room temperature, A is area of contact between anode and electrolyte which is $0.785\,cm^2$ for electrode diameter of 10mm, F is the Faraday constant and C is the molar concentration of Li^+ ions. The impedance parameters derived from the Nyquist plots shown in Figure 5.6 are listed in the Table 5.2 which shows that the change in resistance (R_S) is

not very significant across all the samples. However, the variation of R_{ct} values is relatively large i.e. varying from as low as 44 to as high as 142 ohms.

Table 5.2: Impedance parameters derived by EIS plots of Li$_4$Ti$_{5-x}$V$_x$O$_{12}$ electrodes studied in teflon cell assembly

Samples\Parameters	R_S (Ω)	R_{ct} (Ω)	σ_w (Ω cm^{2}s$^{-1/2}$)	D_{Li+} (cm^{2}s^{-1})
LTO	14.47	93.44	69.35	7.40×10^{-14}
VLTO-05	20.03	129.2	68.91	7.50×10^{-14}
VLTO-10	13.96	123.38	96.56	3.82×10^{-14}
VLTO-15	16.18	98.95	49.65	1.44×10^{-13}
LTOAR	31.15	141.87	212.59	7.88×10^{-15}
VLTO-05AR	11.53	62.95	144.67	1.70×10^{-14}
VLTO-10AR	15.89	131.86	115.86	2.65×10^{-14}
VLTO-15AR	7.79	44.12	41.19	2.09×10^{-13}
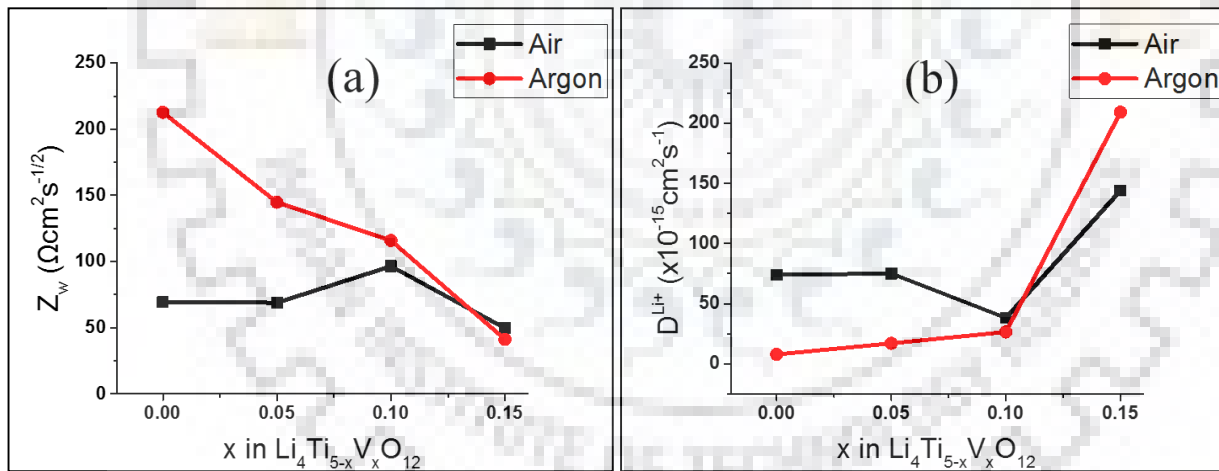
Figure 5.7: (a) Warburg impedance coefficient (σ_w), (b) Lithium ion diffusion coefficient (D_{Li+}) with doping concentration of V in LTO

The σ_w and D_{Li+} of air and argon calcined Li$_4$Ti$_{5-x}$V$_x$O$_{12}$ are plotted and compared in Figure 5.7. The lithium ion diffusion coefficient increases gradually with the increase in V concentration in argon calcined Li$_4$Ti$_{5-x}$V$_x$O$_{12}$ up to x = 0.10 and a larger increase occurs between x = 0.10 and 0.15, however, for air calcined Li$_4$Ti$_{5-x}$V$_x$O$_{12}$ a continuous rise in D_{Li+} was not observed which may be attributed to the variation in particle size of the powder with the increase in doping concentration as described in sec 5.2. As evident from equation (2) D_{Li+} is inversely

proportional to the square of area of contact between anode and electrolyte and reduction in particle size increases this contact area. Argon calcined $Li_4Ti_{5-x}V_xO_{12}$ have much smaller particle size than air calcined $Li_4Ti_{5-x}V_xO_{12}$, therefore D_{Li+} becomes low when calcination is done in argon atmosphere. The D_{Li+} in case of VLTO-15AR is highest since doping concentration is quite high causing σ_w very low which overcomes the particle size effect as D_{Li+} is also inversely proportional to the square of σ_w.

5.4.2 Charge-discharge characteristics
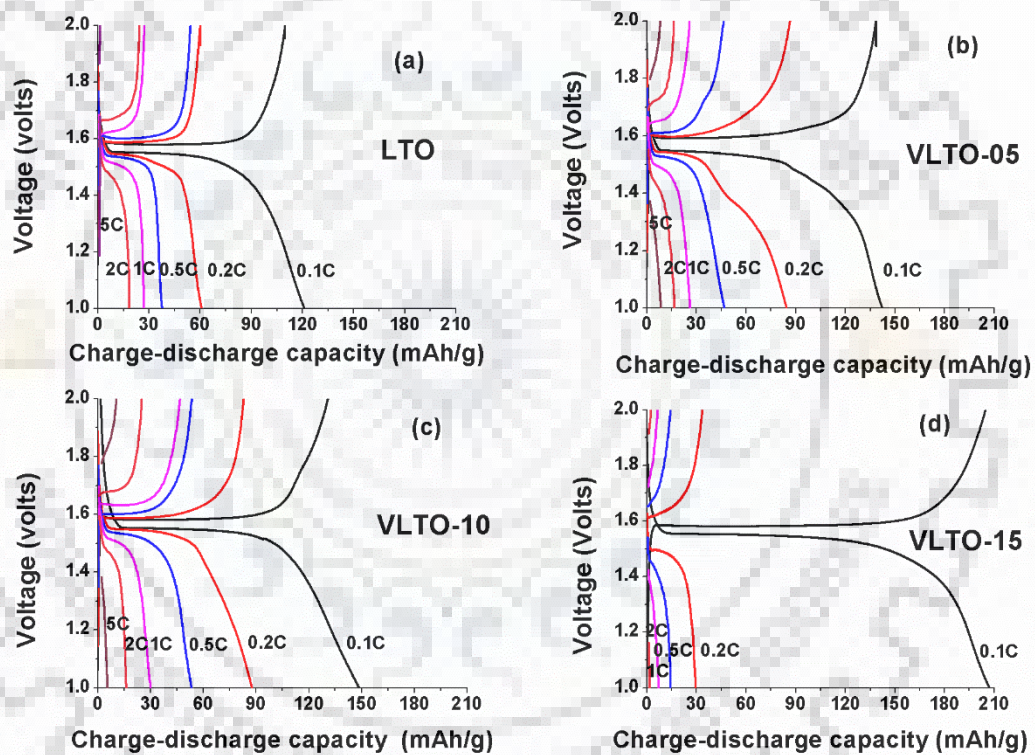
Figure 5.8: Charge-discharge behaviours of air calcined $Li_4Ti_{5-x}V_xO_{12}$ at different C-rates (a) LTO, (b) VLTO-05, (c) VLTO-10 and (d) VLTO-15

The performance of the $Li_4Ti_{5-x}V_xO_{12}$ as anode of lithium ion battery is evaluated by galvanostatic charge-discharge measurements. The electrochemical behaviors of the air calcined $Li_4Ti_{5-x}V_xO_{12}$ are shown in Figure 5.8. The initial charge-discharge capacities at 0.1C obtained for LTO, VLTO-05, VLTO-10 and VLTO-15 are 121mAhg^{-1}, 141mAhg^{-1}, 148mAhg^{-1} and

207mAhg^{-1} respectively which shows Li$^+$ intake capacity increases with the increase in V doping concentration.

It can be considered that corresponding to the maximum discharge capacity obtained for the LTO the excess Li$^+$ that can be accommodated in the structure of stoichiometric formula i.e. Li$_4$Ti$_5$O$_{12}$ is 3. Hence the excess Li$^+$ accommodation for the air calcined V doped LTO i.e. VLTO-05, VLTO-10 and VLTO-15 from their respective discharge curves are estimated to be 2.42, 2.54 and 3.55 respectively which are in accordance with the literature since it is reported by Hain et al. that the maximum Li$^+$ that can be accommodated in LTO is 5 (Hain et al., 2012). The charge and discharge capacities of VLTO-15 are found reducing drastically with increase in C-rate from 0.1 to 0.2 C, however, the reduction in capacity is relatively gradual with further increase in C-rates (i.e. at 0.2, 0.5, 1, 2 and 5C). However, the capacities fall with the increase in C-rate for LTO, VLTO-05 and VLTO-10 are gradual at all the C-rates studied.
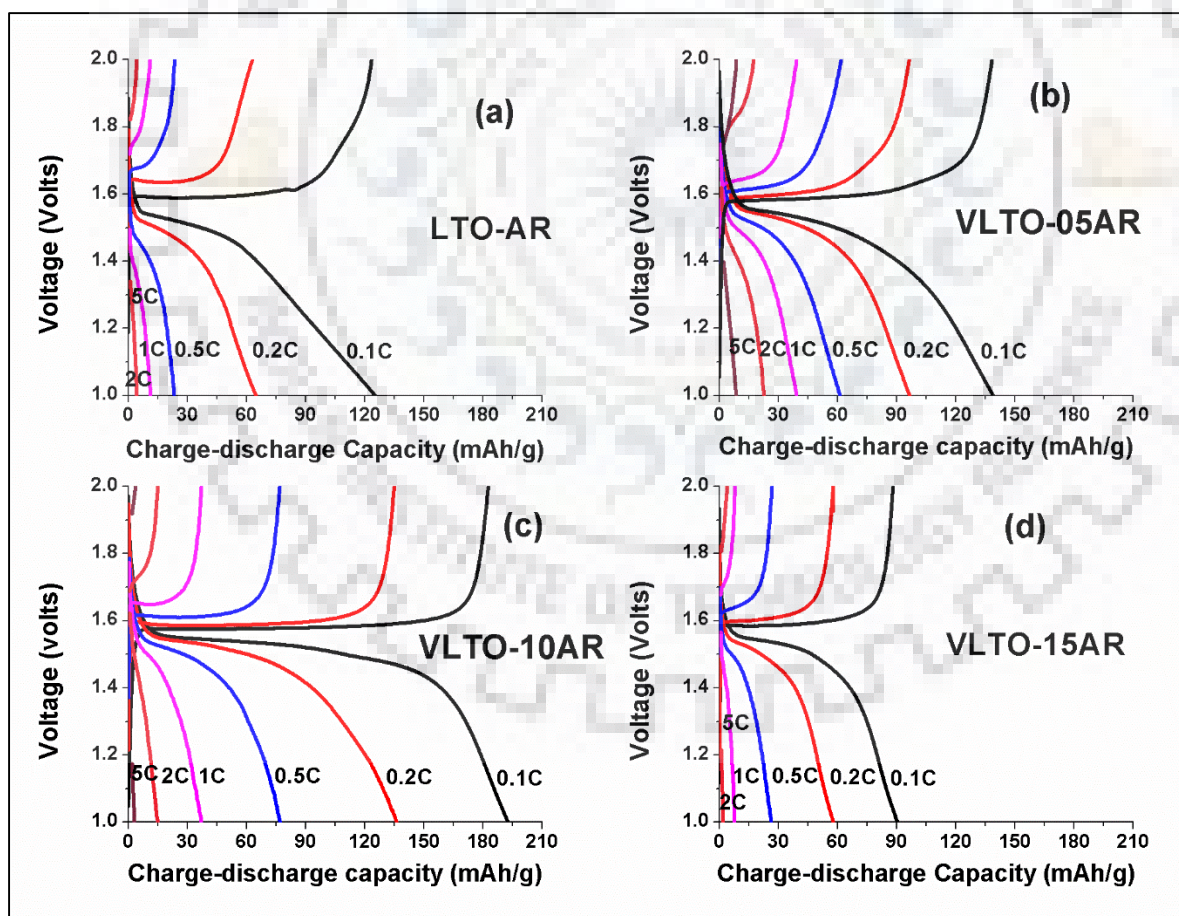
Figure 5.9: Charge-discharge behaviours of argon calcined Li$_4$Ti$_{5-x}$V$_x$O$_{12}$ at different C-rates (a) LTO-AR, (b) VLTO-05AR, (c) VLTO-10AR and (d) VLTO-15AR

The discharge capacities of all air calcined $Li_4Ti_{5-x}V_xO_{12}$ materials for five cycles at each C-rate are observed and are shown in Figure 5.10 (a). All the air calcined V doped LTO except VLTO-15 show better performance than LTO at all C-rates and VLTO-10 has most superior performance. From this it can be concluded that V doping in air calcined LTO is beneficial for better performance as anode of the lithium ion battery if limited to 2wt. %. The charge-discharge behaviors of argon calcined $Li_4Ti_{5-x}V_xO_{12}$ are shown in Figure 5.9. The discharge capacities obtained for LTOAR, VLTO-05AR, VLTO-10AR and VLTO-15AR for the first discharge cycle at 0.1C are 124, 140, 196 and 90mAhg^{-1} respectively.

The excess Li^+ accommodations for the argon calcined V doped LTO i.e. VLTO-05AR, VLTO-10AR and VLTO-15AR are estimated as 2.4, 3.36 and 1.54 respectively from their respective discharge curves. The discharge capacity of VLTO-15AR as anode material of LIB is lower as compared to VLTO-10AR and VLTO-05AR. It is evident from Table 5.1 that the proportion of V^{5+} is lowest in VLTO-15AR means less number of Ti^{4+} ions get reduced to Ti^{3+} ions to compensate the extra charge due to V^{5+}. The same can be observed from the peak position of VLTO-15AR in Figure 5.5(b).

The discharge capacities of the argon calcined $Li_4Ti_{5-x}V_xO_{12}$ for five cycles at each C-rate are shown in Figure 5.10(b). The electrochemical performance of VLTO-10AR is found to be superior among all the samples studied.
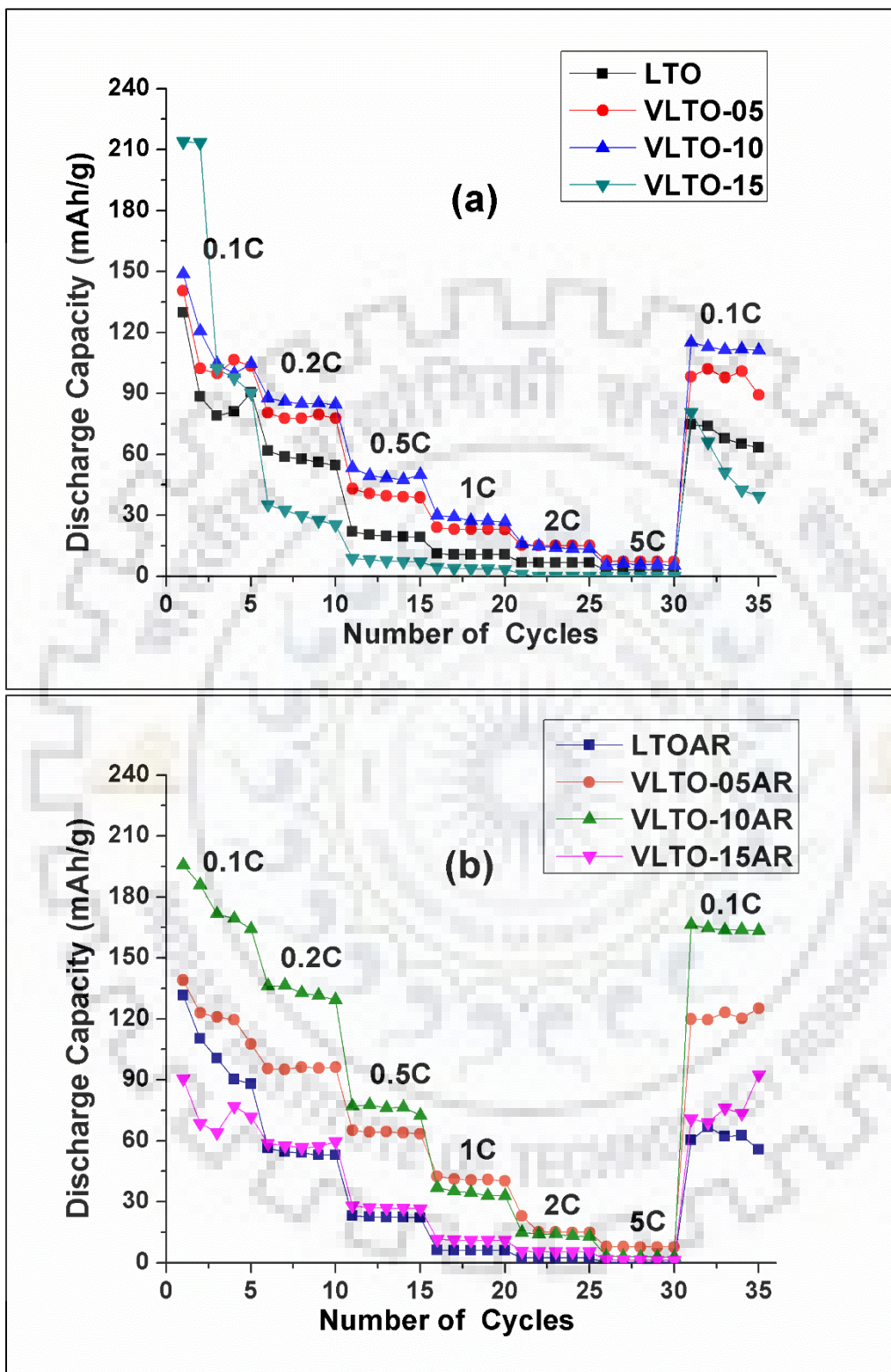
Figure 5.10: Discharge capacities at different C-rates (5 cycles for each rate) of (a) air calcined Li$_4$Ti$_{5-x}$V$_x$O$_{12}$ and (b) argon calcined Li$_4$Ti$_{5-x}$V$_x$O$_{12}$

5.5 Electronic Conductivity Measurement

$Li_4Ti_{4.9}V_{0.1}O_{12}$ composition shows best charge-discharge behavior among air as well as argon calcined $Li_4Ti_{5-x}V_xO_{12}$. Cylindrical pellets were prepared from powder samples of LTO, LTOAR, VLTO-10 and VLTO-10AR for electronic conductivity measurements. The Nyquist plots obtained from potentiostatic EIS performed for pellets of air and argon calcined $Li_4Ti_{5-x}V_xO_{12}$ (x = 0 and 0.1) are shown in the Figure 5.11.
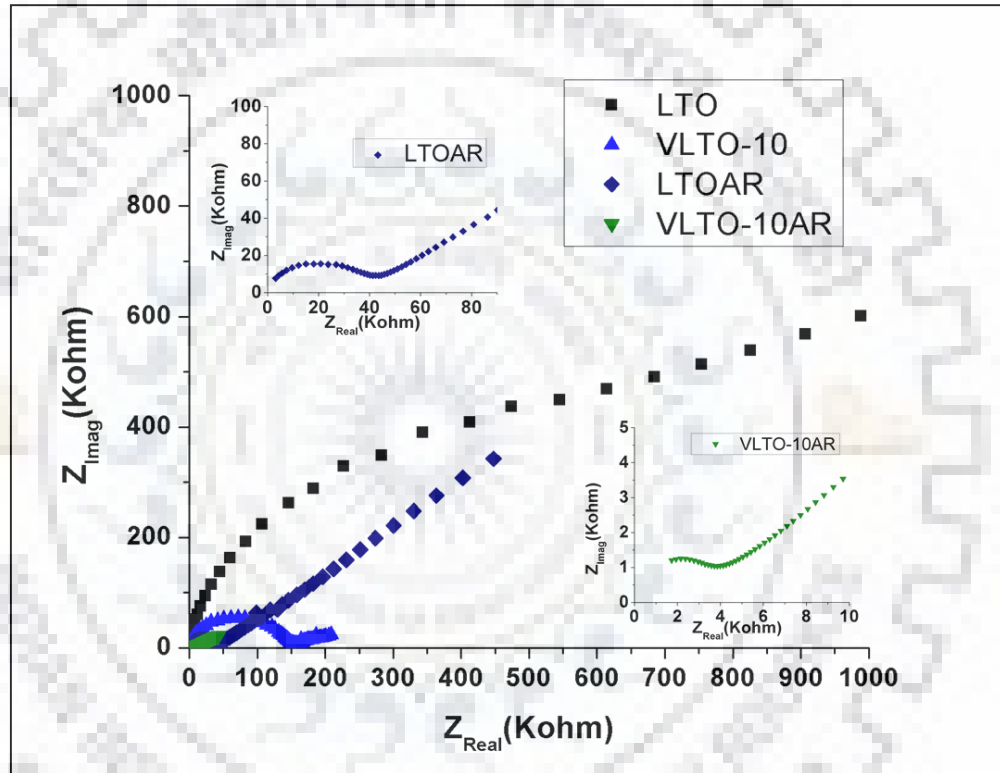
Figure 5.11: EIS Nyquist plots for pellets of air and argon calcined $Li_4Ti_{5-x}V_xO_{12}$ (x = 0, 0.1)

As can be seen from the plots that the impedance spectra do not approach to the real axis in the intermediate frequency range, therefore for the sake of R_{ct} estimate, the curves have been extrapolated following the semicircular variation between Z_{Imag} vs. Z_{Real} and the intersection has been obtained for the calculation of conductivity (Lin et al., 2014). The conductivity values shown in Table 5.3 were estimated using the following relation:

$$\sigma = G\, \frac{l}{A}\ \ Scm^{-1} \hspace{4cm} \text{……. (3)}$$

where G is the conductance = 1/Resistance, l is the thickness of the pellet and A is the circular area of the pellet.

Table 5.3: Resistance (R_{ct}) and estimated conductivity values of air and argon calcined $Li_4Ti_{5-x}V_xO_{12}$ (x = 0 and 0.1)

	LTO	VLTO-10	LTOAR	VLTO-10AR
R_{ct} (KΩ)	~ 1000	150	40	4
σ (S/cm)	2.5×10^{-5}	1.7×10^{-4}	3.6×10^{-3}	1.7×10^{-2}

Higher electronic conductivity of LTOAR powder material is obtained compared to pristine LTO and VLTO-10 implying that with calcination in argon atmosphere enhancement in conductivity becomes more than air calcined V doped LTO. The doping of V increases the conductivity of air calcined LTO about six times and the increase is up to three orders in case of V doped LTO calcined in argon atmosphere. However, the electronic conductivity of air calcined LTO reported in the literature is $< 10^{-9}$ S/cm (Lin et al., 2014) which is quite low than what estimated here so with reference of literature the increase in conductivity is of five orders in case of V doped LTO calcined in air and increment is up to seven orders for V doped LTO is calcined in argon atmosphere than pristine LTO.

In air calcined V doped LTO the doping of V^{5+} in the position of Ti^{4+} in the structure of LTO makes one electron free for each replacement of Ti^{4+} and this increased electronic concentration leads to the enhancement in conductivity (Zhong, 2007). In argon calcined V doped LTO the partial reduction of Ti^{4+} to Ti^{3+} results in increase in conductivity. The conductivity of VLTO-10AR is better than VLTO-10 and LTOAR because doping of V also contributes in reducing T^{4+} to Ti^{3+} in argon calcined LTO as confirmed by XPS analysis done in this work.

5.6. Summary

A systematic comparison of air and argon synthesized V doped LTO is done. The doping of V does not make any changes in the lattice structure of LTO. V doping upto 2wt. % in air calcined LTO reduces the particle size distribution. The calcination in air does not reduce Ti^{4+} to Ti^{3+}, therefore the excess charge of V^{5+} must be compensated by defects generated in the crystal structure. Calcination in argon atmosphere also reduces V from the oxidation state of 5+ to 4+ which play a significant role in conductivity of V doped LTO. The reduction of Ti^{4+} to Ti^{3+} is

enhanced by V doping if calcined in argon atmosphere. The D_{Li+} of V doped LTO increases with the increase of doping concentration. Electrochemically argon calcined $Li_4Ti_{5-x}V_xO_{12}$ in argon atmosphere outperforms the same calcined in air. Electronic conductivity can be increased up to three orders compared to pristine LTO by doping of V followed by calcination in argon atmosphere. $Li_4Ti_{4.9}V_{0.1}O_{12}$ composition calcined in argon atmosphere shows best charge-discharge behavior and suggested to be used as electrode of lithium ion battery instead of pristine LTO.

Hybrid system using bimaterial electrodes of Li$_4$Ti$_5$O$_{12}$ and Activated Carbon

Hybrid system using bimaterial electrodes Li₄Ti₅O₁₂ and activated carbon

In chapters 4 and 5 LTO, LTO-P and VLTO as electrodes of lithium ion battery are discussed. This chapter 6 describes the electrochemical behavior of activated carbon (AC) based supercapacitor. A novel three terminal internal hybrid system of lithium ion battery and supercapacitor using bimaterial electrodes is presented. Three different bimaterial electrodes combination each of using LTO, LTO-P and VLTO-10AR as the battery material and AC as supercapacitor material for each case are used. The hybrid system is put in parallel configuration by short circuiting the non-bimaterial electrode terminals externally. This internal parallel hybrid system is electrochemically characterized using arbin cycler. The results of the hybrid system are also compared with individual LTO based lithium ion battery and activated carbon based supercapacitor systems.

Pulsed application test is also performed for all the three different bimaterial electrodes based hybrid systems. In this test pulsating charge-discharge current is applied to all the hybrid systems and their discharge capacities were measured and the results are compared.

6.1 Activated carbon based supercapacitor

A supercapacitor cell is fabricated using AC as active material for both the electrodes. The copper and the aluminium foils are used as current collector for anode and cathode respectively. Two half-cells are also fabricated using lithium as electrode against both the AC electrodes separately. The electrochemical studies of all the prepared half cells and full cell are conducted by applying constant charge-discharge current. Cyclic voltammetry of the cells are also performed. Similarly full cell is fabricated by taking both electrodes of activated carbon and is electrochemically tested.

6.1.1 Half Cells of AC

6.1.1.1 Half-cell with AC on Cu foil

The prepared electrode of activated carbon on copper foil is shown in Figure 6.1. Half-cell assembly is electrically connected to Arbin cycler and is subjected to charge-discharge test at constant current. The theoretical capacity is considered as 40 mAhg^{-1}. The discharge capacity

obtained at 0.1C as shown in Figure 6.2 (a) is 47mAhg⁻¹. As expected no flatness is observed since the lithium ion storage and release process are is limited to the surface area of the electrode material. The cyclic voltammetry characteristic is shown in Figure 6.2 (b).
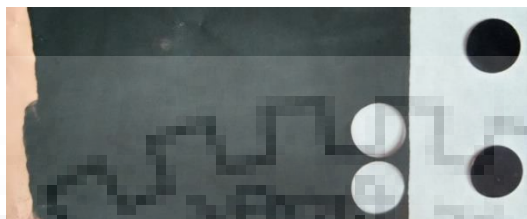
Figure 6.1 Activated carbon slurry pasted on copper foil and punched electrodes

Figure 6.2 (a) Charge-discharge profiles and (b) CV of half-cell of AC with Cu current collector
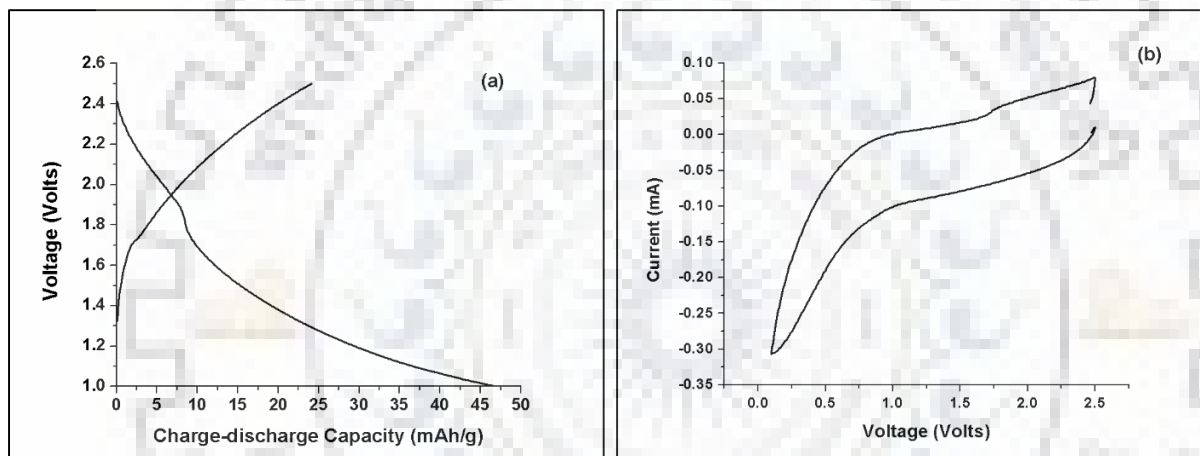
6.1.1.2 Half-cell with AC on Al foil

The prepared electrode of activated carbon on aluminum foil is shown in Figure 6.3. The discharge capacity obtained at 0.1C is 16 mAhg⁻¹ as shown in Figure 6.4 (a).
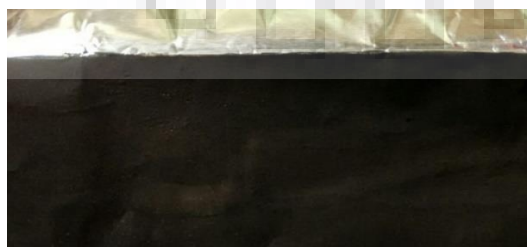
Figure 6.3 Activated carbon slurry pasted on aluminum foil

The cyclic voltammetry characteristic is shown in Figure 6.4 (b).
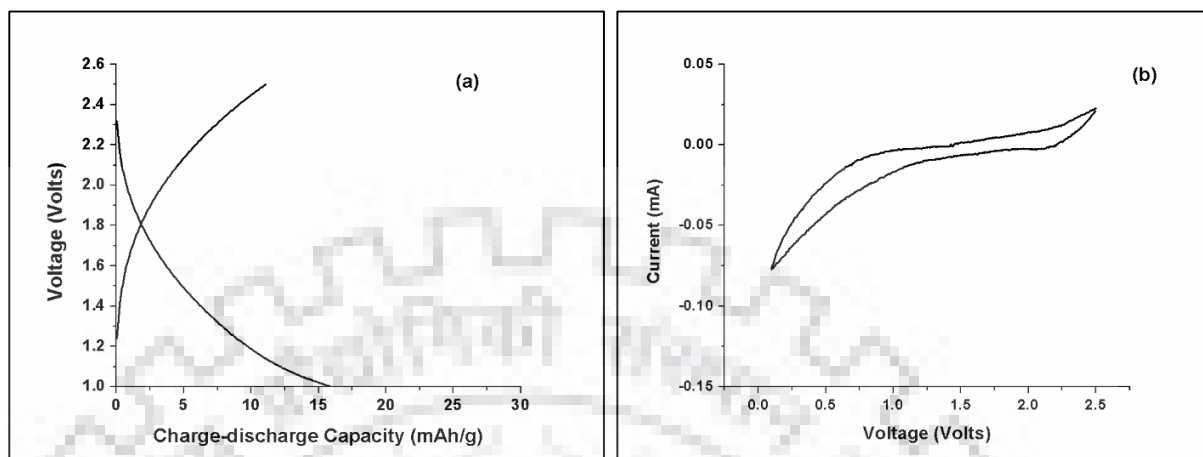
Figure 6.4 (a) Charge-discharge profiles and (b) CV of half-cell of AC with Al current collector

6.1.2 Full Cell of AC

Full cell is fabricated with one electrode of AC pasted on copper foil and another electrode of AC pasted on aluminum foil and designated as AC//AC system. The electrochemical characteristics of activated carbon based full cell is shown in Figure 6.5. The discharge capacity obtained at 0.1C is 19 mAhg^{-1}. The cyclic voltammetry characteristics is shown in Figure 6.5 (b).
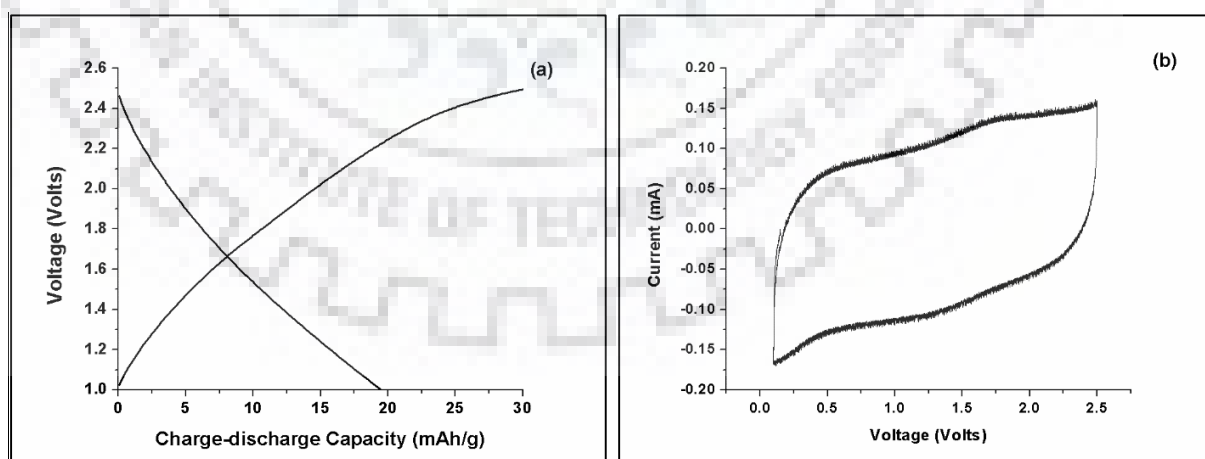
Figure 6.5 (a) Charge-discharge profiles and (b) CV of full-cell of AC

6.2 Hybrid Design

The two terminal internal parallel hybrid of lithium ion battery and supercapacitor proposed in literature normally consists of battery anode and cathode materials mixed with activated carbon in 1:1 ratio or else specified (Cericola et al., 2011). The different approaches for making bimaterial electrodes were explained in Chapter 2 (US patent 5744258, Bai et al. 1998).
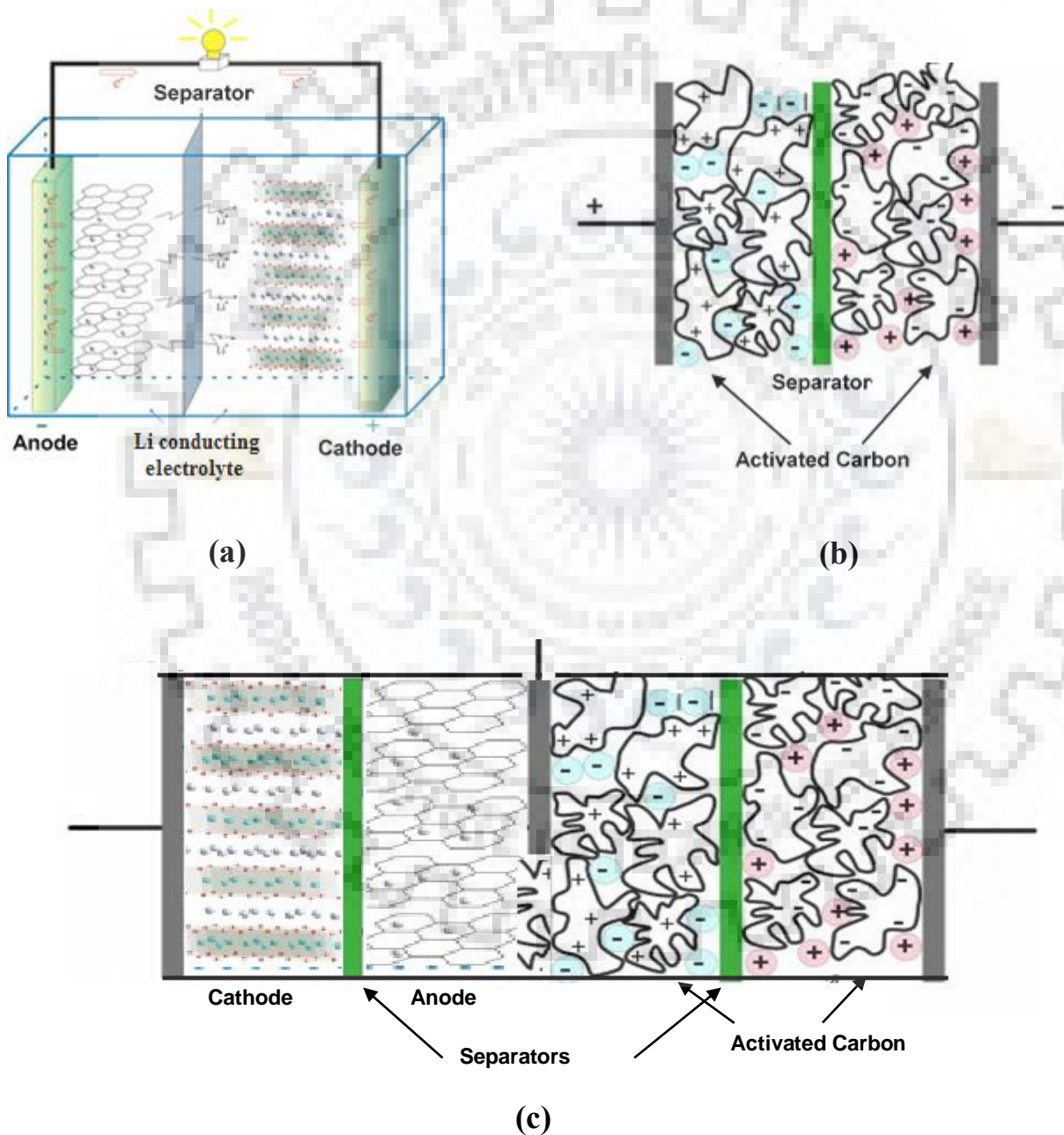
Figure 6.6 Arrangement of electrodes in (a) Lithium ion battery (b) Supercapacitor (c) Lithium ion battery-supercapacitor hybrid system studied

In the present work, a novel three terminal internal parallel hybrid system of lithium ion battery and supercapacitor is studied. The schematic diagram of the system is shown in Figure 6.6 (c). The hybrid system consists of a bimaterial electrode having battery material and supercapacitor material sharing the same collector (copper foil). The supercapacitor electrode facing the supercapacitor side of bimaterial electrode and the battery material electrode facing the battery side of bimaterial electrode make the three terminal hybrid system.

The difference between the bimaterial electrode shown in Figure 2.10 (d) and the proposed bimaterial electrode is the existence of overlapping of battery material and the supercapacitor material in the proposed one. The designed three terminal hybrid system in the cell assembly is shown in Figure 6.7.

Figure 6.7 Photograph of designed three terminal hybrid system in cell assembly

6.3 LTO-AC bimaterial electrode

The bimaterial electrode consisting of LTO and AC and in combination with lithium as counter electrode for the three terminal hybrid system is prepared (Figure 6.8) for electrochemical characterization i.e. charge-discharge test and cyclic voltammetry studies.

The configuration is designated as Li//LTO/AC//Li. The hybrid system is subjected to charge and discharge test at constant current for C rates varying from 0.1C to 5C. $1C = 170 mAhg^{-1}$ is taken as standard for all the hybrid systems studied.
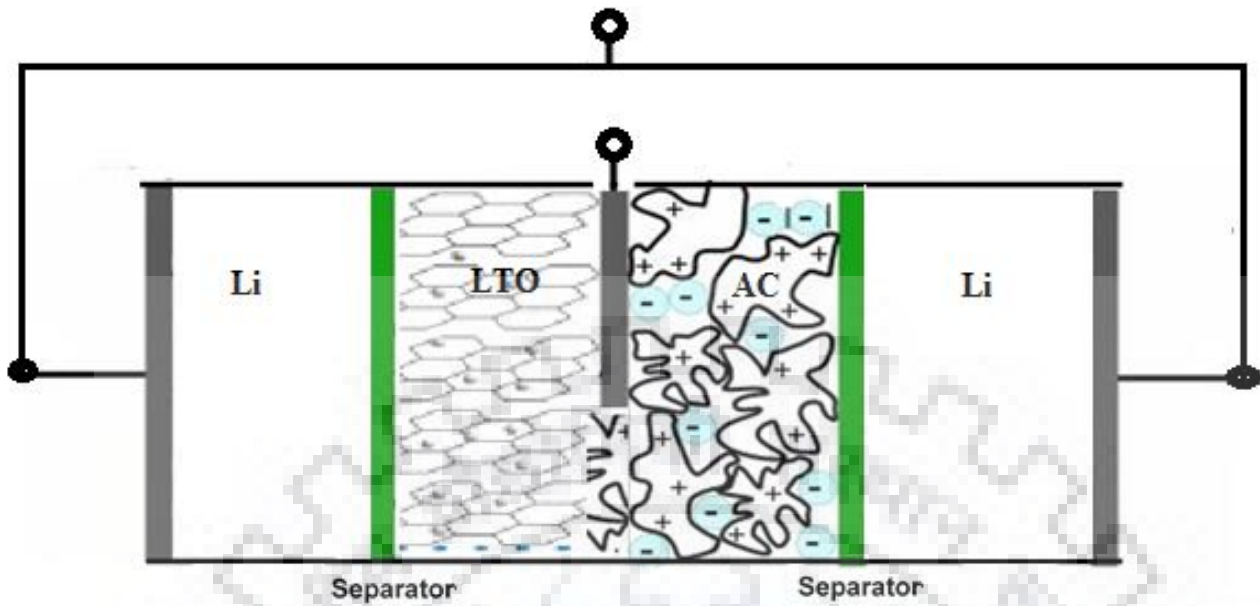
Figure 6.8 Electrode arrangements in the three terminal hybrid system for testing

6.3.1 Galvanostatic charging discharging
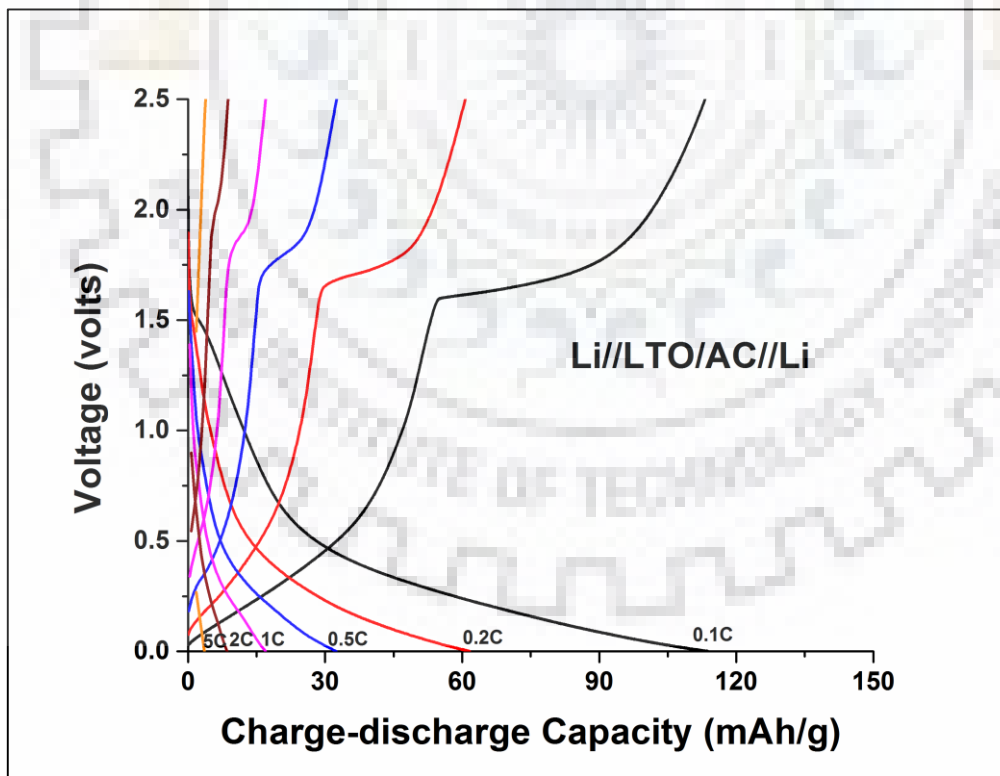
Figure 6.9 Charge-Discharge profiles of Li//LTO/AC//Li hybrid system at different C-rates

The charge-discharge curves shown in Figure 6.9 correspond to Li//LTO/AC//Li hybrid system. The discharge capacities obtained at 0.1C, 0.2C, 0.5C, 1C, 2C and 5C are 113mAhg^{-1}, 62mAhg^{-1}, 34mAhg^{-1}, 18mAhg^{-1}, 9mAhg^{-1} and 4mAhg^{-1} respectively.

The performance of Li//LTO/AC//Li hybrid system is studied for 35 cycles with the increasing C-rates starting with five cycles at 0.1 C-rate and then five cycles at each increased rate (0.2, 0.5, 1, 2 and 5C) followed by five cycles at 0.1 C-rate again. The LTO based battery system and AC based supercapacitor are also subjected to the same pattern of C-rates and the performances of all the three systems are compared as shown in Figure 6.10. As expected the discharge capacities at all C-rates for the hybrid system are higher compared to those of AC based supercapacitor and lower compared to those LTO based battery.
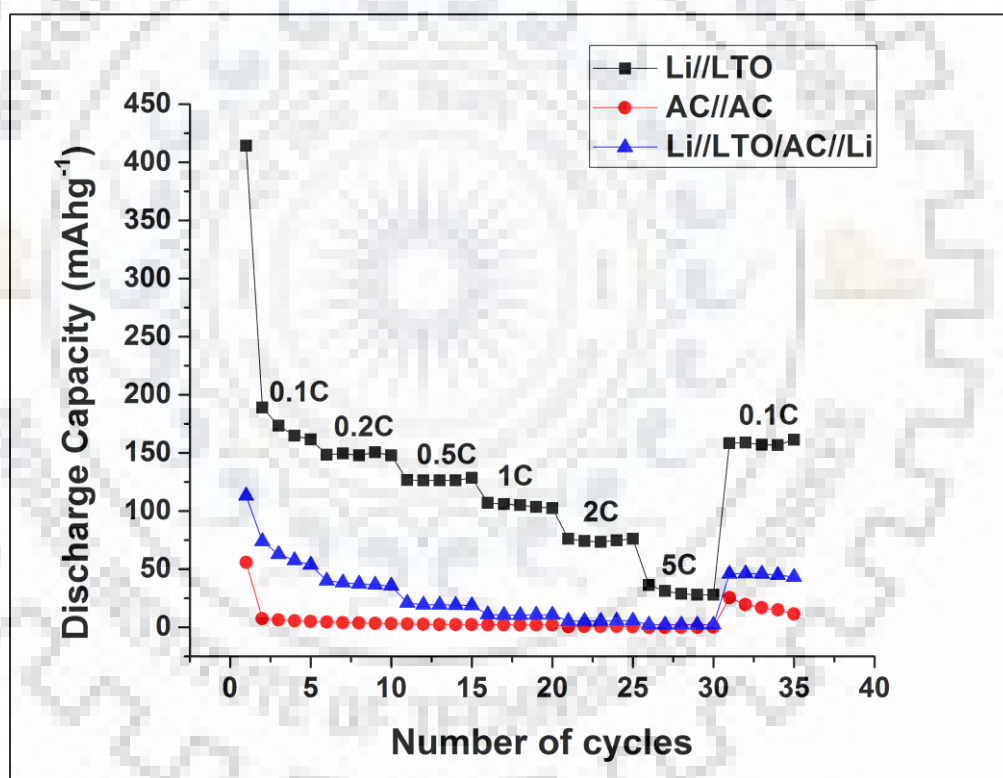
Figure 6.10 Discharge capacities comparison of LTO based battery, AC based supercapacitor and Li//LTO/AC//Li hybrid system at different C-rates

It can be seen from Figure 6.10 that the discharge capacity of all the systems for the very first cycle at 0.1 C-rate is quite high compared to that for the second cycle. This is due to the high irreversible capacity of the acetylene black material used as conductive agent in the preparation of the electrodes. The step pattern is observed for LTO based battery system with the increase in

C-rate. For the AC based supercapacitor system the discharge capacities remains nearly same with the increase in C-rate. The Li//LTO/AC//Li hybrid system also shows step pattern like battery system with the increase in C-rate but for the C-rates higher than 1C, the discharge capacity values are nearly same and equal to those of AC based supercapacitor system. This is because activated carbon reaches faster to the lower voltage level while discharging and the full capacity of battery material is not utilized. The battery material has to be fast enough in charging and discharging process for proper utilization of its capacity in the hybrid system.

6.3.2 Cyclic voltammetry

The cyclic voltammetry characteristics of LTO based battery system (Li//LTO), AC based supercapacitor system (AC//AC) and Li//LTO/AC//Li hybrid system are shown in Figure 6.11. The intercalation peaks corresponds to oxidation and reduction phenomenon occurs at battery electrodes are observed between 1.5-1.7V for both LTO based battery system and Li//LTO/AC//Li hybrid system. The peak to peak potential difference for Li//LTO/AC//Li hybrid system is less as compared to that of LTO based battery system which shows that the internal polarization resistance of hybrid system is low than that of LTO based battery. No oxidation or reduction peak is observed for AC based supercapacitor system in this voltage range.

The profile of CV curve of LTO based battery system in the voltage range of 0-1V corresponds to the SEI layer formation and are in consistent with result reported in (Yi et al., 2009). For AC based supercapacitor the variation in the current in the voltage range of 0 - 1V is due to the intercalation of Li ion inside the carbon structure at such low voltage. The combined effect of AC and LTO in Li//LTO/AC//Li hybrid system is observed in the voltage range of 0-1V where the variation in current is increased up to -0.25 mA.
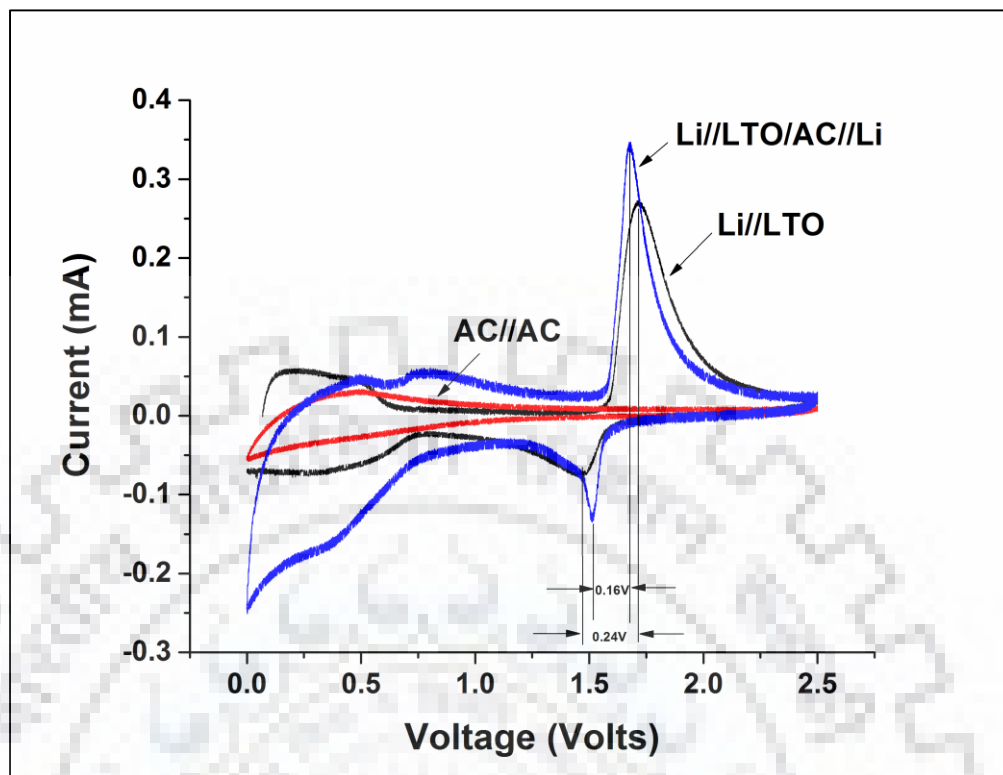
Figure 6.11 Cyclic voltammetry profiles of LTO based battery, AC based supercapacitor and Li//LTO/AC//Li hybrid system

6.4 LTO-P-AC bimaterial electrode

The bimaterial electrode using nanoporous LTO as battery material with AC as supercapacitor material is designated as LTO-P-AC bimaterial electrode and the hybrid configuration for the same is named as Li//LTO-P/AC//Li.

6.4.1 Galvanostatic charging discharging

The charge-discharge profiles of Li//LTO-P/AC//Li hybrid system are shown in Figure 6.12. The discharge capacities of the first cycle at 0.1C, 0.2C, 0.5C, 1C, 2C and 5C are 321mAhg^{-1}, 238mAhg^{-1}, 154mAhg^{-1}, 80mAhg^{-1}, 42mAhg^{-1} and 14mAhg^{-1} respectively.
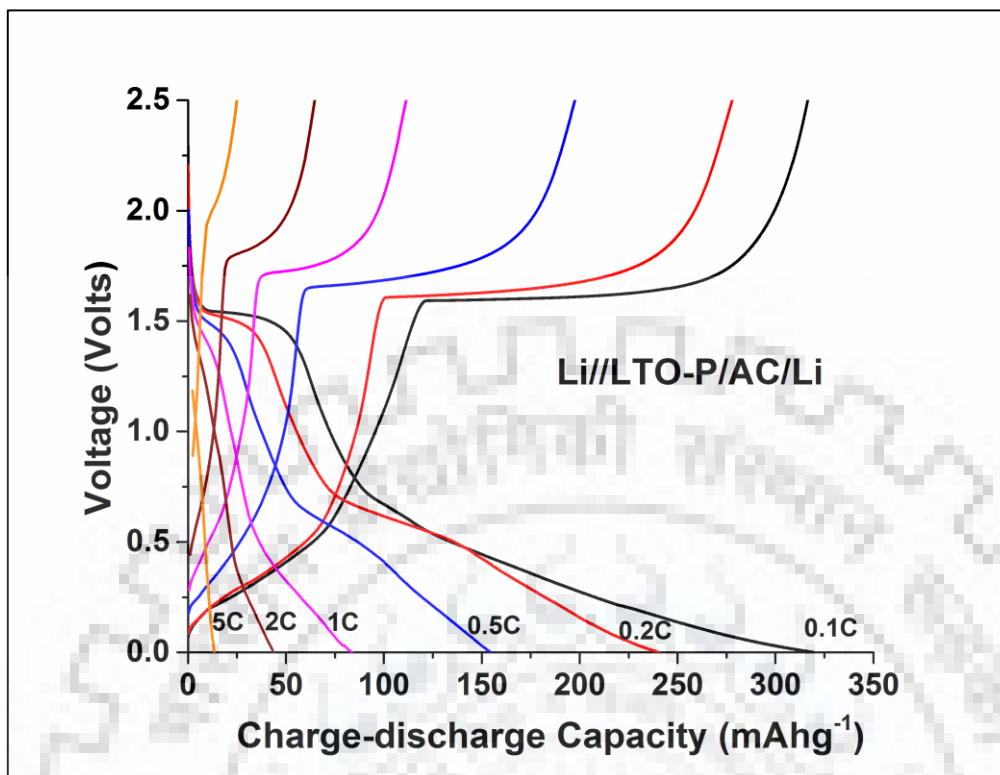
Figure 6.12 Charge-Discharge profiles of Li//LTO-P/AC//Li hybrid system at different C-rates

The flat discharge plateau at 1.55V is observed for Li//LTO-P/AC//Li hybrid system which is not observed in the case of Li//LTO/AC//Li hybrid system. This shows that the LTO-P battery material in the bimaterial electrode is capable to retain the characteristics of battery with fast acting AC supercapacitor material in the same bimaterial electrode. A second discharge plateau at about 0.7V is also observed due to which discharge capacity is further increased.

The performance of Li//LTO-P/AC//Li hybrid system is studied for 35 cycles with the increasing C-rates starting with five cycles at 0.1 C-rate and then five cycles at each increased rate (0.2, 0.5, 1, 2 and 5C) followed by five cycles at 0.1 C-rate again as shown in Figure 6.13. The difference between first and second cycle due to the high irreversible capacity of the acetylene black material used as conductive agent in the preparation of the electrode. The step pattern of discharge capacities is observed with the increase in C-rate. The discharge capacities of Li//LTO-P/AC//Li hybrid system is compared with that of Li//LTO/AC//Li hybrid system and shown in Figure 6.13. The Li//LTO-P/AC//Li hybrid system performs much better at all C-rates compared to Li//LTO/AC//Li hybrid system. This enhancement in the performance of hybrid system is due to the nanoporous structure of LTO-P. The difference between the discharge capacities of the two hybrid systems is decreased with increase in C-rate.

Figure 6.13 Discharge capacities comparison of Li//LTO-P/AC//Li and Li//LTO/AC//Li hybrid systems at different C-rates

6.4.2 Cyclic voltammetry

The cyclic voltammetry characteristics of Li//LTO-P/AC//Li hybrid system is shown in Figure 6.14 along with cyclic voltammetry characteristics of Li//LTO/AC//Li hybrid system for comparison. The huge difference between the peak to peak current values of two hybrid systems indicates the high discharge capacity of Li//LTO-P/AC//Li hybrid system. The second intercalation peak at about 0.7V is observed for Li//LTO-P/AC//Li hybrid system which clearly shows the reversible capacity at this voltage. The flat discharge plateau at the same voltage appears in the charge-discharge characteristics of Li//LTO-P/AC//Li hybrid system confirms the same.
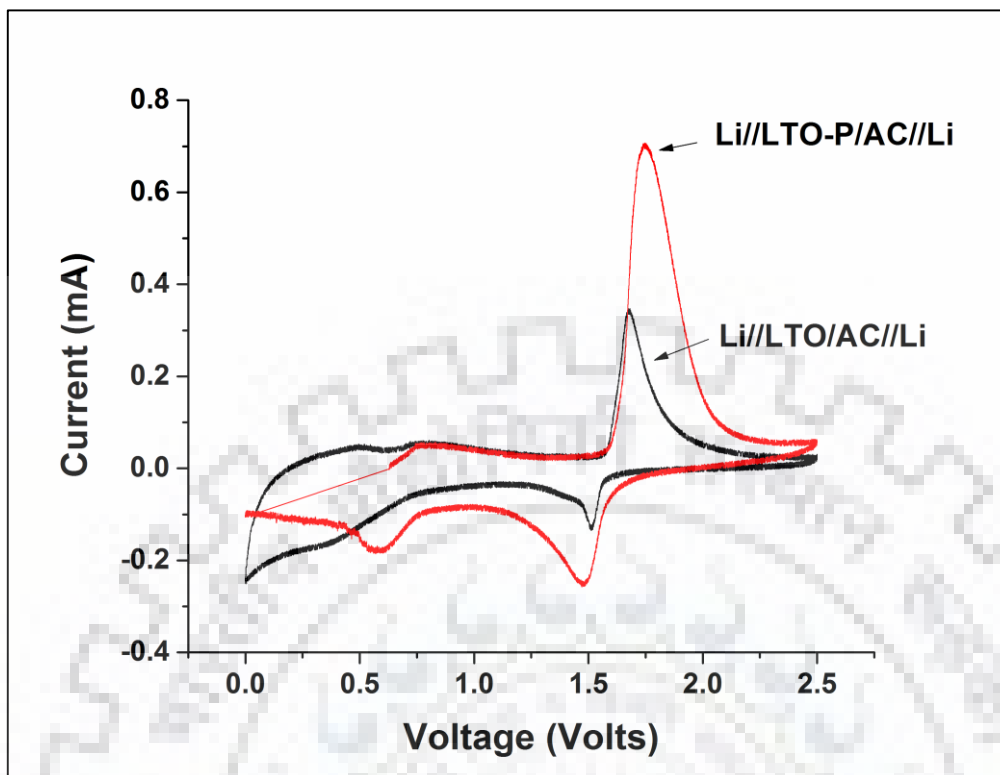
Figure 6.14 Cyclic voltammetry profiles of Li//LTO-P/AC//Li and Li//LTO/AC//Li hybrid systems

6.5 VLTO-10AR-AC bimaterial electrode

The bimaterial electrode using vanadium doped LTO calcined in argon atmosphere (VLTO-10AR) as battery material with AC as supercapacitor material is designated as VLTO-10AR-AC biomaterial electrode and the configuration is named as Li//VLTO-10AR/AC//Li.

6.5.1 Galvanostatic charging discharging

The charge-discharge profiles of Li//VLTO-10AR/AC//Li hybrid system are shown in Figure 6.15. The discharge capacities of the first cycles at 0.1C, 0.2C, 0.5C, 1C, 2C and 5C are 253mAhg^{-1}, 212mAhg^{-1}, 162mAhg^{-1}, 119mAhg^{-1}, 68mAhg^{-1} and 24mAhg^{-1} respectively.

The flat discharge plateau at 1.55V is observed for Li//VLTO-10AR/AC//Li hybrid system similar to Li//LTO-P/AC//Li hybrid system which is not observed in the case of Li//LTO/AC//Li hybrid system. This shows that the VLTO-10AR battery material in the bimaterial electrode is also capable to retain the characteristics of battery with fast acting AC supercapacitor material in the same bimaterial electrode.
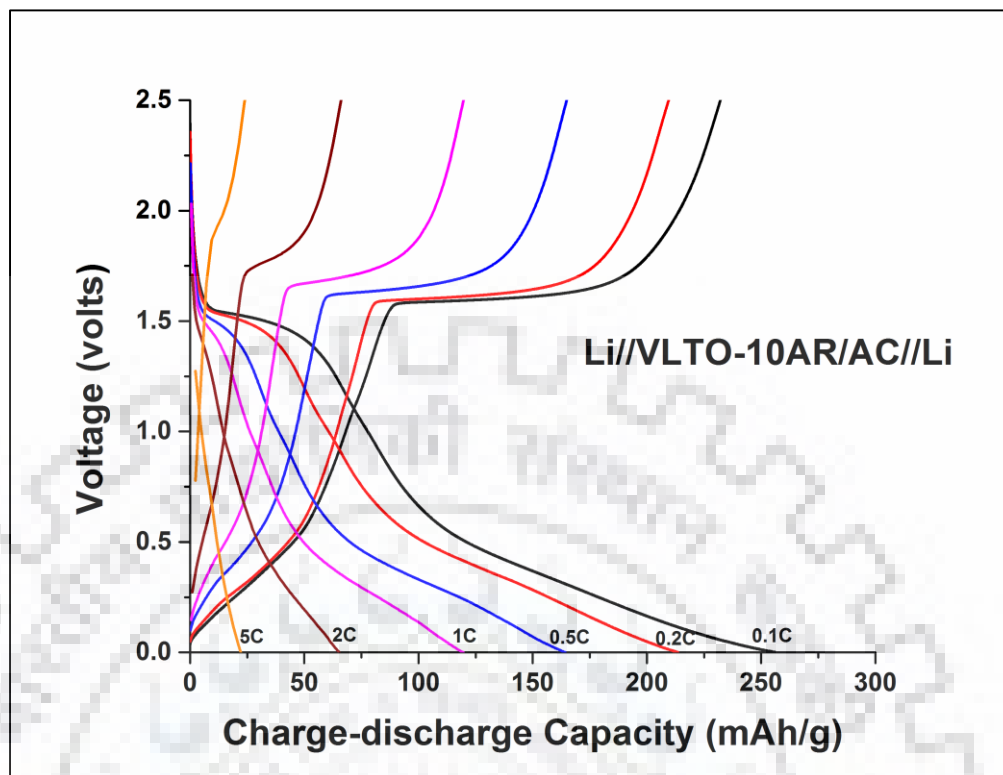
Figure 6.15 Charge-Discharge profiles of Li//VLTO-10AR/AC//Li hybrid system

The performance of Li//VLTO-10AR/AC//Li hybrid system is studied for 35 cycles with the increasing C-rates starting with five cycles at 0.1 C-rate and then five cycles at each increased rate (0.2, 0.5, 1, 2 and 5C) followed by five cycles at 0.1 C-rate again as shown in Figure 6.16. The difference between first and second cycle due to the high irreversible capacity of the acetylene black material used as conductive agent in the preparation of the electrode. The step pattern of discharge capacities is observed with the increase in C-rate. The discharge capacities of Li//VLTO-10AR/AC//Li hybrid system is compared with that of Li//LTO/AC//Li hybrid system and shown in Figure 6.16.

The discharge capacities are increased significantly at all C-rates by using VLTO-10AR as battery material of the bimaterial electrode in the hybrid system. V doped LTO has already proved the enhancement in electrochemical performance compared to pristine LTO as Li-ion battery electrode as discussed in chapter 5.
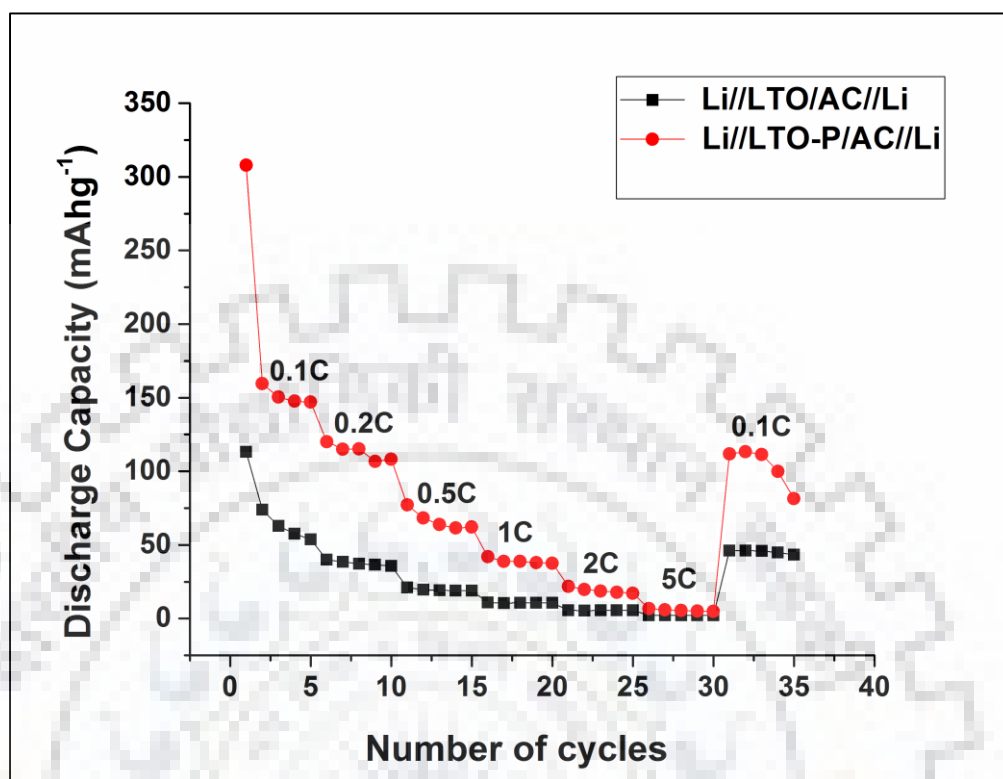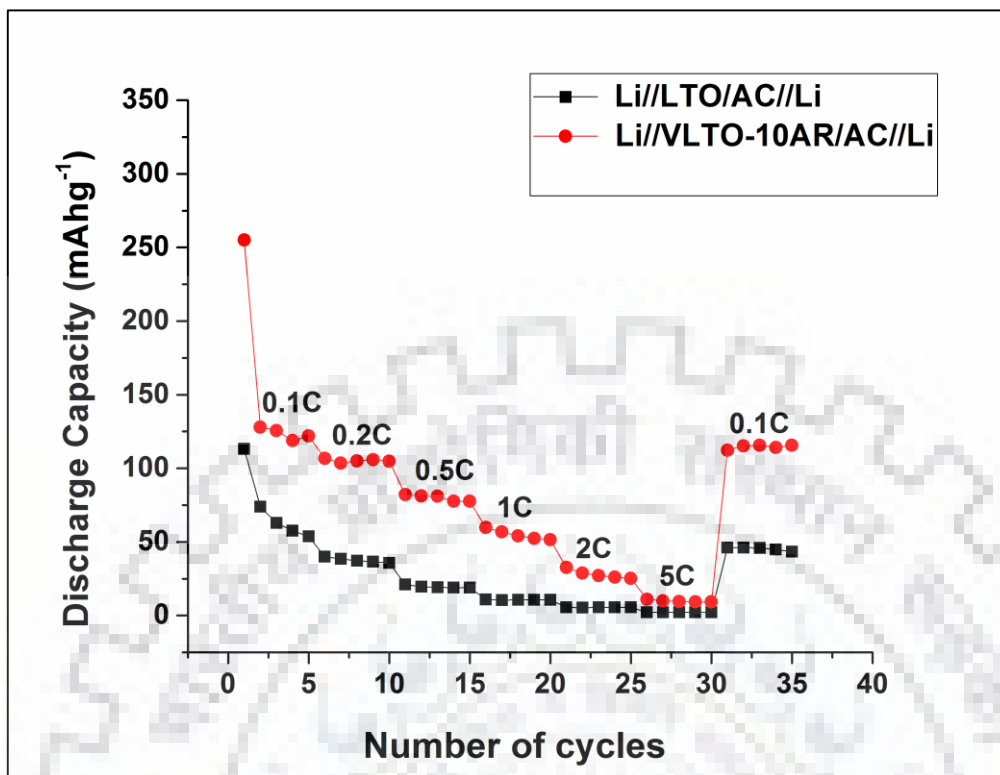
Figure 6.16 Discharge capacities comparison of Li//VLTO-10AR/AC//Li and Li//LTO/AC//Li hybrid systems at different C-rates

6.5.2 Cyclic voltammetry

The cyclic voltammetry characteristics of Li//VLTO-10AR/AC//Li hybrid system is shown in Figure 6.17 along with cyclic voltammetry characteristics of Li//LTO/AC//Li hybrid system for comparison. The difference between the peak to peak current values of two hybrid systems shows the enhancement in reversible capacity of Li//VLTO-10AR/AC//Li hybrid system. Rest of the cyclic voltammetry profile of Li//LTO-10AR/AC//Li hybrid system is similar to that of similar to Li//LTO/AC//Li hybrid system.
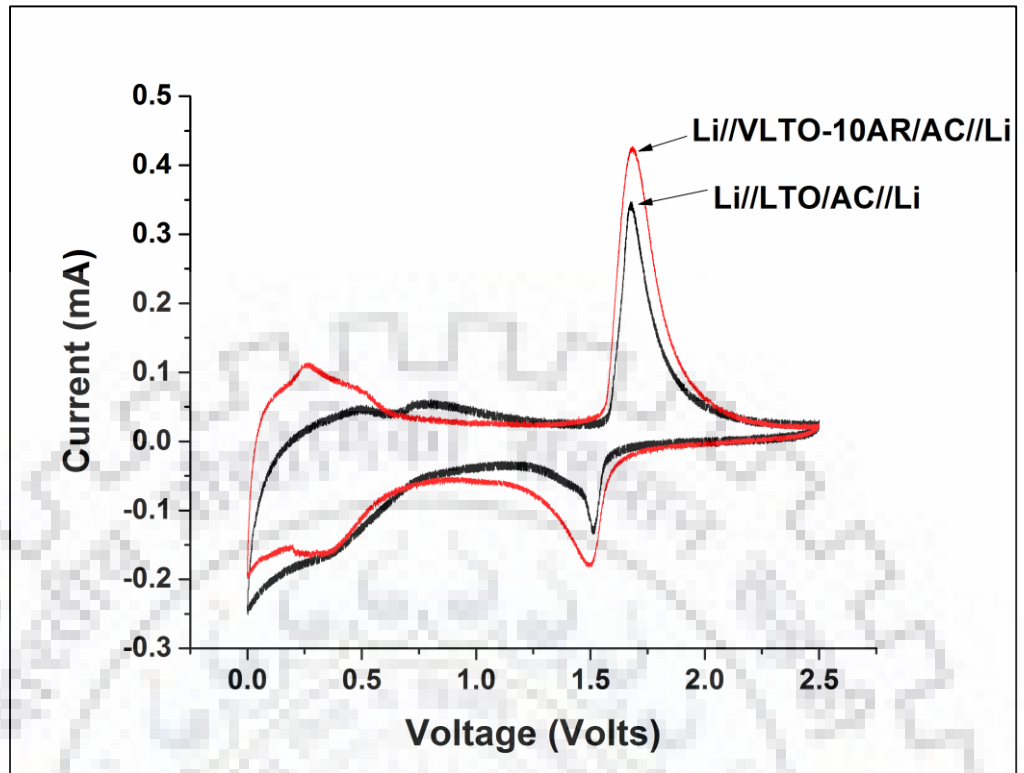
Figure 6.17 CV curves of Li//VLTO/AC//Li and Li//LTO/AC//Li hybrid systems

The discharge capacities for 35 cycles with the increasing C-rates starting with five cycles at 0.1 C-rate and then five cycles at each increased rate (0.2, 0.5, 1, 2 and 5C) followed by five cycles at 0.1 C-rate again of the LTO based battery system, AC based supercapacitor and all the hybrid systems based on LTO-AC, LTO-P-AC and VLTO-10AR-AC bimaterial electrodes prepared in this work are compared as shown in Figure 6.18. This is very much clear that the hybrid system cannot outperform the battery system as far as discharge capacity or we can say energy density is concerned but the capacity of hybrid system can be achieved closer to battery system by enhancing the properties of pristine battery electrode material used in the hybrid system. The discharge capacity values of Li//LTO-P/AC//Li hybrid system reaches very close to LTO based battery system at low C-rates. The Li//VLTO-10AR/AC//Li hybrid system performs much better than LTO based battery system and Li//LTO-P/AC//Li hybrid system at moderate and high C-rates.
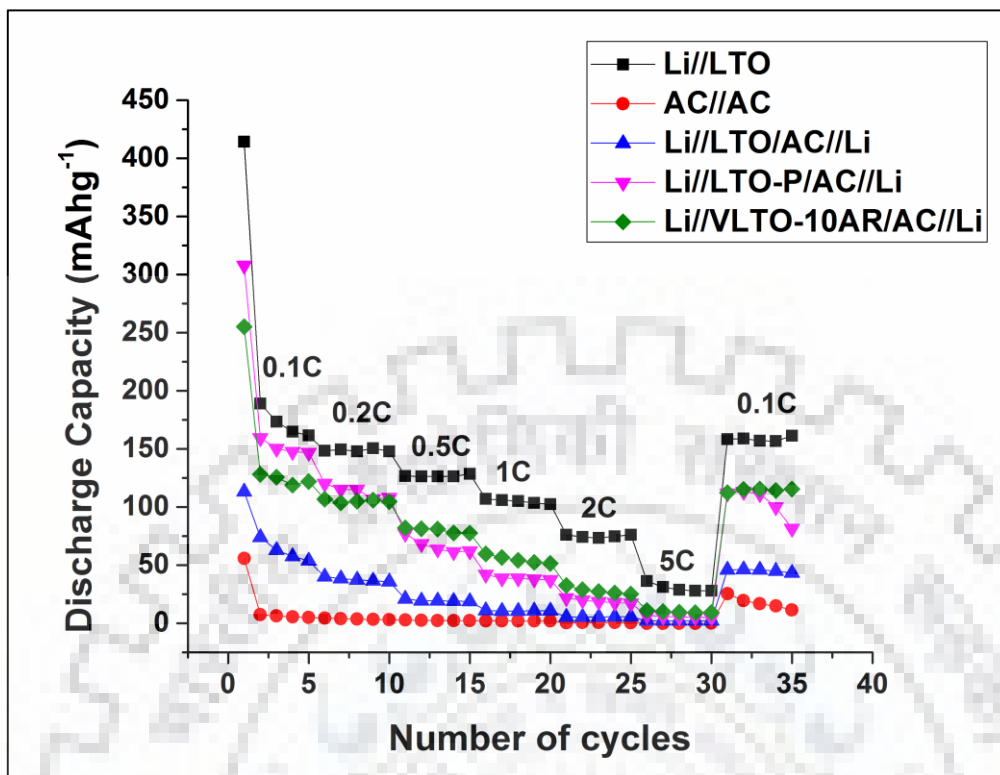
Figure 6.18 Discharge capacities comparison of different hybrid systems along with LTO based battery and AC based supercapacitor at various C-rates

6.6 Pulsed application test

The developed hybrids system are also evaluated in the criteria of specific power by investigating their performances for pulsed applications. The fabricated cells of the hybrid systems are subjected to pulsating current as shown in Figure 6.20. It shows the variation in the level of input current w.r.t. time. Here DT is the duration of time for which the level of applied current is according to high C-rate. T is the time period of the pulse such that the duty cycle [(DT/T) x 100] = 10%. The applied pulse pattern charge and discharge the system between 0 to 2.5 volts. The three different pulse patterns having the applied current levels according to C-rates of 0.1C-1C, 0.5C-5C and 1C-10C are used as input. The same pulse patterns are also applied to LTO based battery and AC based supercapacitor for comparison.
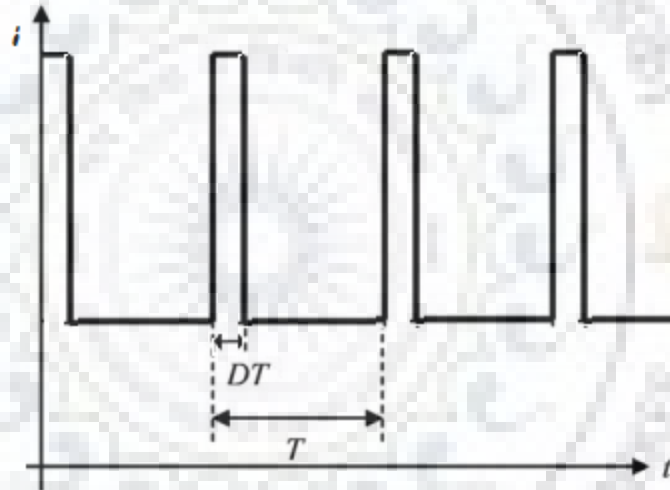
Figure 6.19: Pulse pattern showing the two current levels with duty cycle

6.6.1 L//LTO battery, AC//AC supercapacitor Li//LTO/AC//Li hybrid system

The discharge profiles of LTO based battery, AC based supercapacitor and Li//LTO/AC//Li hybrid system obtained after applying the pulse pattern 0.1C-1C are shown in Figure 6.20. The discharge capacity values for LTO based battery, AC based supercapacitor and Li//LTO/AC//Li hybrid system are $96mAhg^{-1}$, $74mAhg^{-1}$ and $76mAhg^{-1}$ respectively. The flat plateau are obtained for both battery hand hybrid systems. The first cycle discharge capacity of LTO based battery obtained at 0.1C rate (constant current discharging) was $407mAhg^{-1}$ and the first cycle discharge capacity for pulse pattern 0.1C-1C is $96mAhg^{-1}$. This shows that the capacity of battery is very much affected by pulsating current load and reduced to [(96 x 100)/407] = 23.5

117

% of its value at constant current load. In case of Li//LTO/AC//Li hybrid system the capacity is less affected by pulsating current load and reduced to [(76 x 100)/113] = 67.2 % of its value at constant current load. Although the discharge capacity of LTO based battery is more than Li//LTO/AC//Li hybrid system at this pulse rate, the reduction in discharge capacity of LTO based battery is higher.

The power of hybrid system is also tested with two more pulse patterns corresponds to higher C-rates viz. 0.5C-5C and 1C-10C and the comparison is shown in Figure 6.21(a) and (b).
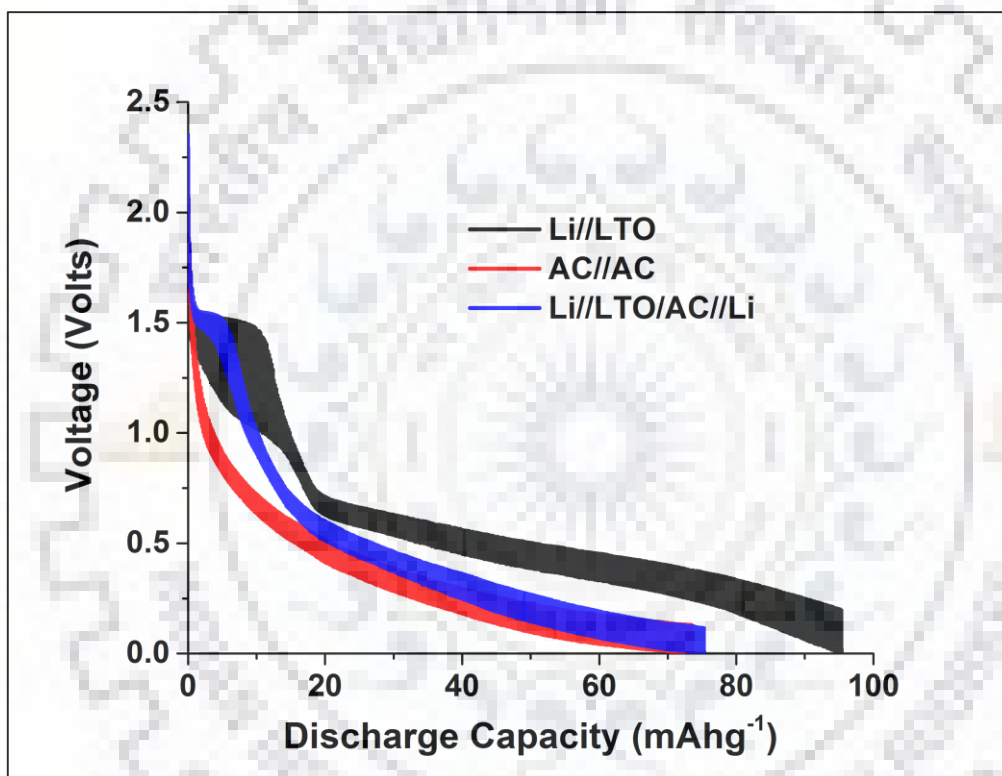
Figure 6.20 Discharge profiles obtained for LTO based battery, AC based supercapacitor and Li//LTO/AC//Li hybrid system at pulse pattern 0.1C-1C

The discharge capacity of LTO based battery obtained at 0.5C-5C and 1C-10C pulse patterns are 29mAhg^{-1} and 5mAhg^{-1} respectively. The discharge capacity of Li//LTO/AC//Li hybrid system obtained at 0.5C-5C and 1C-10C pulse rates are 24mAhg^{-1} and 16mAhg^{-1} respectively.
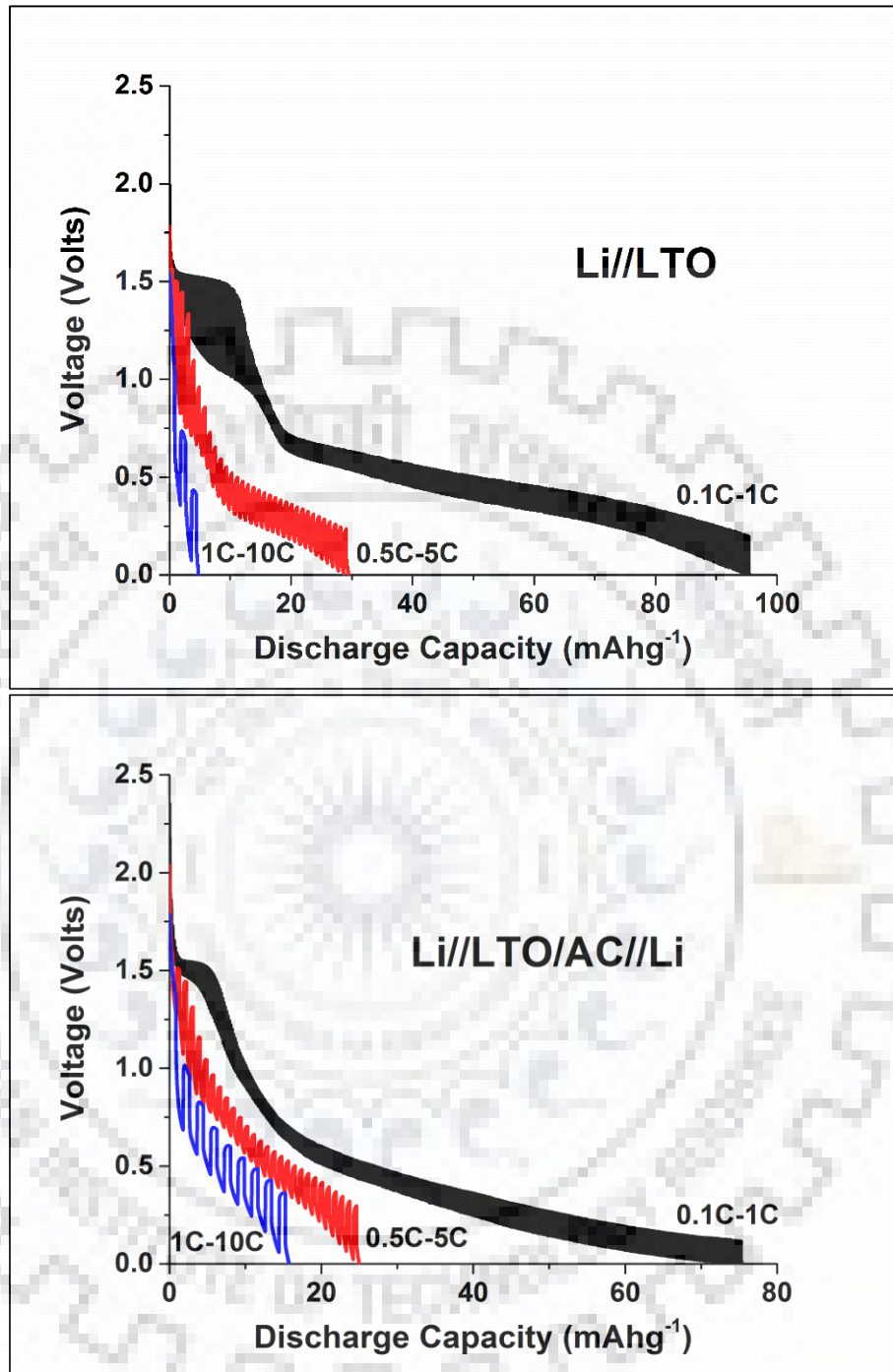
Figure 6.21 Discharge profiles comparison of LTO based battery and Li//LTO/AC//Li hybrid system at 0.1C-1C, 0.5C-5C and 1C-10C pulse patterns

Here Li//LTO/AC//Li hybrid system outperforms LTO based battery at 1C-10C pulse pattern with more than three times discharge capacity. So it is confirmed that the Li//LTO/AC//Li hybrid system is suitable for power applications having pulsating load corresponding to high C-rates. Since it is proven that hybrid systems based on LTO-P-AC and VLTO-10AR-AC

bimaterial electrodes shows better performance for constant current charge-discharge applications, the same are also tested for pulsed application at 0.1C-1C, 0.5C-5C and 1C-10C pulsed rates.

6.6.2 Li//LTO-P/AC//Li hybrid system
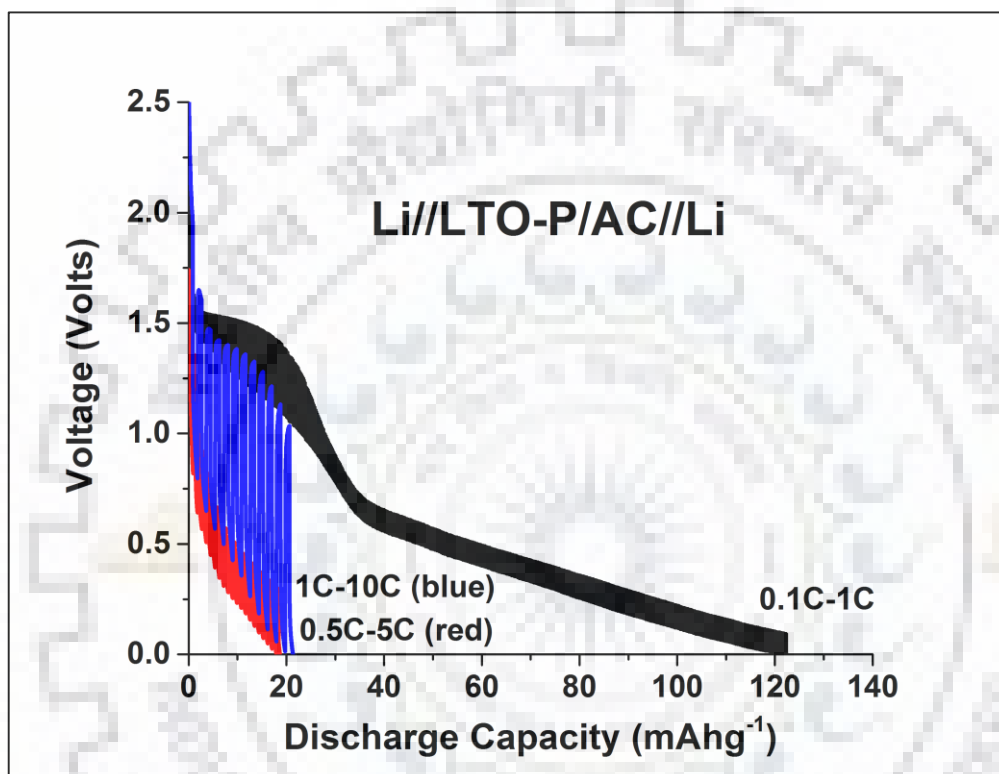
Figure 6.22 Discharge patterns obtained for Li//LTO-P/AC//Li hybrid system at different pulse patterns

The discharge capacity of Li//LTO-P/AC//Li hybrid system obtained at 0.1C-1C, 0.5C-5C and 1C-10C pulse patterns are 122mAhg^{-1}, 22mAhg^{-1} and 20mAhg^{-1} respectively.

The discharge capacities of LTO based battery, Li//LTO/AC//Li hybrid system and Li//LTO-P/AC//Li hybrid system obtained are compared at 0.1C-1C, 0.5C-5C and 1C-10C pulse patterns and are shown in Figure 6.23.
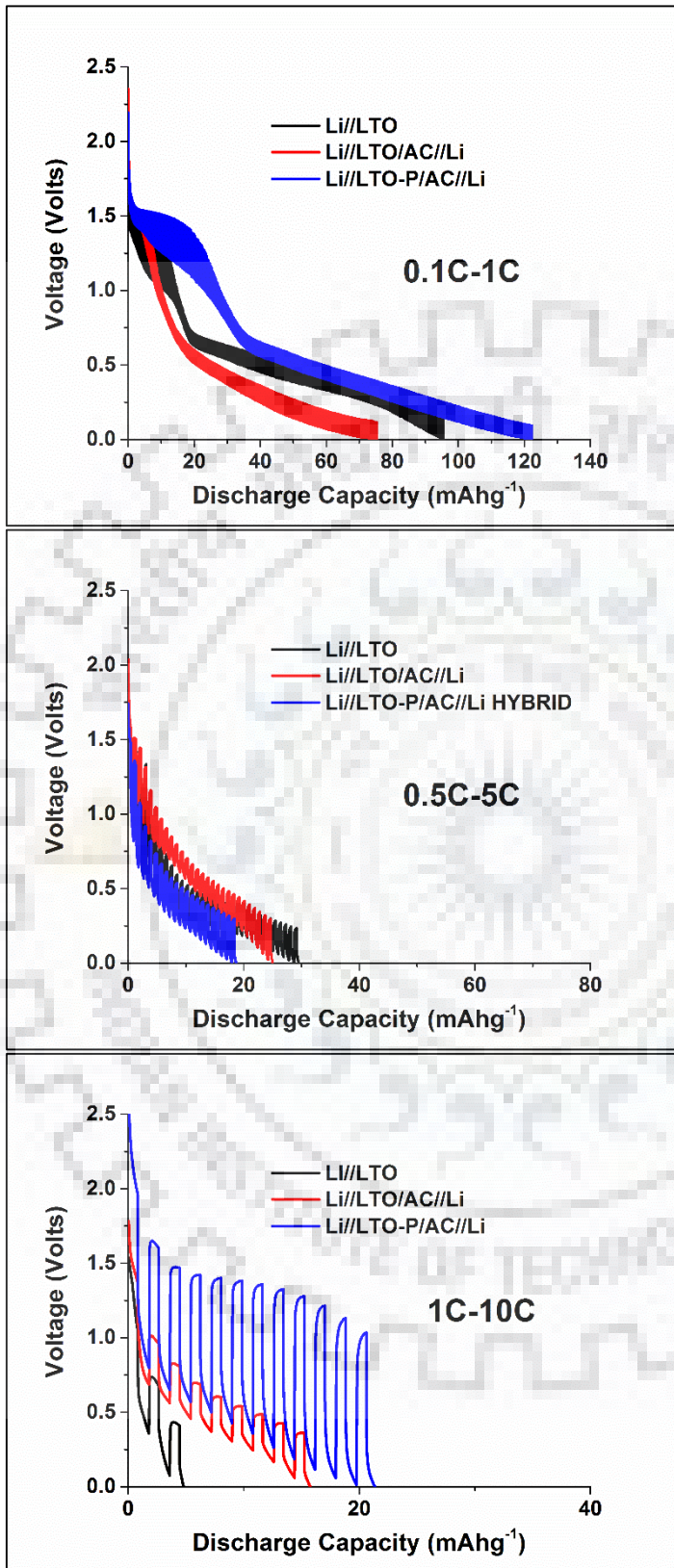
Figure 6.23

Discharge profiles comparison of Li//LTO battery, Li//LTO/AC//Li hybrid system and Li//LTO-P/AC//Li hybrid system for
(a) 0.1C-1C pulse pattern
(b) 0.5C-5C pulse pattern
(c) 1C-10C pulse pattern

By making the LTO nanoporous the discharge capacity of hybrid system is increased from 76mAhg^{-1} to 122mAhg^{-1} for 0.1C-1C pulse pattern which is also higher than the discharge capacity of LTO based battery.

Hence we may say that improvement of battery material in battery – supercapacitor hybrid system is necessary to get the beneficial results. In case of 0.5C-5C and 1C-10C pulse patterns the comparison shows that there is not much difference in discharge capacities of Li//LTO/AC//Li hybrid system and Li//LTO-P/AC//Li hybrid system.

6.6.3 Li//VLTO-10AR/AC//Li hybrid system
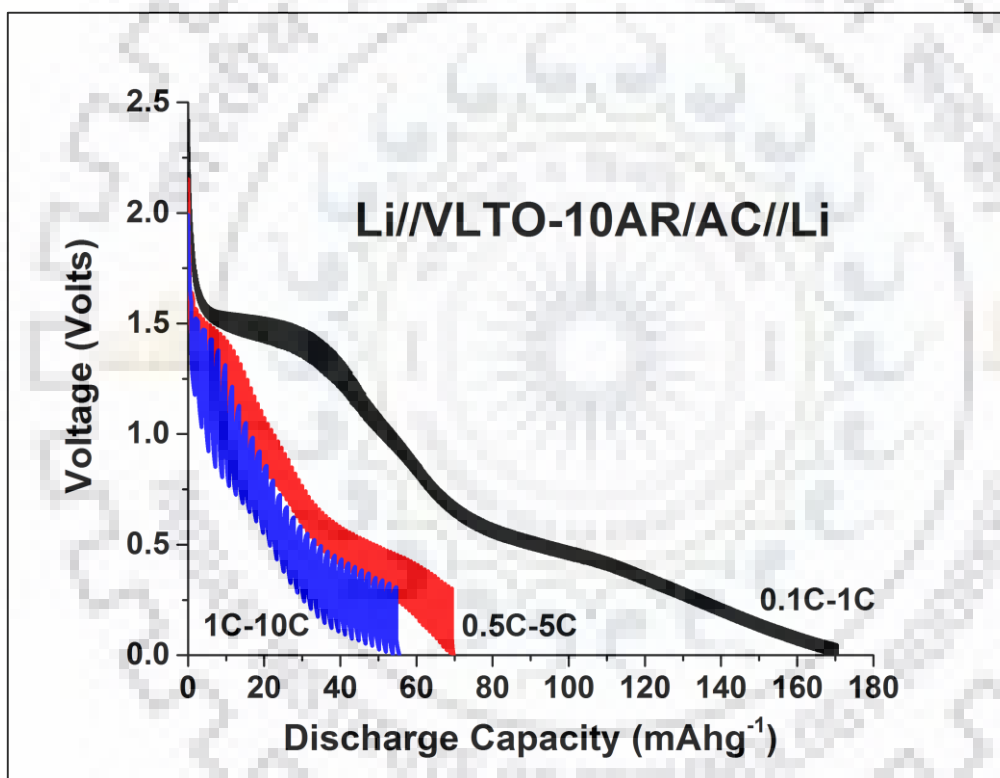
Figure 6.24 Discharge profiles obtained for Li//VLTO-10AR/AC//Li hybrid system at different pulse patterns
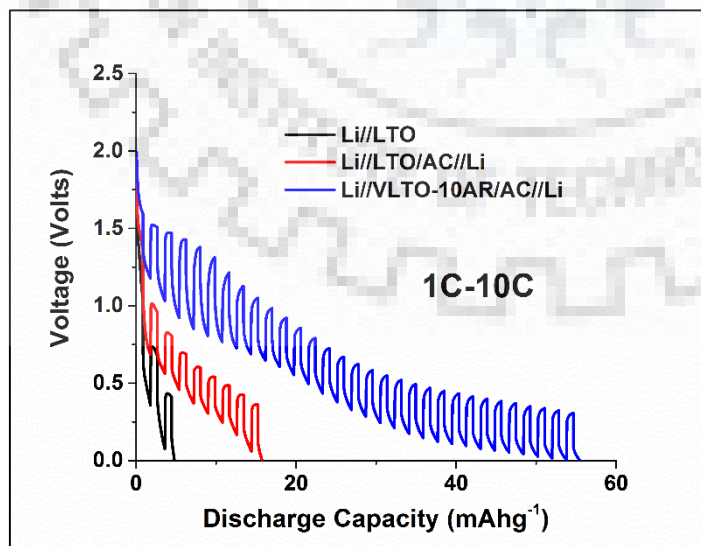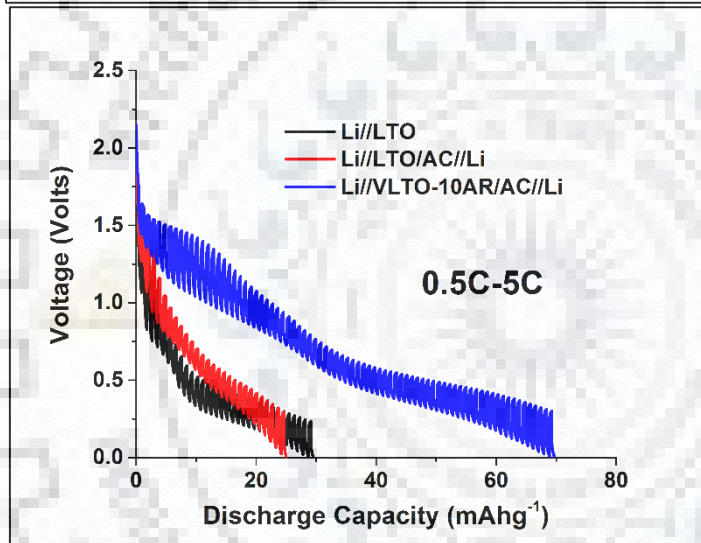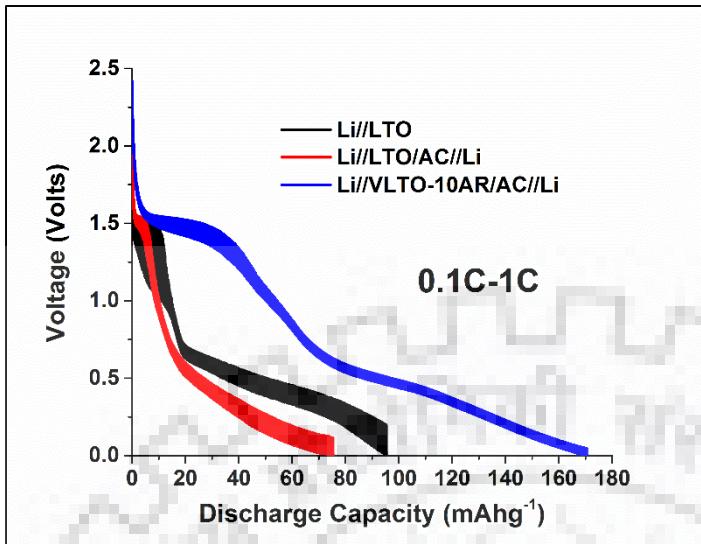
Figure 6.25

Discharge profiles comparison of Li//LTO battery, Li//LTO/AC//Li hybrid system and Li//VLTO-10AR/AC//Li hybrid system for
(a) 0.1C-1C pulse pattern
(b) 0.5C-5C pulse pattern
(c) 1C-10C pulse pattern

The discharge capacities of Li//VLTO-10AR/AC//Li hybrid system obtained at 0.1C-1C, 0.5C-5C and 1C-10C pulse rates are 170mAhg^{-1}, 69mAhg^{-1} and 54mAhg^{-1} respectively as shown in Figure 6.24. The discharge profiles of LTO based battery, Li//LTO/AC//Li hybrid system and Li/VLTO-10AR/AC//Li hybrid system obtained are compared at 0.1C-1C, 0.5C-5C and 1C-10C pulse patterns and are shown in Figure 6.25.A significant enhancement in the discharge capacity is observed by replacing LTO with VLTO-10AR material in the hybrid system.

There discharge profiles at 0.5C-5C and 1C-10C pulse patterns are also compared which shows that the discharge capacities of Li//VLTO-10AR/AC//Li hybrid system are much higher at pulse patterns corresponding to higher C-rates compared to LTO based battery and Li//LTO/AC//Li hybrid system. On the basis of above mentioned observations one can conclude that VLTO-10AR is the best suitable battery material for lithium ion battery-supercapacitor hybrid.

Summary

With the aim of combining the high specific power of the supercapacitor and the high specific energy of the lithium ion battery by means of hybridization a novel three terminal hybrid structure consisting a bimaterial electrode with battery and supercapacitor materials sharing the common collector (Cu foil) on either sides has been investigated. AC based supercapacitor are also investigated in both half-cell and full cell configurations. Hybrid systems were constructed separately with LTO, LTO-P and VLTO-10AR as battery material along with AC as supercapacitor material in all the cases. All the hybrid systems are subjected to constant current charge-discharge at 0.1C, 0.2C, 0.5C, 1C, 2C and 5C. The discharge capacities of all the hybrid systems are compared along with the discharge capacities of LTO based battery system and AC based full cell supercapacitor system.

The Li//VLTO-10AR/AC//Li hybrid system and Li//LTO-P/AC//Li hybrid system shows significant increase in discharge capacities at all C-rates compared to Li//LTO/AC//Li hybrid system. The capacity of Li//LTO-P/AC//Li hybrid system reaches very close to LTO based battery at low C-rates. The Li//VLTO-10AR/AC//Li hybrid system performs much better than Li//LTO/AC//Li and Li//LTO-P/AC//Li LTO hybrid systems at moderate and high C-rates. Cyclic voltammetry is also performed for all the hybrid systems and compared.

The hybrid systems along with battery and supercapacitor systems are also tested for pulsed applications by means of studying their electrochemical behaviors on applying pulsating charge-discharge current.

The pulse patterns chosen having two current levels corresponding to different C-rates are 0.1C-1C, 0.5C-5C and 1C-10C. The duty cycle of the pulse patterns is 10%. VLTO-10AR is found to be the best suitable battery material for lithium ion battery-supercapacitor hybrid among all the materials studied.

Conclusions and Future scope

7.1 Conclusions

The major conclusions of the Ph.D. dissertation work are as follows:

- The internal hybrid of lithium ion battery and supercapacitor with parallel configuration is the area where more focused research work is required so as to enhance the performance of the hybrid device for large scale applications like energy storage for electric vehicle etc.

- LTO is established battery material and therefore one of the most suitable materials to be used in hybrid device. The performance of the device can be enhanced by using LTO with improved properties.

- Porous structure of battery material reduces the diffusion path for Li^+ due to which high rate performance is improved and become more compatible to be used with supercapacitor material in hybrid devices.

- High rate electrochemical performance is achievable by electrical conductivity enhancement. Doping of elements with higher oxidation states than Ti^{4+} (like V^{5+}, Ta^{5+} etc.) in LTO increases its conductivity which can be further enhanced by calcination in reduced atmosphere during synthesis LTO.

- Quantitative analysis of LTO synthesized by sol-gel process with stoichiometric ratio Li:Ti = 4:5 calcined in air shows presence of impurity phase of rutile TiO_2 by an amount of 7.8 wt. %. Theoretical estimation according to the chemical reaction given as

$$5 TiO_2 + 2 Li_2O = Li_4Ti_5O_{12}$$
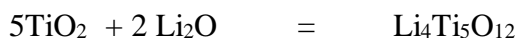
specifies that 10.07 wt. % excess Li is required for phase pure LTO which is also confirmed experimentally by XRD analysis of synthesized powder samples in $Li_{4+x}Ti_5O_{12}$ (x = 0.2, 0.4 and 0.6). The lithium intake capacity of LTO is enhanced for phase pure LTO.

- Carbon nanobeads (CNBs) can be used as template for synthesis of nanoporous LTO to obtain the average pore size of less than 100nm. The three fold increase in surface area by the presence of porosity enhances the discharge capacity of LTO based Li ion battery from 121mAhg^{-1} to 148mAhg^{-1}.

- Doping of vanadium does not change the crystal structure of LTO due to negligibly small difference in ionic radii of V^{5+} and Ti^{4+}. Narrow size distribution in particle size can be achieved by doping of vanadium in LTO followed by calcination in air, for which the reduction of Ti^{4+} ions to Ti^{3+} ions does not occur. Therefore the excess charge at Ti^{4+} site due to V^{5+} is compensated by defects formation in the crystal structure. In case of argon calcined vanadium doped LTO the reduction of Ti^{4+} ions to Ti^{3+} ions is enhanced by V doping.

- The lithium ion diffusivity in vanadium doped LTO is increased up to two orders with the increase of doping concentration from 0 to 3 wt. %. Electronic conductivity can be increased up to three orders compared to pristine LTO by V doping followed by calcination in argon atmosphere. The discharge capacity of LTO is enhanced up to 2 wt. % of V doping. $Li_4Ti_{4.9}V_{0.1}O_{12}$ calcined in argon atmosphere is found to have superior properties among all the synthesized materials for use of anode material of Li-ion battery.

- A novel three terminal hybrid structure consisting a bimaterial electrode with battery and supercapacitor materials sharing the common collector on either side investigated, shows that the discharge capacities are increased significantly at all C-rates by using LTO-P-AC and VLTO-10AR-AC as bimaterial electrode in the hybrid system as compared to LTO-AC. The discharge capacity of Li//LTO-P/AC//Li hybrid system reaches very close to LTO based battery at low C-rates. The Li//VLTO-10AR/AC//Li hybrid system performs much better than Li//LTO/AC//Li and Li//LTO-P/AC//Li hybrid system at moderate and high C-rates.

- The pulsating current discharge the battery very fast. The discharge capacity of LTO based battery is 407 mAhg^{-1} at constant current of 0.1C rate which reduces to 96 mAhg^{-1} at pulsating current having 0.1C-1C pattern. The discharge capacity is further reduced to 5 mAhg^{-1} for 1C-10C pulse pattern. Li//LTO/AC//Li hybrid system whose discharge

capacity is 113 mAhg^{-1} at constant current of 0.1C rate reduces to 76 mAhg^{-1} at a pulsating current having 0.1C-1C pattern which is further reduced to 16 mAhg^{-1} for 1C-10C pulse pattern. Therefore it is inferred that at high rate pulsating current Li//LTO/AC//Li hybrid system sustained more capacity compared to LTO based battery.

- The effect of pulsating current can be reduced to a large extent by enhancing the properties of LTO. The discharge capacities of Li//LTO-P/AC//Li and Li//VLTO-10AR/AC//Li hybrid system for pulse pattern 0.1C-1C are 122 mAhg^{-1} and 170mAhg^{-1} respectively which are much higher than LTO based battery and Li//LTO/AC//Li hybrid system.

- The Li//VLTO-10AR/AC//Li hybrid system with a discharge capacity of 70 mAhg^{-1} and 54mAhg^{-1} for high C-rate pulse patterns of 0.5C-5C and 1C-10C with duty cycle of 10% respectively found to be the best internal parallel hybrid system among all the systems studied.

7.2 Future scope

There is a vast scope of further development in high energy density and high power density energy storage systems as their demand is increasing with time. Although a number of important conclusions have been drawn from the present study, but several phenomena reported here need further investigation to enhance the knowledge. Some suggestions for future work have been listed below:

1. The other methods to improve the properties of LTO material can be adopted viz. carbon coating, making nanorods of LTO etc.

2. The novel hybrid system can be further investigated with different anode materials with high discharge capacity.

3. Bimaterial electrodes of cathode material and supercapacitor material can also be studied as per the proposed hybrid system.

4. The current sharing between battery material and supercapacitor material has to be investigated by advanced in situ techniques.

5. A comparative study of different available hybrid designs may be accomplished to understand the effect of electrode designs on the performance of the hybrid systems in a better way.

6. High performance 3D structures of electrode materials can be used in the hybrid system to enhance their performance.

References

References

Algharaibeh, Z., Liu, X., & Pickup, P. G. (2009). An asymmetric anthraquinone-modified carbon / ruthenium oxide supercapacitor. *Journal of Power Sources*, *187*, 640–643.

Alias, N. A., Kufian, M. Z., Teo, L. P., Majid, S. R., & Arof, A. K. (2009). Synthesis and characterization of $Li_4Ti_5O_{12}$. *Materials Chemistry and Physics*, *486*, 645–648.

Arbizzani, C., Beninati, S., Lazzari, M., Soavi, F., & Mastragostino, M. (2007). Electrode materials for ionic liquid-based supercapacitors. *Journal of Power Sources*, *174*, 648–652.

Arbizzani, C., Biso, M., Cericola, D., Lazzari, M., Soavi, F., & Mastragostino, M. (2008). Safe , high-energy supercapacitors based on solvent-free ionic liquid electrolytes. *Journal of Power Sources*, *185*, 1575–1579.

Arbizzani, C., Mastragostino, M., & Soavi, F. (2001). New trends in electrochemical supercapacitors. *Journal of Power Sources*, *100*, 164–170.

Armand, M. (1994). The history of polymer electrolytes. *Solid State Ionics*, *69*, 309–319.

Bach, S. (1999). Electrochemical properties of sol – gel $Li_{4/3}Ti_{5/3}O_4$. *Journal of Power Sources*, *81–82*, 273–276.

Bai, L., Changming, L., & Thomas, G. (1998). High power, high energy, hybrid electrode an electrical energy storage device made therefrom. *US Patent 5744258*.

Balducci, A., Bardi, U., Caporali, S., Mastragostino, M., & Soavi, F. (2004). Ionic liquids for hybrid supercapacitors. *Electrochemistry Communications*, *6*, 566–570.

Balducci, A., Henderson, W. A., Mastragostino, M., Passerini, S., Simon, P., & Soavi, F. (2005). Cycling stability of a hybrid activated carbon // poly (3-methylthiophene) supercapacitor with N -butyl- N -methylpyrrolidinium bis (trifluoromethanesulfonyl) imide ionic liquid as electrolyte. *Electrochimica Acta*, *50*, 2233–2237.

Becker, H. I. (1957). Low voltage electrolytic capacitor. *US Patent 2800616*.

Biendicho, J. J., & West, A. R. (2012). Impedance characterisation of $LiFePO_4$ ceramics. *Solid State Ionics*, *226*, 41–52.

Bobade, S. M., Gulwade, D. D., Kulkarni, A. R., & Gopalan, P. (2005). Dielectric properties of A- and B-site-doped $BaTiO_3$(I): La- and Al-doped solid solutions. *Journal of Applied*

Physics, 97, *74105*.

Brousse, T., Taberna, P., Crosnier, O., Dugas, R., Guillemet, P., Scudeller, Y., … Simon, P. (2007). Long-term cycling behavior of asymmetric activated carbon / MnO_2 aqueous electrochemical supercapacitor. *Journal of Power Sources*, *173*, 633–641.

Brousse, T., Taberna, P., & Simon, P. (2006). $TiO_2(B)$ / activated carbon non-aqueous hybrid system for energy storage. *Journal of Power Sources*, *158*, 571–577.

Burke, A. (2008). Proc. the 18th International Seminar on Double Layer Capacitors and Similar Energy Storage Device, Deerfield Beach, Florida.

Cericola, D., & Kötz, R. (2012). Hybridization of rechargeable batteries and electrochemical capacitors: Principles and limits. *Electrochimica Acta*, *72*, 1-17.

Cericola, D., Novák, P., Wokaun, A., & Kötz, R. (2011). Hybridization of electrochemical capacitors and rechargeable batteries: An experimental analysis of the different possible approaches utilizing activated carbon, $Li_4Ti_5O_{12}$ and $LiMn_2O_4$. *Journal of Power Sources*, *196*, 10305-10313.

Chen, C. H., Vaughey, J. T., Jansen, A. N., Dees, D. W., Kahaian, A. J., Goacher, T., & Thackeray, M. M. (2001). Studies of Mg-Substituted $Li_{4-x}Mg_xTi_5O_{12}$ Spinel Electrodes ($0 \leq x \leq 1$) for Lithium Batteries. *Journal of Electrochemical Society*, *148*(1), 103–105.

Chen, C., Spears, M., Wondre, F., & Ryan, J. (2003). Crystal growth and superconductivity of $LiTi_2O_4$ and $Li_{1+1/3}Ti_{2-1/3}O_4$. *Journal of Crystal Growth*, *250*(1–2), 139–145.

Chen, F., Li, R., Hou, M., Liu, L., Wang, R., & Deng, Z. (2005). Preparation and characterization of ramsdellite $Li_2Ti_3O_7$ as an anode material for asymmetric supercapacitors. *Electrochimica Acta*, *51*, 61–65.

Chen, J., Yang, L., Fang, S., Hirano, S., & Tachibana, K. (2012). Synthesis of hierarchical mesoporous nest-like $Li_4Ti_5O_{12}$ for high-rate lithium ion batteries. *Journal of Power Sources*, *200*, 59–66.

Chen, J.-S., Stolojan, V., & Silva, S. R. P. (2015). Towards type-selective carbon nanotube growth at low substrate temperature via photo-thermal chemical vapour deposition. *Carbon*, *84*, 409–418

Chen, L., Lai, Q., Hao, Y., Zhao, Y., & Ji, X. Y. (2009). Investigations on capacitive properties

of the AC / V_2O_5 hybrid supercapacitor in various aqueous electrolytes. *Journal of Alloys and Compounds*, *467*, 465–471.

Christiansen, B. Z., West, K., Jacobsen, T., & Atlung, S. (1988). Lithium insertion in different TiO_2 modifications. *Solid State Ionics*, *28–30*, 1176–1182.

Colbow, K. M., Dahn, J. R., & Haering, R. R. (1989). Structure and electrochemistry of the spinel oxides $LiTi_2O_4$ and $Li_{4/3}Ti_{5/3}O_4$. *Journal of Power Sources*, *26*(3–4), 397–402.

Das, S., Chakraborty, S., Parkash, O., Kumar, D., Bandyopadhyay, S., Samudrala, S. K., … Maiti, H. S. (2008). Vanadium doped tin dioxide as a novel sulfur dioxide sensor. *Talanta*, *75*(2), 385–389.

Deschanvres, A; Raveau, B.; Sekkal, Z. (1971). Mise En Evidence Et Etude Cristallographioue D'une Nouvelle Solution Solide De Type Spinelle $Li_{l+x}Ti_{2-x}O_4$ $0 \leq x \leq 0.33$. *Materials Research Bulletin*, *6*, 699–704.

Dougal, R. A., Member, S., Liu, S., & White, R. E. (2002). Power and Life Extension of Battery – Ultracapacitor Hybrids. *IEEE Transactions on Components Packaging and Manufacturing Technology*, *25*(1), 120–131.

Duffy, N. W., Baldsing, W., & Pandolfo, A. G. (2008). The nickel – carbon asymmetric supercapacitor — Performance , energy density and electrode mass ratios. *Electrochimica Acta*, *54*, 535–539.

Ferg, E., Gummow, R. J., & Kock, A. De. (1994). Spinel Anodes for Lithium-Ion Batteries, *141*(11), 9–12.

Ganesh, V., Pitchumani, S., & Lakshminarayanan, V. (2006). New symmetric and asymmetric supercapacitors based on high surface area porous nickel and activated carbon. *Journal of Power Sources*, *158*, 1523–1532.

Gao, J., Jiang, C., Ying, J., & Wan, C. (2006). Preparation and characterization of high-density spherical $Li_4Ti_5O_{12}$ anode material for lithium secondary batteries. *Journal of Power Sources*, *155*, 364–367.

Garg, Ashish, Kar, Soumya, Dixit, Anju, & Agrawal, D. C. (2007). Sol-Gel Synthesis and Characterization of $BiFeO_3$-$PbTiO_3$ Thin Films. *MRS Proceedings,* 997.

Ghosh, S., Mitra, S., & Barpanda, P. (2016). Sonochemical Synthesis of Nanostructured Spinel

Li$_4$Ti$_5$O$_{12}$ Negative Insertion Material for Li-ion and Na-ion Batteries. *Electrochimica Acta*, *222*, 898–903.

Goodenough, J. B., & Kim, Y. (2010). Challenges for rechargeable Li batteries. *Chemistry of Materials*, *22*(3), 587–603.

Gopalan, P., Bhandari, S., Kulkarni, A. R., & Palkar, V. R. (2002). Effect of preparative parameters on the electrical conductivity of Li$_2$SO$_4$ ± Al$_2$O$_3$ composites. *Materials Research Bulletin*, *37*, 2043–2053.

Goriparti, S., Miele, E., De Angelis, F., Di Fabrizio, E., Proietti Zaccaria, R., & Capiglia, C. (2014). Review on recent progress of nanostructured anode materials for Li-ion batteries. *Journal of Power Sources*, *257*, 421–443.

Gu, Y., Guo, Z., & Liu, H. (2014). Structure and electrochemical properties of Li$_4$Ti$_5$O$_{12}$ with Li excess as an anode electrode material for Li-ion batteries. *Electrochimica Acta*, *123*, 576–581.

Hain, H., Scheuermann, M., Heinzmann, R., Wünsche, L., Hahn, H., & Indris, S. (2012). Study of local structure and Li dynamics in Li$_{4+x}$Ti$_5$O$_{12}$ (0 ≤ x ≤ 5) using ^{6}Li and ^{7}Li NMR spectroscopy. *Solid State Nuclear Magnetic Resonance*, *42*, 9–16.

Hao, Y. J., Lai, Q. Y., Wang, L., Xu, X., & Chu, H. Y. (2010). Electrochemical performance of a high cation-deficiency Li$_2$Mn$_4$O$_9$ / active carbon supercapacitor in LiNO$_3$ electrolyte. *Synthetic Metals*, *160*(7–8), 669–674.

Hao, Y., Lai, Q., & Lu, J. (2007). Effects of dopant on the electrochemical properties of Li$_4$Ti$_5$O$_{12}$ anode materials. *Ionics*, (3), 369–373.

Hao, Y., T, Q. L., Xu, Z., Liu, X., & Ji, X. (2005). Synthesis by TEA sol – gel method and electrochemical properties of Li$_4$Ti$_5$O$_{12}$ anode material for lithium-ion battery. *Solid State Ionics*, *176*, 1201–1206.

Harrison, M.R.; Edwards, P.P.; Goodenough, J. B. (1984). A Study of the Li$_{1+x}$Ti$_{2-x}$O$_4$ Spine1 System by Diffuse-Reflectance Spectroscopy. *Journal of Solid State Chemistry*, 426–437.

Holland, C. E., Weidner, J. W., Dougal, R. A., & White, R. E. (2002). Experimental characterization of hybrid power systems under pulse current loads. *Journal of Power Sources*, *109*, 32–37.

Hsiao, K. C., Liao, S. C., & Chen, J. M. (2008). Microstructure effect on the electrochemical property of $Li_4Ti_5O_{12}$ as an anode material for lithium-ion batteries. *Electrochimica Acta*, *53*(24), 7242–7247.

Hu, C., & Tsou, T. (2002a). Capacitive and textural characteristics of hydrous manganese oxide prepared by anodic deposition. *Electrochimica Acta*, *47*, 3523–3532.

Hu, C., & Tsou, T. (2002b). Ideal capacitive behavior of hydrous manganese oxide prepared by anodic deposition. *Electrochemistry Communications*, *4*, 105–109.

Hu, X., Deng, Z., Suo, J., & Pan, Z. (2009). A high rate, high capacity and long life ($LiMn_2O_4$+ AC)/$Li_4Ti_5O_{12}$ hybrid battery–supercapacitor. *Journal of Power Sources*, *187*(2), 635-639.

Hu, X., Huai, Y., Lin, Z., Suo, J., & Deng, Z. (2007). A ($LiFePO_4$–AC)∕$Li_4Ti_5O_{12}$ Hybrid Battery Capacitor. *Journal of the Electrochemical Society*, *154*(11), A1026-A1030.

Hu, X., Lin, Z., Yang, K., Huai, Y., & Deng, Z. (2011). Effects of carbon source and carbon content on electrochemical performances of $Li_4Ti_5O_{12}$ / C prepared by one-step solid-state reaction. *Electrochimica Acta*, *56*(14), 5046–5053.

Huang, S., Wen, Z., Zhu, X., & Lin, Z. (2007). Effects of dopant on the electrochemical performance of $Li_4Ti_5O_{12}$ as electrode material for lithium ion batteries. *Journal of Power Sources*, *165*, 408–412.

Hubbard, C. R., Evans, E. H., & Smith, D. K. (1976). The reference intensity ratio, I/Ic, for computer simulated powder patterns. *Journal of Applied Crystallography*, *9*(2), 169-174.

Hung, P., Chang, K., Lee, Y., Hu, C., & Lin, K. (2010). Ideal asymmetric supercapacitors consisting of polyaniline nanofibers and graphene nanosheets with proper complementary potential windows. *Electrochimica Acta*, *55*(20), 6015–6021.

Idota, Y. (1997). Tin-Based Amorphous Oxide: A High-Capacity Lithium-Ion-Storage Material. *Science*, *276*(5317), 1395–1397.

Johnston, D. C., Prakash, H., & Zachariasen, W. H. (1973). High Temperature Suprconductivity in Li-Ti-O Ternary System, *8*(53), 777–784.

Kalhammer, F. R. (1995). Performance and Availability of Batteries for Electric Vehicles: *A Report of the Battery Technical Advisory Panel. California Air Resources Board*

Karthikeyan, K., Aravindan, V., Lee, S. B., Jang, I. C., Lim, H. H., Park, G. J., … Lee, Y. S. (2010). A novel asymmetric hybrid supercapacitor based on Li_2FeSiO_4 and activated carbon electrodes. *Journal of Alloys and Compounds*, *504*(1), 224–227.

Kawai, H., Nagata, M., Tabuchi, M., Tukamoto, H., & West, A. R. (1998). Novel 5 V Spinel Cathode $Li_2FeMn_3O_8$ for Lithium Ion Batteries. *Chemistry of Materials*, (17), 3266–3268.

Khomenko, V. (2008). High-energy density graphite / AC capacitor in organic electrolyte. *Journal of Power Sources*, *177*, 643–651.

Khomenko, V., Raymundo-Piñero, E., & B´eguin, F. (2006). Optimisation of an asymmetric manganese oxide / activated carbon capacitor working at 2 V in aqueous medium. *Journal of Power Sources*, *153*, 183–190.

Konno, H., Kasashima, T., & Azumi, K. (2009). Application of Si – C – O glass-like compounds as negative electrode materials for lithium hybrid capacitors. *Journal of Power Sources*, *191*, 623–627.

Kubiak, P., Garcia, A., Womes, M., Aldon, L., Olivier-Fourcade, J., Lippens, P. E., & Jumas, J. C. (2003). Phase transition in the spinel $Li_4Ti_5O_{12}$ induced by lithium insertion - Influence of the substitutions Ti/V, Ti/Mn, Ti/Fe. *Journal of Power Sources*, *119–121*, 626–630.

Kuperman, A., & Aharon, I. (2011). Battery-ultracapacitor hybrids for pulsed current loads: A review. *Renewable and Sustainable Energy Reviews*, *15*(2), 981–992.

Lam, L. T., & Louey, R. (2006). Development of ultra-battery for hybrid-electric vehicle applications. *Journal of Power Sources*, *158*, 1140–1148.

Li, X., Qu, M., & Yu, Z. (2009). Structural and electrochemical performances of $Li_4Ti_{5-x}Zr_xO_{12}$ as anode material for lithium-ion batteries. *Journal of Alloys and Compounds*, *487*, L12–L17.

Liang, Y., Li, H., & Zhang, X. (2008). A novel asymmetric capacitor based on $Co(OH)_2$ / USY composite and activated carbon electrodes. *Materials Science and Engineering A*, *473*, 317–322.

Lim, J., Choi, E., Mathew, V., Kim, D., Ahn, D., Gim, J., … Kim, J. (2011). Enhanced High-Rate Performance of $Li_4Ti_5O_{12}$ Nanoparticles for Rechargeable Li-Ion Batteries, 275–280.

Lin, C., Ding, B., Xin, Y., Cheng, F., Lai, M. O., Lu, L., & Zhou, H. (2014). Advanced

electrochemical performance of $Li_4Ti_5O_{12}$-based materials for lithium-ion battery: Synergistic effect of doping and compositing. *Journal of Power Sources*, *248*, 1034–1041.

Lin, C., Ritter, J. A., Popov, B. N., & White, R. E. (1999). A Mathematical Model of an Electrochemical Capacitor with Double-Layer and Faradaic Processes. *Journal of Electrochemical Society*, *146*(9), 3168–3175.

Liu, H., He, P., Li, Z., Liu, Y., & Li, J. (2006). A novel nickel-based mixed rare-earth oxide / activated carbon supercapacitor using room temperature ionic liquid electrolyte. *Electrochimica Acta*, *51*, 1925–1931.

Liu, J., Li, X., Yang, J., Geng, D., Li, Y., Wang, D., … Verbrugge, M. W. (2012). Microwave-assisted hydrothermal synthesis of nanostructured spinel $Li_4Ti_5O_{12}$ as anode materials for lithium ion batteries. *Electrochimica Acta*, *63*, 100–104.

Lu, W., Belharouak, I., Liu, J., & Amine, K. (2007). Electrochemical and Thermal Investigation of $Li_{4/3}Ti_{5/3}O_4$ spinel. *Journal of Electrochemical Society*, *154(2)* 114–118.

Luo, J., & Xia, Y. (2009). Electrochemical profile of an asymmetric supercapacitor using carbon-coated $LiTi_2(PO_4)_3$ and active carbon electrodes. *Journal of Power Sources*, *186*, 224–227.

Lv, Y., Zhang, H., Cao, G., Wang, B., & Wang, X. (2011). Phenol-formaldehyde resin-assisted synthesis of pure porous $Li_4Ti_5O_{12}$ for rate capability improvement. *Materials Research Bulletin*, *46*(12), 2312–2316.

Mahajan, S., Thakur, O. P., Prakash, C., & Sreenivas, K. (2011). Effect of Zr on dielectric , ferroelectric and impedance properties of $BaTiO_3$ ceramic. *Bulletin of Materials Science*, *34*(7), 1483–1489.

Mahmoud, A., Amarilla, J. M., Lasri, K., & Saadoune, I. (2013). Influence of the synthesis method on the electrochemical properties of the $Li_4Ti_5O_{12}$ spinel in Li-half and Li-ion full-cells. A systematic comparison. *Electrochimica Acta*, *93*, 163–172.

Maisnam, M., Phanjoubam, S., Sarma, H. N. K., Devi, L. R., Thakur, O. P., & Prakash, C. (2005). BH loop properties of V5+ substituted Li-Zn-Ti ferrites. *Indian Journal of Physics and Proceedings of The Indian Association for the Cultivation of Science,* 79(9), 981-983).

Maloney, R. P., Kim, H. J., & Sakamoto, J. S. (2012). Lithium titanate aerogel for advanced lithium-ion batteries. *ACS Applied Materials and Interfaces*, *4*(5), 2318–2321.

Martın, P., Lo, M. L., Pico, C., & Veiga, M. L. (2007). $Li_{(4-x)/3}Ti_{(5-2x)/3}Cr_xO_4$ $(0 \leq x \leq 0.9)$ spinels: New negatives forlithium batteries. *Solid State Sciences*, *9*(3), 521–526.

Mastragostino, M., & Soavi, F. (2007). Strategies for high-performance supercapacitors for HEV. *Journal of Power Sources*, *174*, 89–93.

Mizushima, K., Jones, P.C., Wiseman, P.J., Goodenough, J.B. (1980) $LixCoO_2$ $(0<x<l)$: A new cathode material for batteries of high energy density. *Materials Research Bulletin*, *15*, 783 – 789.

Mosa, J., Vélez, J. F., Lorite, I., Arconada, N., & Aparicio, M. (2012). Film-shaped sol – gel $Li_4Ti_5O_{12}$ electrode for lithium-ion microbatteries. *Journal of Power Sources*, *205*, 491– 494.

Moseley, P. T., Nelson, R. F., & Hollenkamp, A. F. (2006). The role of carbon in valve-regulated lead – acid battery technology ☪. *Journal of Power Sources*, *157*, 3–10.

Moshopoulou, E. G. (1999). Superconductivity in the Spinel Compound $LiTi_2O4$. *Journal of the American Ceramic Society*, *82*(12), 3317–3320.

Mosqueda, H. A., Crosnier, O., Athouël, L., Dandeville, Y., Scudeller, Y., Guillemet, P., … Brousse, T. (2010). Electrolytes for hybrid carbon – MnO 2 electrochemical capacitors. *Electrochimica Acta*, *55*, 7479–7483.

Mukherjee, S., Gupta, R., Garg, A., Mukherjee, S., Gupta, R., & Garg, A. (2013). Dielectric response and magnetoelectric coupling in single crystal gallium ferrite. *AIP ADVANCES*, *3*, 52115.

Murphy, D., Cava, R., Zahurak, S., & Santoro, A. (1983). Ternary Li_xTiO_2 phases from insertion reactions. *Solid State Ionics*, *9–10*, 413–417.

Naoi, K., Ishimoto, S., Isobe, Y., & Aoyagi, S. (2010). High-rate nano-crystalline $Li_4Ti_5O_{12}$ attached on carbon nano-fibers for hybrid supercapacitors. *Journal of Power Sources*, *195*(18), 6250–6254.

Nishi, Y., Azuma, H., Omaru, A. (1990) Non aqueous electrolyte cell *U. S. Patent 4959281*.

Ng, S. H., Wang, J., Wexler, D., Konstantinov, K., Guo, Z. P., & Liu, H. K. (2006). Highly reversible lithium storage in spheroidal carbon-coated silicon nanocomposites as anodes for lithium-ion batteries. *Angewandte Chemie - International Edition*, *45*(41), 6896–6899.

Nohara, S., Asahina, T., Wada, H., Furukawa, N., Inoue, H., Sugoh, N., … Iwakura, C. (2006). Hybrid capacitor with activated carbon electrode , $Ni(OH)_2$ electrode and polymer hydrogel electrolyte. *Journal of Power Sources*, *157*, 605–609.

Ohzuku, T., Makimura, Y., (2001) Layered lithium insertion material of $LiNi_{1/2}Mn_{1/2}O_2$: A possible alternative to $LiCoO_2$ for advanced lithium-ion batteries. *Chemistry Letters*, *642 (30)*, 744 – 745.

Ohzuku, T., Ueda, A., & Yamamota, N. (1995). Zero-Strain Insertion Material of $Li[Li_{1/3}Ti_{5/3}]O4$ for Rechargeable Lithium Cells. *Journal of Electrochemical Society*, *142*(5), 5–9.

Ouyang, C. Y., Zhong, Z. Y., & Lei, M. S. (2007). Ab initio studies of structural and electronic properties of $Li_4Ti_5O_{12}$ spinel. *Electrochemistry Communications*, *9*(5), 1107–1112.

Pasquier, A. Du, Plitz, I., Menocal, S., & Amatucci, G. (2003). A comparative study of Li-ion battery , supercapacitor and nonaqueous asymmetric hybrid devices for automotive applications. *Journal of Power Sources*, *115*, 171–178.

Perret, P., Khani, Z., Brousse, T., Bélanger, D., & Guay, D. (2011). Carbon / PbO_2 asymmetric electrochemical capacitor based on methanesulfonic acid electrolyte. *Electrochimica Acta*, *56*(24), 8122–8128.

Qu, Q., Li, L., Tian, S., Guo, W., Wu, Y., & Holze, R. (2010). A cheap asymmetric supercapacitor with high energy at high power : Activated carbon//$K_{0.27}MnO_2.0.6H_2O$. *Journal of Power Sources*, *195*, 2789–2794.

Qu, Q. T., Shi, Y., Li, L. L., Guo, W. L., Wu, Y. P., Zhang, H. P., … Holze, R. (2009). $V_2O_5.0.6H_2O$ nanoribbons as cathode material for asymmetric supercapacitor in K_2SO_4 solution. *Electrochemistry Communications*, *11*(6), 1325–1328.

Qu, Q. T., Shi, Y., Tian, S., Chen, Y. H., Wu, Y. P., & Holze, R. (2009). A new cheap asymmetric aqueous supercapacitor : Activated carbon // $NaMnO_2$. *Journal of Power Sources*, *194*, 1222–1225.

Rajarathinam, S., Mitra, S., & Petla, R. K. (2013). Li_2MnO_3 rich-$LiMn_{0.33}Co_{0.33}Ni_{0.33}O_2$ integrated nano-composites as high energy density lithium-ion battery cathode materials. *Electrochimica Acta*, *108*, 135–144.

Rao, C. V., & Rambabu, B. (2010). Nanocrystalline $LiCrTiO_4$ as anode for asymmetric hybrid

supercapacitor. *Solid State Ionics*, *181*(17–18), 839–843.

Reale, P., Panero, S., Scrosati, B., Garche, J., Wohlfahrt-Mehrens, M., & Wachtler, M. (2004). A Safe, Low-Cost, and Sustainable Lithium-Ion Polymer Battery. *Journal of The Electrochemical Society*, *151*(12), A2138.

Reeves-Mclaren, N., Smith, R. I., & West, A. R. (2011). Lithium-ion conduction pathways in complex lithium spinels $Li_2MGe_3O_8$ (M = Ni or Zn). *Chemistry of Materials*, *23*(15), 3556–3563.

Roberts, A. J., & Slade, R. C. T. (2010). Effect of specific surface area on capacitance in asymmetric carbon /α-MnO_2. *Electrochimica Acta*, *55*, 7460–7469.

Robertson, A. D., Trevino, L., Tukamoto, H., & Irvine, J. T. . (1999). New inorganic spinel oxides for use as negative electrode materials in future lithium-ion batteries. *Journal of Power Sources*, *81–82*, 352–357.

Rossouw, M. H. and Thackeray, M. M. (1991). Lithum Manganese Oxides from Li_2MnO_3 for Rechargable Lithium Battery Applications, *Materials Research Bulletin, 26*, 463–473.

Rouya, E., Cattarin, S., Reed, M. L., Kelly, R. G., & Zangari, G. (2012). Electrochemical Characterization of the Surface Area of Nanoporous Gold Films. *Journal of The Electrochemical Society*, *159*(4), K97.

Safronov, D. V, Novikova, S. A., Skundin, A. M., & Yaroslavtsev, A. B. (2012). Lithium Intercalation and Deintercalation Processes in $Li_4Ti_5O_{12}$ and $LiFePO_4$. *Inorganic Materials*, *48*(1), 57–61.

Saroha, R., Panwar, A. K., Sharma, Y., Tyagi, P. K., & Ghosh, S. (2017). Development of surface functionalized ZnO-doped $LiFePO_4$/C composites as alternative cathode material for lithium ion batteries. *Applied Surface Science*, *394*, 25–36.

Scharner, S.; Weppner, W ; Schmid-Beurmann, P. (1999). Evidence of Two-Phase Formation upon Lithium Insertion into the $Li_{1.33}Ti_{1.67}O_4$ Spinel. *Journal of Electrochemical Society*, *146*(3), 857–861.

Sengupta, R., Bhattacharya, M., Bandyopadhyay, S., & Bhowmick, A. K. (2011). A review on the mechanical and electrical properties of graphite and modified graphite reinforced polymer composites. *Progress in Polymer Science (Oxford)*, *36*(5), 638–670.

Shao, D., He, J., Luo, Y., & Liu, W. (2012). Synthesis and electrochemical performance of nanoporous $Li_4Ti_5O_{12}$ anode material for lithium-ion batteries, *c*, 2047–2053.

Shard, A. G., 2014. Detection limits in XPS for more than 6000 binary systems using Al and Mg Kα X-rays. *Surface and Interface Analysis*, *46*, 175–185.

Sharma, N., Kumar, S., Mall, A. K., Gupta, R., & Garg, A. (2017). Sr and Mn Co-doped sol-gel derived $BiFeO_3$ ceramics with enhanced magnetism and reduced leakage current enhanced magnetism and reduced leakage current. *Materials Research Express*, *4*, 015702.

Shen, K., Chen, H., Klaver, F., Mulder, F. M., & Wagemaker, M. (2014). Impact of particle size on the non-equilibrium phase transition of lithium-inserted anatase TiO_2. *Chemistry of Materials*, *26*(4), 1608–1615.

Shin, J. W., Chung, K. Y., Ryu, J. H., Park, I. W., & Yoon, D. H. (2012). Effects of Li/Ti ratios on the electrochemical properties of $Li_4Ti_5O_{12}$ examined by time-resolved X-ray diffraction. *Applied Physics A*, *107*(4), 769–775.

Sikha, G., & Popov, B. N. (2004). Performance optimization of a battery – capacitor hybrid system. *Journal of Power Sources*, *134*, 130–138.

Simon, P., & Gogotsi, Y. (2008). Materials for electrochemical capacitors. *Nature Materials*, *7*, 845–854.

Singh, B., Ghosh, S., Aich, S., & Roy, B. (2017). Low temperature solid oxide electrolytes (LT-SOE): A review. *Journal of Power Sources*, *339*, 103–135.

Singh, D., Mulder, F., Abdelkader, A., Wagemaker, M. (2013) Facile Micro Templating LiFePO4 Electrodes for High Performance Li-Ion Batteries. *Advnced Energy Materials*, *3(5)*, 572–578.

Snook, G. A., Kao, P., & Best, A. S. (2011). Conducting-polymer-based supercapacitor devices and electrodes. *Journal of Power Sources*, *196*(1), 1–12.

Song, H., Jeong, T.-G., Moon, Y. H., Chun, H.-H., Chung, K. Y., Kim, H. S., … Kim, Y.-T. (2014). Stabilization of oxygen-deficient structure for conducting $Li_4Ti_5O_{12-\delta}$ by molybdenum doping in a reducing atmosphere. *Scientific Reports*, *4*, 4350.

Song, X. Y., & Kinoshita, K. (1996). Microstructural Characterization of Lithiated Graphite. *Journal of Electrochemical Society*, *143*(6), L120–L123.

Sorensen, E. M., Barry, S. J., Jung, H., Rondinelli, J. R., Vaughey, J. T., Poeppelmeier, K. R., … Materials, A. V. (2006). Three-Dimensionally Ordered Macroporous $Li_4Ti_5O_{12}$: Effect of Wall Structure on Electrochemical Properties, (10), 482–489.

Sun, K., Lee, Y., Han, K., Joon, Y., Gu, M., Park, N., & Ho, S. (2004). Electrochemical supercapacitor based on polyaniline doped with lithium salt and active carbon electrodes. *Solid State Ionics*, *175*, 765–768.

Thackeray, M.M., David, W.I.F., Bruce, P.G., Goodenough, J.B. (1983) Lithium insertion into manganese spinels. *Materials Research Bulletin*, *18,* 461–472.

Thakur, O. P., & Prakash, C. (2009). Structural and electrical properties of Nb^{5+} substituted PZT ceramics. *Modern Physics Letters*, *468*(30), 356–359.

Tsai, P. C., Hsu, W. D., & Lin, S. K. (2014). Atomistic Structure and Ab Initio Electrochemical Properties of $Li_4Ti_5O_{12}$ Defect Spinel for Li Ion Batteries. *Journal of the Electrochemical Society*, *161*(3), A439–A444.

Venkateswarlu, M., Chen, C. H., Do, J. S., Lin, C. W., Chou, T. C., & Hwang, B. J. (2005). Electrochemical properties of nano-sized $Li_4Ti_5O_{12}$ powders synthesized by a sol – gel process and characterized by X-ray absorption spectroscopy, *146*, 204–208.

Wang, D., Li, F., & Cheng, H. (2008). Hierarchical porous nickel oxide and carbon as electrode materials for asymmetric supercapacitor. *Journal of Power Sources*, *185*, 1563–1568.

Wang, G., Zhang, B., Yu, Z., & Qu, M. (2005). Manganese oxide / MWNTs composite electrodes for supercapacitors. *Solid State Ionics*, *176*(9), 1169–1174.

Wang, H., Gao, Q., & Hu, J. (2010). Asymmetric capacitor based on superior porous Ni – Zn – Co oxide / hydroxide and carbon electrodes. *Journal of Power Sources*, *195*, 3017–3024.

Wang, H., & Yoshio, M. (2006). Graphite , a suitable positive electrode material for high-energy electrochemical capacitors. *Electrochemistry Communications*, *8*, 1481–1486.

Wang, H., & Yoshio, M. (2008a). Effect of cation on the performance of AC / graphite capacitor. *Electrochemical and Solid-State Letters*, *10*, 382–386.

Wang, H., & Yoshio, M. (2008b). Performance of AC / graphite capacitors at high weight ratios of AC / graphite. *Journal of Power Sources*, *177*, 681–684.

Wang, H., & Yoshio, M. (2010). Effect of water contamination in the organic electrolyte on the performance of activated carbon / graphite capacitors. *Journal of Power Sources*, *195*, 389–392.

Wang, H., Yoshio, M., Thapa, A. K., & Nakamura, H. (2007). From symmetric AC / AC to asymmetric AC / graphite , a progress in electrochemical capacitors. *Journal of Power Sources*, *169*, 375–380.

Wang, Y., Wang, Z., & Xia, Y. (2005). An asymmetric supercapacitor using RuO_2/TiO_2 nanotube composite and activated carbon electrodes. *Electrochimica Acta*, *50*, 5641–5646.

Wang, Y., & Xia, Y. (2005). A new concept hybrid electrochemical surpercapacitor : Carbon / $LiMn_2O_4$ aqueous system. *Electrochemistry Communications*, *7*, 1138–1142.

Wanger, C. D., Riggs, W. M., Davis, L. E., Moulder, J. F. and Muilenberg, G. E. (1981). Handbook of X-ray Photoelectron Spectroscopy *Perkin-Elmer Corp., Physical Electronics Division, Eden Prairie, Minnesota, USA, 1979. 190pp.*

Wen, Z., Gu, Z., Huang, S., Yang, J., Lin, Z., & Yamamoto, O. (2005). Research on spray-dried lithium titanate as electrode materials for lithium ion batteries. *Journal of Power Sources*, *146*(1–2), 670–673.

Winter, M., Besenhard, J. O., Spahr, M. E., & Novák, P. (1998). Insertion Electrode Materials for Rechargeable Lithium Batteries. *Advanced Materials*, *10*(10), 725–763.

Wolfenstine, J., & Allen, J. L. (2008). Electrical conductivity and charge compensation in Ta doped $Li_4Ti_5O_{12}$. *Journal of Power Sources*, *180*(1), 582–585.

Wolfenstine, J., Lee, U., & Allen, J. L. (2006). Electrical conductivity and rate-capability of $Li_4Ti_5O_{12}$ as a function of heat-treatment atmosphere. *Journal of Power Sources*, *154*(1), 287–289.

Xiao-feng, W., Dian-bo, R., & Zheng, Y. (2006). Application of spherical $Ni(OH)_2$/CNTs composite electrode in asymmetric supercapacitor. *Transactions of Nonferrous Metals Society of China*, *16*, 1129–1134.

Xu, B., Qian, D., Wang, Z., & Meng, Y. S. (2012). Recent progress in cathode materials research for advanced lithium ion batteries. *Materials Science and Engineering: R: Reports*, *73*(5), 51-65.

Yang, J., Takeda, Y., Imanishi, N., & Yamamoto, O. (1999). Ultrafine Sn and SnSb$_{0.14}$ Powders for Lithium Storage Matrices in Lithium-Ion Batteries. *Journal of The Electrochemical Society*, *146*(11), 4009.

Yi, T. F., Shu, J., Zhu, Y. R., Zhu, X. D., Yue, C. B., Zhou, A. N., & Zhu, R. S. (2009). High-performance Li$_4$Ti$_{5-x}$V$_x$O$_{12}$ (0≤ x ≤0.3) as an anode material for secondary lithium-ion battery. *Electrochimica Acta*, *54*(28), 7464–7470.

Yi, T. F., Shu, J., Zhu, Y. R., Zhu, X. D., Zhu, R. S., & Zhou, A. N. (2010a). Advanced electrochemical performance of Li$_4$Ti$_{4.95}$V$_{0.05}$O$_{12}$ as a reversible anode material down to 0 V. *Journal of Power Sources*, *195*(1), 285–288.

Yi, T., Jiang, L., Shu, J., Yue, C., Zhu, R., & Qiao, H. (2010b). Recent development and application of Li$_4$Ti$_5$O$_{12}$ as anode material of lithium ion battery. *Journal of Physical and Chemistry of Solids*, *71*(9), 1236–1242.

Yoon, J., Bang, H. J., Prakash, J., & Sun, Y. (2008). Comparative study of Li[Ni$_{1/3}$Co$_{1/3}$Mn$_{1/3}$]O$_2$ cathode material synthesized via different synthetic routes for asymmetric electrochemical capacitor applications. *Materials Chemistry and Physics*, *110*, 222–227.

Yoon, S., Park, C.-M., & Sohn, H.-J. (2008). Electrochemical Characterizations of Germanium and Carbon-Coated Germanium Composite Anode for Lithium-Ion Batteries. *Electrochemical and Solid-State Letters*, *11*(4), A42.

Yu, N., Gao, L., Zhao, S., & Wang, Z. (2009). Electrodeposited PbO$_2$ thin film as positive electrode in PbO$_2$/AC hybrid capacitor. *Electrochimica Acta*, *54*, 3835–3841.

Yu, Z., Zhang, X., Yang, G., Liu, J., Wang, J., Wang, R., & Zhang, J. (2011). High rate capability and long-term cyclability of Li$_4$Ti$_{4.9}$V$_{0.1}$O$_{12}$ as anode material in lithium ion battery. *Electrochimica Acta*, *56*(24), 8611–8617.

Yuan, A., Wang, X., Wang, Y., & Hu, J. (2010). Comparison of nano-MnO$_2$ derived from different manganese sources and influence of active material weight ratio on performance of nano-MnO$_2$ / activated carbon supercapacitor. *Energy Conversion and Management*, *51*(12), 2588–2594.

Yuan, A., & Zhang, Q. (2006). A novel hybrid manganese dioxide / activated carbon supercapacitor using lithium hydroxide electrolyte. *Electrochemistry Communications*, *8*, 1173–1178.

Yuan, C., Zhang, X., Wu, Q., & Gao, B. (2006). Effect of temperature on the hybrid supercapacitor based on NiO and activated carbon with alkaline polymer gel electrolyte. *Solid State Ionics*, *177*, 1237–1242.

Zangari, G., & Lambeth, D. N. (1994). Porous aluminum oxide templates for nanometer-sized cobalt array. *IEEE Transactions on Magnetics*, *33(5)*, 3010-3012.

Zhang, Q., & Li, X. (2013). Recent developments in the doped-$Li_4Ti_5O_{12}$ anode materials of lithium-ion batteries for improving the rate capability. *International Journal of Electrochemical Science*, *8*(5), 6449–6456.

Zhang, Q. Y., Zhang, C. L., Li, B., Jiang, D. D., Kang, S. F., Li, X., & Wang, Y. G. (2013). Preparation and characterization of W-doped $Li_4Ti_5O_{12}$ anode material for enhancing the high rate performance. *Electrochimica Acta*, *107*, 139–146.

Zhang, Q., Zhang, C., Li, B., Kang, S., Li, X., & Wang, Y. (2013). Preparation and electrochemical properties of Ca-doped $Li_4Ti_5O_{12}$ as anode materials in lithium-ion battery. *Electrochimica Acta*, *98*, 146–152.

Zhang, S. S. (2006). The effect of the charging protocol on the cycle life of a Li-ion battery. *Journal of Power Sources*, *161*(2), 1385–1391.

Zhao, H., Li, Y., Zhu, Z., Lin, J., Tian, Z., & Wang, R. (2008). Structural and electrochemical characteristics of $Li_{4-x}Al_xTi_5O_{12}$ as anode material for lithium-ion batteries. *Electrochimica Acta*, *53*, 7079–7083.

Zhao, Y., Wang, Y. Y., Lai, Q. Y., Chen, L. M., Hao, Y. J., & Ji, X. Y. (2009). Pseudocapacitance properties of $AC/LiNi_{1/3}Co_{1/3}Mn_{1/3}O_2$ asymmetric supercapacitor in aqueous electrolyte. *Synthetic Metals*, *159*, 331–337.

Zhong, Z. (2007). Synthesis of Mo^{4+} Substituted Spinel $Li_4Ti_{5-x}Mo_xO_{12}$. *Electrochemical and Solid-State Letters*, *10(12)*, A267–A269.

Zihong, S., & Anbao, Y. (2009). Electrochemical Performance of Nickel Hydroxide / Activated Carbon Supercapacitors Using a Modified Polyvinyl Alcohol Based Alkaline. *Chinese Journal of Chemical Engineering*, *17*(1), 150–155.

Zuo, W., Li, R., Zhou, C., Li, Y., Xia, J., & Liu, J. (2017). Battery-Supercapacitor Hybrid Devices : Recent Progress and Future Prospects. *Advanced Science*, *4*(7), 1600539.